SIGNAL IN HUMAN MOTOR UNSTEADINESS: DETERMINING THE ACTION AND ACTIVITY OF MUSCLES

by

Jason James Kutch

A dissertation submitted in partial fulfillment
of the requirements for the degree of
Doctor of Philosophy
(Applied and Interdisciplinary Mathematics)
in The University of Michigan
2008

Doctoral Committee:

Professor Anthony M. Bloch, Co-Chair
Associate Professor Arthur D. Kuo, Co-Chair
Professor Edward L. Stuenkel
Assistant Professor Victoria Booth
Professor William Rymer, Northwestern University

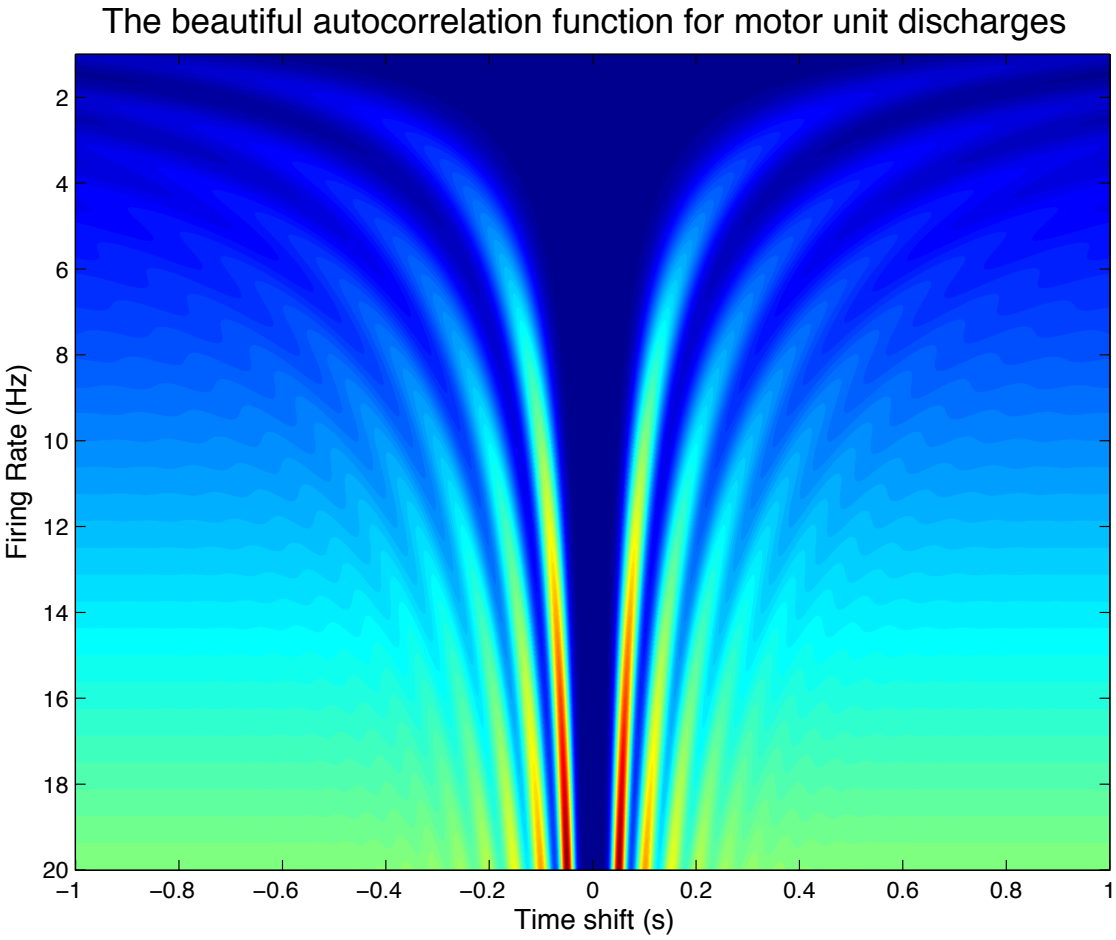
The beautiful autocorrelation function for motor unit discharges
Firing Rate (Hz)
2
4
6
8
10
12
14
16
18
20
−1
−0.8
−0.6
−0.4
−0.2
0
0.2
0.4
0.6
0.8
1
Time shift (s)

"Bernard of Chartres used to say that we are like dwarfs on the shoulders of giants, so that we can see more than they, and things at a greater distance, not by virtue of any sharpness of sight on our part, or any physical distinction, but because we are carried high and raised up by their giant size"

–*Metalogicon*, John of Salisbury, 1159 A.D.

To my parents, Evelyn and Harry Kutch, for being principal giants in my life, and working so hard to hoist me to an extraordinary vantage point. To my wife, Darice Wong (Ph.D.!), for being my giant rock of happiness, and for finishing her dissertation first, making my journey more comfortable and more certain.

ACKNOWLEDGEMENTS

For developing my early interest in biomechanics and the neural control of movement, I thank Professor Tom Buchanan at the University of Delaware. For instilling a sense that any biological problem becomes tractable when viewed quantitatively, I thank Professor John Hopfield at Princeton University.

I must first thank my advisor, Tony Bloch, for opening the doors of an applied math graduate program to a mechanical engineering undergraduate, and encouraging me to explore a variety of topics that interested me. This exploration took me into some rich ideas in theoretical neuroscience, though it ultimately convinced me that my success depended on my ability to put rigorous mathematical analysis together with experimentation.

My previous interest in biomechanics brought be to add a second advisor, Art Kuo. I am very thankful to Art, for establishing my collaboration with the Rehabilitation Institute of Chicago, and for instilling in me the importance of precise and engaging scientific communication. Hours spent in his office discussing (arguing over) scientific story-lines and conceptual figures have been extremely rewarding.

After I defended my dissertation proposal in the summer of 2005, I began experimental work at the Rehabilitation Institute of Chicago (RIC). I am deeply grateful to Nina Suresh for bringing me into the RIC community, introducing me to the single motor unit lab, and fostering (reining-in) my initial thinking on the problems of motor unit coordination.

While at RIC, Zev Rymer became my third advisor, and generously supported my experiments. From January 2006 to September 2007 I resided primarily in Chicago and worked on the experiments that make up this dissertation. Zev was instrumental in guiding my experiments and making them more efficient by highlighting the interesting paths and wisely steering me clear of dead-ends. With Zev's mentorship, I applied for and received a predoctoral training grant from the NIH. Going through this process was a big step in my professional development, and I'm grateful to Zev for guiding me through it. Zev, leading a group of my friends and colleagues at RIC, transformed me from a theorist to a theorist/experimentalist, a transformation for which I am eternally grateful.

I had the opportunity while working at RIC to mentor three students, and I would like to thank them for their work. Matthieu Chardon worked with me in the summer of 2006 on some early computer models of force covariance mapping which helped me to better visualize the potential of the approach. Stan Chikando worked on early versions of the EMG-weighted averaging technique (Spring 2007) and the development of efficient database software for cataloging human neurophysiology data (Summer 2007). During the summer of 2007, Ben Sinder developed computer simulations of EMG-weighted averaging that were very useful in assessing the confounding effects of correlation.

I would like to thank all the members of the Sensory Motor Performance Program at RIC for helping me in any way they could. I would like to especially thank Carol Mottram for her help in the lab and all the discussions we've had. I would also like to thank Debbie Znajda, Sue Penwarden, Joan Ciapas, and Rene Hall for all their help handling the administrative issues of paychecks, housing, grants, scheduling, etc. This work would not have been possible without them. Thanks to Emil Davchev

for saving my computer on more than one occasion. Thanks also to the research engineers Winsean Lin, Janina Madoff, and Andrew Mazotas for technical help in the lab, and to Vik Chib and Assaf Pressman for many stimulating discussions.

At the University of Michigan, thanks to Art's students Peter Adamczyk, Shawn O'Connor, and Steve Collins for being just about the toughest seminar crowd you could ask for. Thanks to my office mates Mark Iwen and Joel Lepak for getting me to program in C++ and throwing the frisbee. Thanks to the Mathematics administrative staff, particularly Tara McQueen, Laura Hornbeck, and Bert Ortiz for making things easier.

Thanks to anyone I've failed to mention for forgiving me.

I'd like to thank my biological siblings, Lynn Sulpizi and Steve Kutch, for keeping me on track by asking me when I would be finished so I could get a job and they could retire, and my non-biological siblings, Mark Brown and Julian Ehlers, for always reminding me not to be incompetent, whether climbing mountains in the magnificent Canadian Rockies or Selkirks, or writing a dissertation.

My wife Darice constantly inspires me to grow intellectually, athletically, artistically, culinarily, and personally. Thinking back on the last 6 years, the mountains we've climbed, the challenges we've met, the blissful Saturdays biking from Evanston to the Field Museum to the beach to BBQ and back, I am thoroughly convinced that going to South Africa in 2001 and missing all these things would have been the worst decision I could have possibly made.

TABLE OF CONTENTS

LIST OF FIGURES

Figure

LIST OF SYMBOLS

Symbol	
t	Continuous time
Δt	Time shift
n	Discrete time
Y	Endpoint force vector
$F^{(i)}$	Contribution to the endpoint force vector from muscle i
Y_{T}	Desired endpoint force vector (task vector)
θ	Task direction
ϵ	Measurement noise
d	Dimension of task space
a	Mechanical action vector (muscle or motor unit)
α	Mechanical action direction
A	Mechanical action matrix
m	Number of actuators (muscles or motor units)
u	Muscle activity
E	Muscle electromyographic (EMG) signal
m_{syn}	Number of muscle synergies
W	Muscle synergy coupling matrix
A_{syn}	Muscle synergy mechanical action matrix
u_{syn}	Muscle synergy input commands
S	Motor unit spike train
z	STA trajectory (motor unit) or EWA trajectory (muscle)
Z	Matrix of STA or EWA trajectories
test	Number of a motor unit being examined
alt	Number of a motor unit not being examined
$C_{\mathrm{test,alt}}(t)$	Contribution function for the influence of alt discharges on the STA of test
$C(t)$	Matrix of contribution functions
s	Index of synchronization
$s_{i,j}$	Index of synchronization between motor units i and j
g	Motor unit twitch gain
T	Motor unit twitch waveform (or muscle impulse response)
x	Time delay between discharges in two motor units
P	Motor unit peak force
θ_r	Angular range

CHAPTER I

Introduction

Ranging from barely perceptible to problematic, unsteadiness is a feature of human movement. Some part of this unsteadiness is likely due to fluctuations in muscle tension, partially generated by spinal motoneurons sending impulsive and somewhat random excitation to muscle fibers. The hypothesis of this work is that unsteadiness in movement reflects, in some way, both the internal wiring of the central nervous system (CNS) and the physical geometry of the connection between muscles and the skeleton. This dissertation seeks to exploit human movement unsteadiness to bring important insights into problems in motor neuroscience and biomechanics: how different muscles are coordinated and precisely how individual muscles move body segments. Muscle coordination can be severely impaired by stroke (Dewald et al., 1995), and a detailed understanding of muscle action is likely necessary to accurately predict and improve outcomes of tendon transfer surgeries aimed at restoring function to paralyzed limbs (Towles et al., 2004).

There are some key concepts and terminology that will run throughout this work, so we introduce them here. The *endpoint* is the segment of the body being used to interact with the world. In the case of typing on a computer, the endpoint is the fingertip (Figure 1.1A). If a person reaches out to push open a door, the endpoint

is the palm of the hand (Figure 1.1B). The *task space* is a set of movements of the endpoint in which the experimenter is interested. For instance, the experimenter may be interested in up/down and left/right movements of the end of the index finger, but may be uninterested in forward/backward movements, thus defining a task plane of interest (Figure 1.1A). Alternatively, the experimenter may be interested in all possible physical translations of the palm, but not in rotations, defining a task cube of interest (Figure 1.1B).

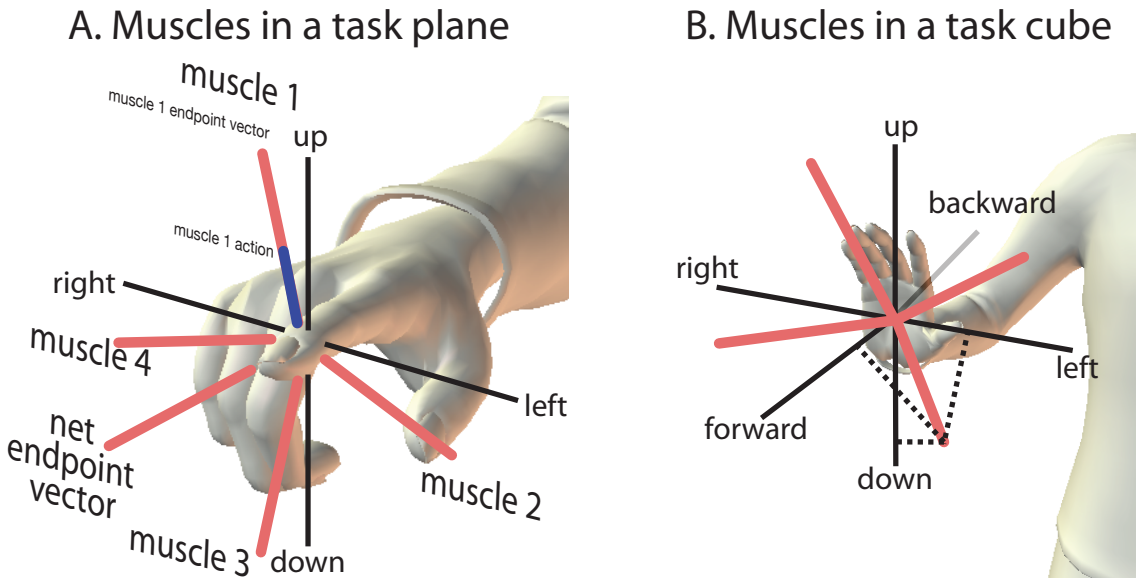

Figure 1.1: Muscles are vectors that move endpoints in task space. A. Muscle actions in a task plane. B. Muscle actions in a task cube, dashed lines highlight that that the vectors are 3 dimensional.

Having the notions of endpoint and task space allows us to form an understanding of muscle action useful for this work. Think of a muscle as a vector in task space, pushing the endpoint in a particular direction (Figure 1.1). This concept simplifies the complex internal architecture of how muscles pull on the skeleton and focuses instead on the result of muscle contraction. The force vector generated at the endpoint by muscle contraction will be referred to as the muscle's endpoint vector, and

will be denoted $F^{(i)}$ for muscle number i.

A muscle's endpoint vector can be controlled by the nervous system, but also has a component that depends only on the musculoskeletal geometry. The part of a muscle's endpoint vector that is assumed (at this point) intrinsic to how the muscle attaches to the skeleton is called the muscle's mechanical action (or just action, for short). A muscle's action is a vector whose direction represents the direction the endpoint would move if that muscle were activated. A muscle's action also has a magnitude because, for instance, two muscles may have the same action direction, but one may have twice the mechanical leverage of the other. The action vector of a muscle i is denoted $a^{(i)}$. The part of a muscle's endpoint vector that is varied by the nervous system to accomplish tasks is a scalar value called the muscle's activity, denoted u_i for muscle number i. The muscle's activity scales its action to produce its endpoint vector, which can be expressed for muscle number i as $F^{(i)} = a^{(i)}u_i$.

Endpoint vectors from different muscles will sum to form a net force vector in task space. The endpoint will actually move according to this vector; we refer to the net vector as the *net endpoint vector*, which will have both a *net endpoint direction* and *net endpoint magnitude*. The CNS coordinates different muscles so that the endpoint can perform desired tasks. The desired net endpoint vector will be called the *task vector*, and denoted Y_{T}. An *isometric* task is one where all body segments are fixed in space, and the endpoint exerts force against a constraint. Isometric tasks are important for obtaining more interpretable experimental findings. The net endpoint vector can be interpreted as the instantaneous direction and magnitude of limb movement if the constraint were suddenly removed.

A physiological structure that will be important in this work is the *motor unit*. The motor unit is defined to be a motoneuron in the spinal cord, along with the set of

muscle fibers it excites. One motoneuron may excite several hundred muscle fibers, but it is generally true that each muscle fiber is excited by only one motoneuron. Given our description of task space and mechanical action above, it is as equally appropriate to discuss motor unit mechanical action as it is muscle mechanical action. Motor unit mechanical action is a vector describing the magnitude and direction of how the endpoint is moved if a single motor unit is active. Motor units also have endpoint vectors formed by motor unit activity scaling motor unit action.

Chapter II introduces two key questions in movement neuroscience that this dissertation will consider. First, it is generally true that the number of muscles acting in a task space exceeds the dimension of the task space. This fact affords the CNS a certain amount of choice when deciding how much activity each muscle should have to make the net endpoint vector match as close to the task vector as possible. This problem is often referred to as the *muscle redundancy problem*, and many theories of how the CNS uses redundant muscles have been proposed. Second, though motor units within a muscle are generally understood to function as a unit, several studies have shown different motor units within the same muscle may behave differently depending on the task direction. Whether these differences relate to differences in motor unit mechanical action remains an open question. Since these scientific questions will be approached using unsteadiness in human movement, Chapter II also presents a brief review of previous findings on the source of unsteadiness.

Chapter III introduces an original experimental and computational technique coined *force covariance mapping* (FCM). FCM is based on the principle of *signal-dependent noise*: the variability in the tension generated by a muscle is proportional to the average tension generated. Applying FCM experimentally involves having a subject push (against a force sensor) to different stationary task vectors distributed

uniformly around task space. As the subject attempts to hold a particular stationary task vector, unsteadiness will cause the net endpoint vector exerted by the subject to fluctuate. Applying FCM across the task plane shown in Figure 1.1A, it was found that in some task directions the net endpoint vector always had essentially the same direction and only fluctuated in magnitude. For other task directions, the net endpoint vector fluctuated in both magnitude and direction. The former observation implies that a single muscle is providing most of the control (*prime mover strategy*), while the latter observation implies a significant contribution from multiple muscles having different actions (*cooperation strategy*). The CNS strategies inferred from FCM are discussed in regard to the muscle redundancy problem and muscle synergy hypothesis. FCM may also provide more information about how the CNS coordinates muscles compared to a traditional dimensionality analysis.

This work then turns to the problem of using unsteadiness to determine muscle mechanical action. Chapter IV provides a rigorous mathematical framework for analyzing spike-triggered averaging (STA), a widely-used tool in motor neuroscience, for understanding the mechanical action of single motor units. STA uses the discharges from a single motor unit to filter fluctuations in the net endpoint vector, potentially revealing force generating characteristics of the motor unit being studied. STA thus produces a motor unit action estimate (MUAE) for a particular motor unit, referred to as the *MUAE vector*. In analytical equations, when the task vector was multidirectional (i.e. the task space is multidimensional), motor unit discharge rates did not affect the MUAE direction. However, weak synchronization of discharge times among motor units with different mechanical action directions did profoundly affect the MUAE direction. Novel predictive equations are presented that relate motor unit synchronization to MUAE direction distortion. This theoretical analysis lays

the groundwork for the second experiment of this dissertation, described in Chapter V.

Studying whether motor unit control within a muscle is related to differences in motor unit mechanical action, directly at the motor unit level, presents significant difficulties. An alternative approach was taken, aimed at providing global information about this hypothesis. Chapter V shows how the concept of STA can be generalized to use a complex electrical signal, such as surface EMG, instead of a single motor unit discharges. The technique that arose from this analysis is coined EMG-weighted averaging (EWA). EWA provides a *muscle* action estimate, also referred to as the *MAE vector*. MAE vectors for two index finger muscles across tasks in the plane (Figure 1.1A) were experimentally measured. Significant shifts were found in the MAE direction for both muscles as a function of task direction. These findings indicate that representing a muscle with a single vector describing its action may not be valid even for constant posture tasks, and supports the idea that the CNS can control muscle action as well as activity.

When the human motor system is unimpaired, it is able to minimize the effects of unsteadiness on accomplishing tasks. However, if human motor unsteadiness is carefully measured, it can reveal a wealth of information about how muscles are coordinated and how single muscles move body segments. The experimental methods and computational analyses presented in this dissertation will hopefully provide a means of harnessing the information contained in human motor unsteadiness.

CHAPTER II

Background

This chapter presents an overview of two key problems in movement neuroscience: 1) how do redundant muscles cooperate to achieve tasks? and 2) is muscle action direction fixed? Some common approaches to these problems are reviewed, and concrete examples are given to discuss these problems in a mathematical context. First, one source of human motor unsteadiness is discussed, so that examples of how unsteadiness may provide key insights into the relevant problems will be clear as the chapter progresses.

2.1 Movement unsteadiness

Unsteadiness in human movement may be generated by many processes, both central and peripheral. Motoneurons in the spinal cord may not receive steady commands (Lowery and Erim, 2005). Motoneurons may not generate a steady output even when provided a steady input because of fluctuations in membrane voltage threshold (Binder and Powers, 2001). Information in the brain is largely transmitted in the form of action potentials, brief electrical discharges that initiate chemical events in target cells (Rieke et al., 1997). At some point, these all-or-none events must be filtered so that our movements are smooth. Thus, even if a motoneuron were to generate a completely regular spike train, muscle force will still be unsteady because

of un-fused motor twitches (Thomas et al., 1991). After receiving excitation from motoneurons, motor unit force output is generally smooth, but it retains oscillations due to the action potential input (Figure 2.1). For inputs at sufficiently low rates, the fluctuations in the net endpoint magnitude generated by a single motor unit will be substantial. This work will be focused on the effects of movement unsteadiness, with less emphasis on its exact source.

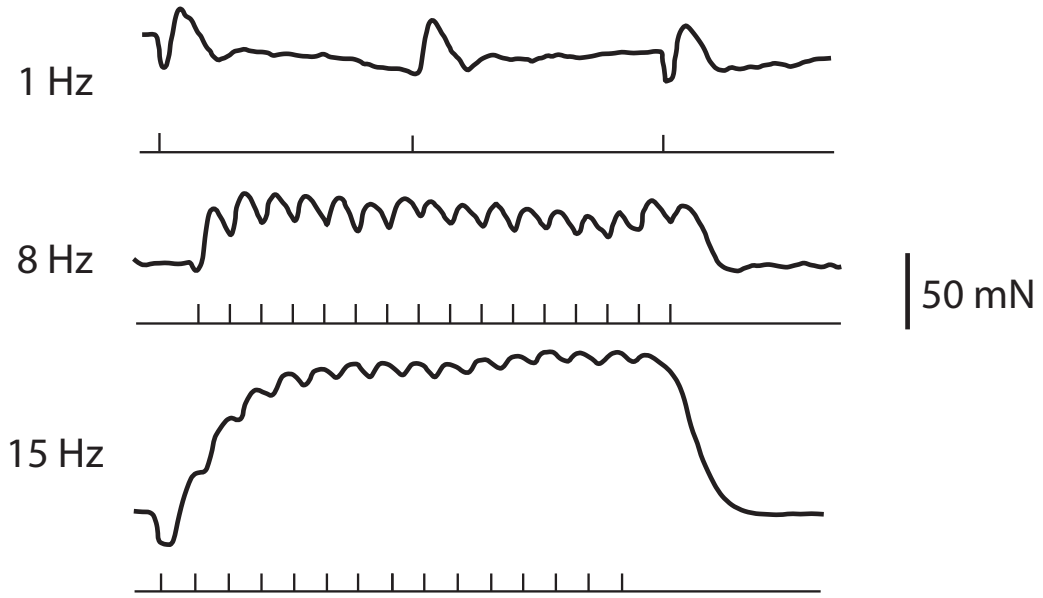

Figure 2.1: Motor unit force is not steady, even given steady input. The different panels show the force recorded when a single human motor unit was stimulated with regular spike trains at various frequencies. Notice that force fluctuations about the average steady state level can be significant. Adapted from Thomas et al. (1991).

Fluctuations in the net endpoint magnitude are also present when motor units are activated under natural conditions. For isometric force generated by the index finger, net endpoint magnitude variability is on the order of 5% of average net endpoint magnitude (Moritz et al., 2005). Fluctuations in net endpoint magnitude are time-locked to single motor unit discharges, as revealed by the spike-triggered averaging technique (Stein et al., 1972). Thus, fluctuations in motor unit force will generate

measurable fluctuations in the net endpoint vector.

When considering the mechanical action and activity of muscles, the muscle-level consequences of the motor unit force fluctuations are of interest. Fluctuations in force generated by a single muscle exhibit *signal-dependent noise*: the variability in muscle endpoint magnitude increases with increasing average muscle endpoint magnitude (Galganski et al., 1993; Moritz et al., 2005). This scaling relation may be related to physiological properties of the motoneuron pool (Jones et al., 2002): since motor units are activated in an orderly manner by strength, stronger motor units are recruited when larger forces are required. These stronger motor units will generate larger force fluctuations, which may contribute to signal-dependent noise.

This work will seek to make use of signal-dependent noise to infer the activity of muscles from observed net endpoint vector fluctuations, and exploit the fact that increases in muscle force will be accompanied by specific changes in the net endpoint vector to estimate muscle mechanical action.

2.2 How do redundant muscles cooperate to achieve tasks?

Nikolai Bernstein (1896-1966) was probably the first to formulate the degrees of freedom problem in motor control (Macpherson, 1991). The problem is that the CNS is confronted with choice when deciding how to move the body to accomplish any task. This problem may appear at the kinematic level: your elbow can be a great many places while maintaining your hand at a fixed location in space. The degrees of freedom problem may also appear at the muscle level: after the CNS has decided where to put your elbow relative to your hand, there may be many combinations of muscle activities that can accomplish the desired goal. The degrees of freedom problem at the muscle level is referred to as the *muscle redundancy problem*; it will

be a major question that this work will address experimentally.

2.2.1 Muscles are not redundant because of incomplete task spaces

The muscle redundancy problem is often casually articulated by scientists by saying: "every joint has more muscles crossing it than degrees of freedom." In the context of the terminology of the introduction in Chapter I, the muscle redundancy problem is that each task space has more muscle action vectors in it than the dimension of the task space. However, the task space is defined by the experimenter. What says that, if the task space is simply made to include more degrees of freedom, the redundancy would not disappear? What if the CNS has all the information it needs to set the exact activity of all muscles, but the experimenter is ignoring some of this information by throwing degrees of freedom away?

The problem is that muscle can only pull. This evolutionary restriction requires that there are more muscles in *any* task space than the dimension of the task space. If m is the number of muscles and d is the dimension of the task space, then $m \geq d+1$ (see Appendix for proof). Given that muscles only generate tension, the muscle redundancy problem is probably better stated as the muscle redundancy *necessity*. The CNS will always have to make a choice when controlling muscles, and this choice will likely not go away by picking a certain task space.

For example, imagine two actuators that can both push and pull (not muscles) in a one-dimensional task space (Figure 2.2A). We would say that these actuators are redundant, because you could push the endpoint in either direction using only one of these actuators. It is possible, in this case, that the experimenter simply made a poor choice when defining the task space. The one-dimensional task space is actually a part of a complete two-dimensional task space, which has two actuators, and is therefore not redundant (Figure 2.2B). Thus, recognizing the complete task space

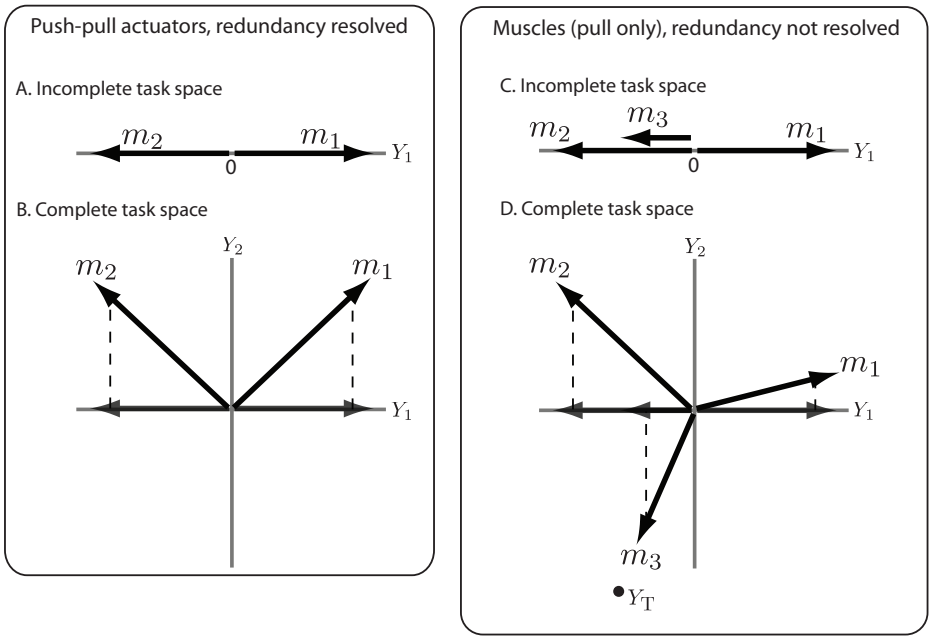

Figure 2.2: Muscle redundancy relates to the fact that muscles can only pull. When actuators can both push and pull, they may be redundant for a subspace (A) of the complete task space (B). However, when muscles are vectors that can only be weighted positively, the redundancy for the subspace (C) persists when the complete task space (D) is shown.

eliminated the apparent redundancy in the one-dimensional subspace.

Now, imagine that the actuators are actually muscles, only able to produce tension (positive force). The experimenter again defines a one dimensional task space (Figure 2.2C), and this time it has 3 muscles in it because the complete two-dimensional task space must have at least 3 muscles (Figure 2.2D). Three muscles controlling a single degree of freedom are certainly redundant if there are muscles that can generate both positive and negative endpoint vectors. The experimenter later realizes that the true task space for the system was two-dimensional, and draws it accordingly. Now there are three muscles in a two-dimensional task space, and these muscles are still redundant; for a task vector in the action direction of one of the muscles (Y_{T} in Figure 2.2D), the task could be accomplished by that muscle alone. Or, that muscle could pull harder, and the other two muscles could counteract the excess

force producing the same net endpoint vector.

2.2.2 The question of one or multiple muscles

One of the most basic questions that can be asked about a redundant set of muscles is whether a given task is being performed by primarily one muscle (prime mover strategy), or if the CNS is coordinating multiple muscles with different mechanical actions (cooperation strategy)? Of course, if no muscle has its mechanical action vector aligned with the task vector, only the cooperation strategy makes sense. However, when the task vector is well aligned with the mechanical action vector of a muscle, the CNS is faced with choosing between the cooperation and the prime mover strategy.

As a simple example, imagine 3 muscles in a two-dimensional task space. Muscle 1 pulls straight to the right ($a^{(1)} = [1, 0]^T$), muscle 2 pulls straight up ($a^{(2)} = [0, 1]^T$), and muscles 3 pulls straight down ($a^{(3)} = [0, -1]^T$). These mechanical actions are placed as columns of a matrix A. Once we choose a vector $\bar{u}$ specifying the average activity in each muscle, the average net endpoint vector will be $\bar{Y} = A\bar{u}$. If we have a task vector $Y_{\mathrm{T}} = [1, 0]^T$, we can either use a prime mover strategy $\bar{u} = [1, 0.1, 0.1]$ or a cooperation strategy $\bar{u} = [1, 1, 1]^T$. Note, however, that for these muscles and $Y_{\mathrm{T}} = [1, 1]^T$, there is no prime mover strategy available because there is no muscle mechanical action in the task vector direction.

Does the CNS always use the prime mover strategy when available? Buchanan et al. (1986; 1989) considered a 2-dimensional task space at the wrist consisting of rotations of the elbow and forearm. They studied electromyographic (EMG) data from a number of relevant muscles, and they did not find any task directions in which one muscle appeared to be a prime mover. In contrast, many authors claim that index finger force generated in abduction (away from the other fingers) is primar-

ily attributable to the first dorsal interosseous (FDI) muscle (Flament et al., 1993; Semmler and Nordstrom, 1998; Thomas et al., 1986), though this assumption has recently been challenged (Keenan et al., 2006). In addition, the EMG data of Hoffman and Strick (1999) suggest that there may be task directions in the task space of human wrist movements that are controlled using the prime mover strategy, though the authors did not comment on this possibility.

Being able to investigate prime mover versus cooperation strategies is clinically relevant. Hoffman and Strick (1995) showed that after motor cortex lesion in the monkey, movements involving combinations of wrist flexion and radial deviation changed from straight trajectories to piecewise trajectories involving radial deviation first followed by wrist flexion. Given the mechanical action directions of the wrist muscles (Hoffman and Strick, 1999), it is possible that the motor cortex lesion causes a smooth cooperation strategy to be replaced by two sequential prime mover strategies.

Whether the net endpoint vector is generated by a prime mover or cooperation strategy is a question about one task in particular. The next three sections introduce theories of how the CNS might activate multiple redundant muscles to achieve *all* tasks in a task space.

2.2.3 The muscle synergy hypothesis

One approach to muscle redundancy is to hypothesize that the CNS does not control each muscle individually, but forms muscle groups that can be controlled independently. The synergy hypothesis considers movement control hierarchically: a task vector Y_{T} is formed by the CNS, and this task vector is transformed into activity in a group of synergies (Figure 2.3). Each synergy specifies activity ratios for all muscles that are involved in the task. In this way, it is proposed that the

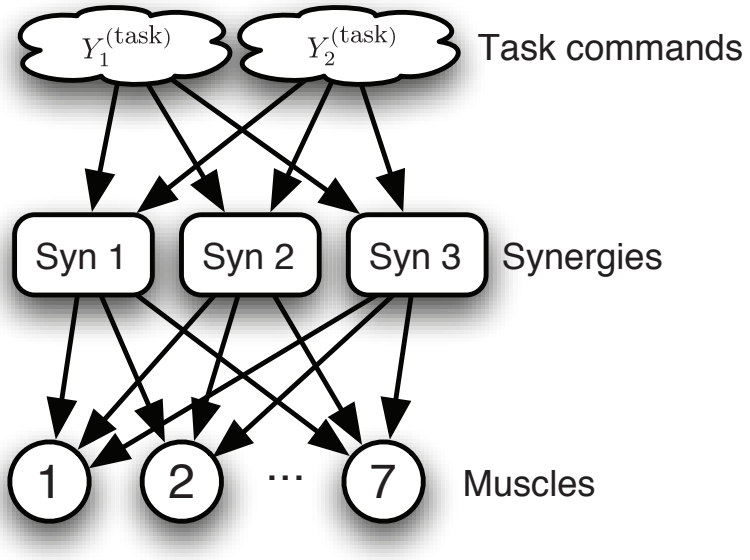

Figure 2.3: Schematic diagram of the muscle synergy hypothesis. Components of the task vector Y_T are transformed into the activity of synergies. Each synergy fixes the activity of a group of muscles. In this way, the CNS controls synergies rather than muscles, resulting in fewer degrees-of-freedom to control.

complexity of control is reduced because muscle groups are controlled rather than the muscles themselves (Lee, 1984; Macpherson, 1991).

Researchers typically test the muscle synergy hypothesis by applying a feature extraction algorithms, such as variants of principal components analysis, to electromyographic (EMG) signals from multiple muscles during movement. Three time-varying patterns of muscle activity are sufficient to describe the activity in 13 hindlimb muscles of the frog during kicking in different directions (d'Avella et al., 2003). Four patterns of muscle activity are sufficient to describe the activity in > 8 cat hindlimb muscles during postural response to translations of the support surface in 16 different directions (Ting and Macpherson, 2005). EMG activity from 8 muscles controlling the human elbow can be described by only 2 variables during isometric elbow flexion/extension, and these variables are clearly related to joint torque and total muscle activity (Kutch and Buchanan, 2001). Finally, four to five patterns of time-varying

muscle activity are sufficient to describe the activity in up to 19 human shoulder and arm muscles during reaching movements in vertical planes (d'Avella et al., 2006). One possible interpretation of these findings is that muscle synergies are enforced by fixed neural constraints, and the CNS uses these constraints as a substrate for reducing degrees of freedom.

One problem with the muscle synergy hypothesis, in light of the discussion of complete and incomplete task spaces in Section 2.2.1, is that forming muscle synergies can not eliminate redundancy. Muscle synergies are often viewed as linear transformations applied to the muscle mechanical action matrix A (Ting and Macpherson, 2005; Tresch et al., 2006). The net endpoint vector Y is ordinarily expressed as $Y = Au$. Under the modern mathematical interpretation of the muscle synergy hypothesis, $Y = AWu_{\text{syn}}$. If m is the number of muscles and m_{syn} is the number of synergies, W is a $m \times m_{\text{syn}}$ matrix, where the ith column specifies the contribution of each muscle to the ith synergy. The u_{syn} vector contains a weighting for each synergy, and is assumed to be positive. The product $A_{\text{syn}} = AW$ has column i specifying the mechanical action of the ith *synergy*. In order to perform all tasks by coordinating a set of synergies, there must be $m_{\text{syn}} \geq d + 1$ synergies, where d is the task space dimension, because the synergy activities u_{syn} are assumed to be positive. Thus, the CNS is still faced with choice when deciding on the synergy activities u_{syn}, and thus synergies do not eliminate redundancy.

2.2.4 The optimization hypothesis

A long-standing hypothesis about how the CNS eliminates muscle redundancy proposes that, for any given task vector, the CNS chooses to activate muscles so that performance criteria are optimized. It has been proposed that muscle activity patterns may be explained by minimizing some measure of effort (Buchanan and

Shreeve, 1996; van Bolhuis and Gielen, 1999; Fagg et al., 2002), or by maximizing accuracy (Harris and Wolpert, 1998; Todorov, 2002; Haruno and Wolpert, 2005). Some optimization criteria compare very nicely with experimental data.

The problem with the optimization approach is that it is very difficult to say with certainty that "the CNS is minimizing X." It has been pointed out that minimizing effort and maximizing accuracy may be equivalent for isometric tasks, as the presence of signal-dependent noise encourages the minimization of squared muscle force (van Bolhuis and Gielen, 1999; Todorov, 2002). Also, many optimization criteria based on physiological muscle properties generate similar results (Buchanan and Shreeve, 1996), meaning that experimental data may be unable to argue definitively for some criteria over another.

This work is more interested in providing experimental support for statements of the form "it is more likely that the CNS resolves redundancy using synergies as compared to optimization", or visa versa. As an example, we consider the relation between optimization and the prime mover strategy versus cooperation strategy (Section 2.2.2). Consider a hypothetical task space at the end of the index finger consisting of four muscles: muscle A pulls up, muscle D, pulls down, muscle B pulls right and down, muscle C pulls left and down (Figure 2.4). This simple example shows that, for task vectors aligned with muscle mechanical action vectors, optimization will sometimes favor the prime mover strategy and sometimes favor the cooperation strategy, depending on the geometric relations among the muscle mechanical action vectors. Alternatively, if all muscles are part of synergies containing muscles with different mechanical actions, the prime mover strategy will never be observed because activity of any synergy will involve the coactivation of multiple muscles. Depending on experimental observations of CNS control strategies, it may be possible to argue

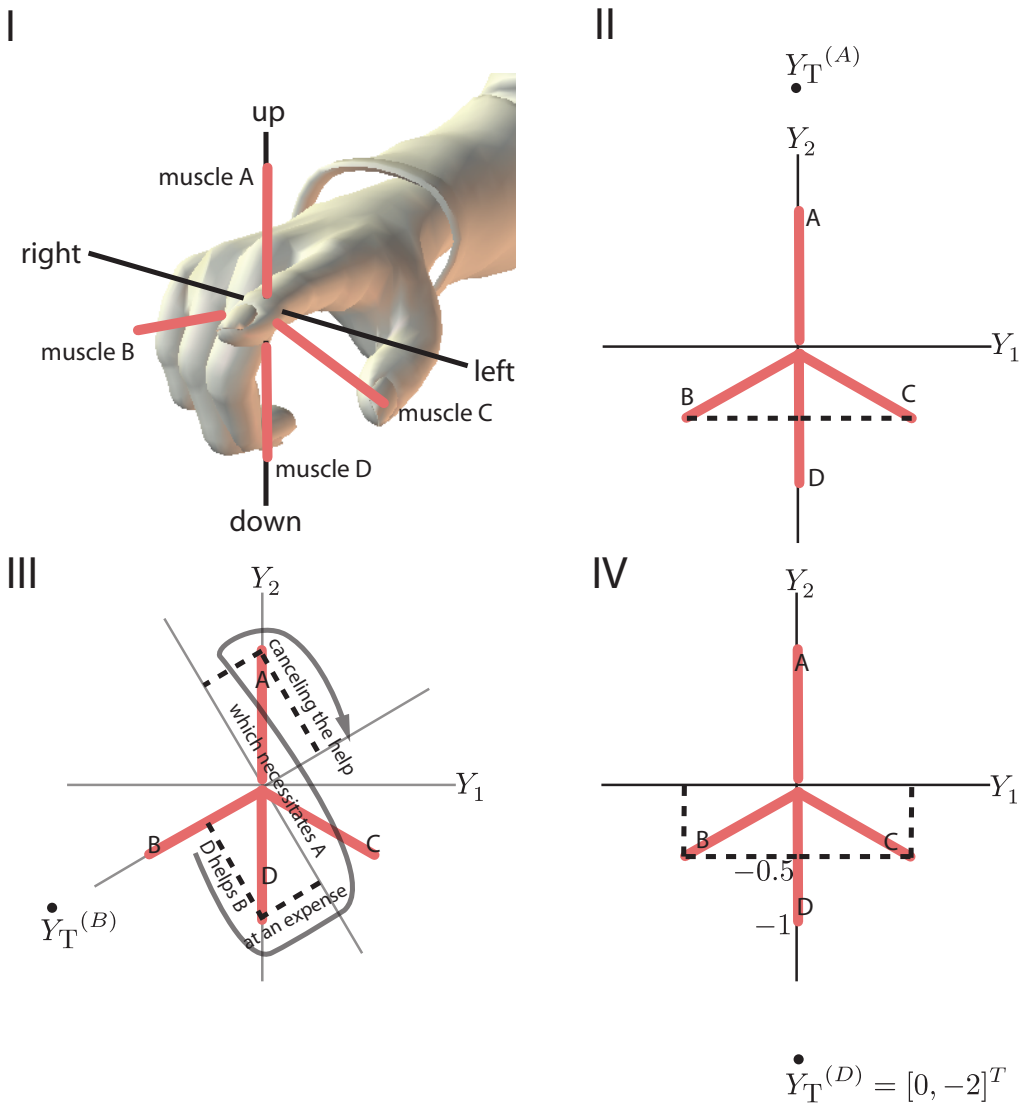

Figure 2.4: Relation between optimization and prime mover versus cooperation strategy. I. Four muscles in a task space. II. For a task vector $Y_T{}^{(A)}$ in the direction of muscle A's mechanical action, minimizing effort clearly dictates that muscle A function as a prime mover, because activity in any other muscle would be detrimental to the task. III. For a task vector $Y_T{}^{(B)}$, muscle D is in a position to assist muscle B. However, this assistance comes at the expense of an unwanted endpoint vector contribution perpendicular to the task direction, which necessitates that muscle A is activated. However, the activity of muscle A generates an unwanted endpoint contribution in the direction opposite to $Y_T{}^{(B)}$, canceling the help provided by muscle D. Thus, the optimal strategy for minimizing effort is still to use muscle B as a prime mover. IV. If a muscle has two muscles within 90° on either side, then it becomes advantageous to use the cooperation strategy. The prime mover strategy would have $u = [0, 0, 0, 2]^T$ (A,B,C,D) to achieve the task vector $Y_T{}^{(D)}$. A possible cooperation strategy is $u = [0, 1, 1, 1]^T$. If the CNS is minimizing $\sum_i u_i^2$, then the prime mover strategy has a cost of 4, while the cooperation strategy as a cost of 3, making it a more optimal strategy.

for one hypothesis or another.

2.2.5 The uncontrolled manifold hypothesis

Another possibility for eliminating redundancy is the *uncontrolled manifold hypothesis*. This hypothesis, most often applied to kinematic redundancy, states that only some kinematic degrees of freedom are relevant to performing a task; these are stabilized with the remaining allowed to fluctuate (Latash et al., 2002; Todorov and Jordan, 2002). For instance, when visual feedback is provided to a human subject about the total vertical force generated by index and middle finger, force is distributed among the fingers to stabilize moment about a point between the fingers at the expense of destabilizing total force (Latash et al., 2001). Recently, the uncontrolled manifold hypothesis has been discussed in terms of the muscle redundancy problem (Krishnamoorthy et al., 2007).

A simple example will illustrate the key concept of the uncontrolled manifold hypothesis applied to muscle activity. Consider three muscles in a two-dimensional task space, with mechanical actions of equal magnitude distributed through the plane with 120° between each pair (Figure 2.5I). The mechanical action matrix for this muscle system is

$$A = \begin{bmatrix} 1 & -0.5 & -0.5 \\ 0 & 0.866 & -0.866 \end{bmatrix} \tag{2.1}$$

The *null space* of a matrix is the set of vectors that, when multiplied by the matrix, become the zero vector. The null space of A is any vector of the form $[\alpha, \alpha, \alpha]^T$ for some positive number α. The null space is easy to see for this set of muscles because if the three muscles pull equally hard, the net endpoint vector is zero. For this example, the null space can be thought of as a line in activity space (Figure 2.5II).

The idea of the uncontrolled manifold is that the component of the activity vector that is in the null space can do whatever it wants, and no effect will be seen on the net endpoint vector. At the same time, there is (in this example) one less degree of freedom, so redundancy is eliminated. Let v_n denote a vector in the null space, and let v_1 and v_2 be two other linearly independent vectors not in the null space. The activity vector u required to achieve some task vector Y_{T} can be expressed as some linear combination of v_1, v_2, and v_n according to $u = b_1v_1 + b_2v_2 + b_nv_n$ for scalars b_1, b_2, and b_n. Applying A to u, we find

$$Au = A(b_1v_1 + b_2v_2 + b_nv_n) = \begin{bmatrix} | & | \\ Av_1 & Av_2 \\ | & | \end{bmatrix} \begin{bmatrix} b_1 \\ b_2 \end{bmatrix} = Y_{\mathrm{T}} \tag{2.2}$$

b_nAv_n disappears because v_n is in the null space of A. We can now invert the matrix $[Av_1, Av_2]$, multiply by the task vector Y_{T}, to obtain $[b_1, b_2]^T$. The activity vector will then be $u = b_1v_1 + b_2v_2 + [\text{any number}]v_n$.

In the example presented, the prime mover strategy will only appear if the null space vector v_n has a zero contribution to the activity vector. The uncontrolled manifold hypothesis encourages the cooperation strategy, because there are many combinations of multiple muscles that will have no effect on the net endpoint vector. It is not possible to have uncontrolled activity of a single muscle because it will always have an effect on the task vector.

2.2.6 Example: using signal-dependent noise to determine average muscle activities

Variability in a muscle endpoint vector likely provides information about average muscle activity. Here is an example of how unsteadiness may be exploited to provide additional information about muscle activity.

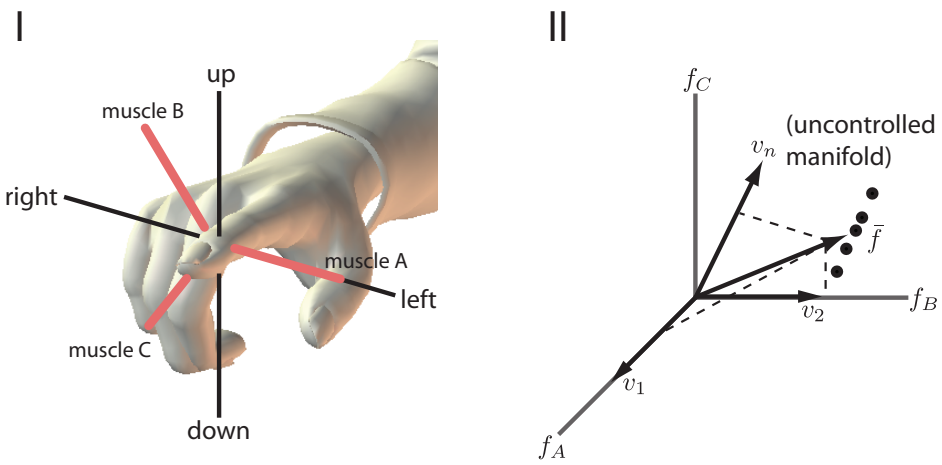

Figure 2.5: Using the uncontrolled manifold hypothesis for eliminating muscle redundancy. I. A set of three muscles pulling 120° apart in a 2-dimensional task space. II. This set of muscle mechanical action vectors has a null space along the line $[1, 1, 1]^T$. There is enough information in the 2-dimensional task vector to uniquely determine v_1 and v_2. A activity vector can then be chosen by adding appropriate contributions from v_1 and v_2 along with any contribution from v_n. Thus, the activity vector can fluctuate along an uncontrolled manifold (the null space) while still achieving the task.

Consider a 1-dimensional task space having "forward" and "backward" directions. Muscle 1 pushes the endpoint forward while muscle 2 pulls the endpoint back (Figure 2.6A). We denote the net endpoint vector Y, though in this case it is simply a scalar. Assuming the magnitude of the action vectors are equal for muscles 1 and 2, and both equal to unity, the average net endpoint vector can be expressed:

$$\bar{Y} = \bar{u_1} - \bar{u_2} \tag{2.3}$$

where $\bar{u_1}$ is the average activity in the first muscle and $\bar{u_2}$ is the average activity in the second muscle. Assume that the standard deviation of muscle activity is proportional to average muscle activity, and that both muscles have the same (known) constant of proportionality. Then, $\sigma_1 = k\bar{u_1}$ and $\sigma_2 = k\bar{u_2}$. If the standard deviation of the net endpoint magnitude is denoted it σ_Y,

$$\sigma_Y^2 = k^2(\bar{u_1}^2 + \bar{u_2}^2) \tag{2.4}$$

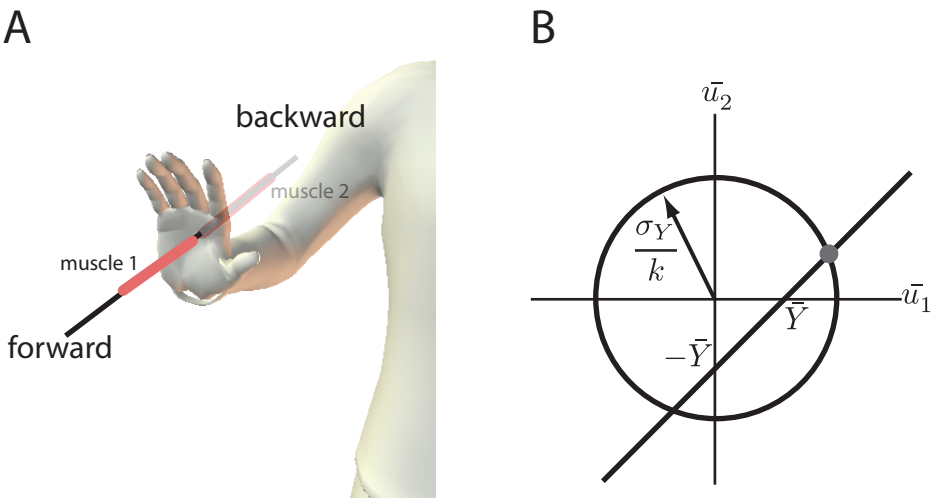

Figure 2.6: Unsteadiness can uniquely determine muscle activity. A. A one dimensional task space, with muscle mechanical actions. Hypothetical muscle 1 pushes the hand forward while hypothetical muscle 2 pulls the hand back. B. In the space of activities, an average net endpoint vector $\bar{Y}$ only constrains $(\bar{u_1}, \bar{u_2})$ to be along a line, while a measurement of the task vector variance adds a circular constraint, thus uniquely specifying a contribution from each muscle.

Can the pair of average activities $(\bar{u_1}, \bar{u_2})$ used to perform the task be determined?. Visualize the$(\bar{u_1}, \bar{u_2})$ plane (Figure 2.6B). Equation 2.3 is not sufficient to know exactly what combination of average activities were used because this equation only defines a line in the $(\bar{u_1}, \bar{u_2})$ plane. However, introducing the information gained from measuring the standard deviation of the the net endpoint vector magnitude, expressed in Equation 2.4, a circular constraint appears in the $(\bar{u_1}, \bar{u_2})$ plane. Provided that $\sigma_Y / k \geq \bar{Y}$, there is a unique solution with $\bar{u_1}$ and $\bar{u_2}$ greater than zero.

2.3 Are muscles fixed vectors in task space?

The smallest physiological structure that the CNS could use to control the net endpoint vector is the motor unit, consisting of one motoneuron in the spinal cord and the set of muscle fibers it excites. An elegant study by Westling and colleagues (1990) demonstrated that a single stimulation pulse applied to a single human motor

unit generated a straight force trajectory in a task plane perpendicular to the long axis of the thumb. These trajectories left the origin along a straight line, peaked in magnitude, and returned to the origin along the same straight line. These results suggest that motor unit mechanical action can be understood as fixed vector in an isometric task space.

The CNS likely does not send an individual command to every motor unit. Given feedback about the discharges of two motor units, humans generally can not make the stronger motor unit discharge while having the weaker motor unit not discharge (Fetz, 2007). Studies of discharge times from motor unit pairs reveal more synchronous discharges than would be expected by chance, likely indicating shared synaptic input (Sears and Stagg, 1976). Certain muscles do not have very different mechanical actions in some task spaces (An et al., 1983); thus in many cases there may not be an advantage to having motor units receive different commands.

However, what if a group of motor units, historically defined to be part of one muscle, did have different mechanical action vectors? If the activity of these motor units reflected their mechanical action, the CNS could tune the mechanical action vector for the muscle to generate force most efficiently for the given task vector. For example, the cat hindlimb muscle *biceps femoris* has three *neuromuscular compartments* that are innervated by separate nerve branches. The compartments have different mechanical functions (Chanaud et al., 1991) and are roughly used accordingly (Chanaud and Macpherson, 1991). This dissertation will be concerned with such a correspondence between motor unit mechanical action and activity even for muscles that are not thought to be compartmentalized.

The following sections review key findings about motor unit activity, and explores mechanisms that could change the mechanical action vector of a muscle.

2.3.1 Henneman Size Principle

Elwood Henemann's seminal work stressed that motoneuron size determines its recruitment threshold (Henneman et al., 1965b), and proposed that small and large motor neurons should receive equal synaptic input (Henneman et al., 1965a). He argued then that motoneurons controlling a particular muscle are recruited primarily on the basis of input resistance, an intrinsic property of motoneurons closely linked to motoneuron size (Loeb and Ghez, 2000). These findings have come to be known as the *size principle* of motor unit recruitment.

A rigid interpretation of the size principle would suggest that all the motor units of a given muscle would receive the same input regardless of differences in mechanical action direction among the units. The size principle would predict that one common descending command is provided to a group of motoneurons exciting a muscle (Figure 2.7). In general, smaller motoneurons would excite motor units that have smaller mechanical action magnitude. The input resistance of the motoneurons would dictate that, for the same descending command, the smaller motoneurons would be activated first. In this scheme for motoneuron recruitment, the controlled muscle would have one effective mechanical action direction; differences in motor unit mechanical action direction would not be exploited.

2.3.2 Differential tuning of motor units within a muscle

Though the size principal provides a general description of how motor units are recruited to do work in multidimensional task spaces (Thomas et al., 1986), the completeness of this theory has been questioned. For example, Desmedt and Godaux (1981) found that, in about 8% of the motor unit pairs examined in the human first dorsal interosseous, the activation order switched when the task direction

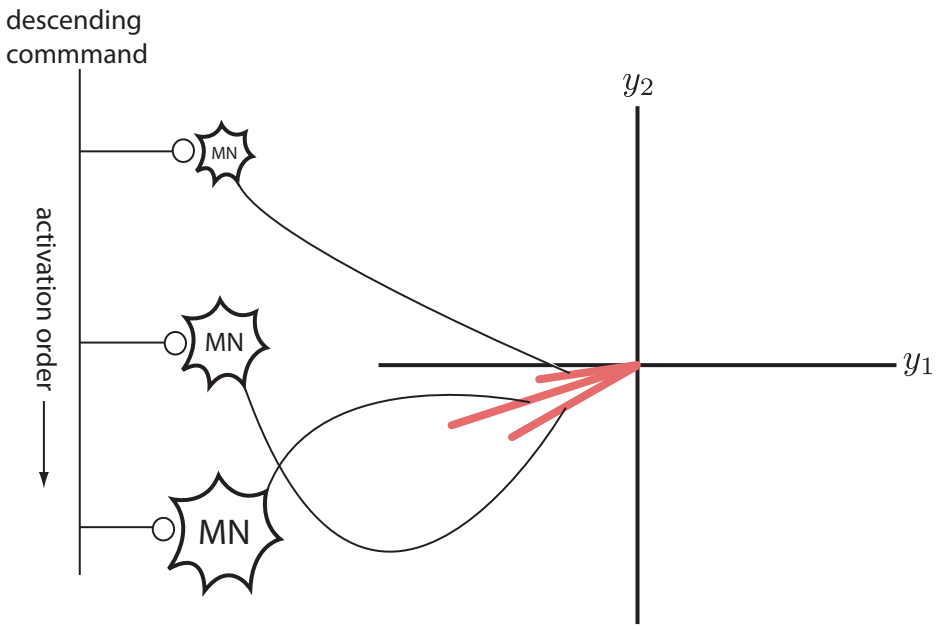

Figure 2.7: The size principle applied to motor units of a muscle in a 2-dimensional task space. Three illustrative motor units have differences in mechanical action and magnitude. The size principle states that a single descending command is distributed to all the motoneurons, so that motor units are activated in order of mechanical action magnitude. In this scheme, differences in mechanical action direction are ignored.

changed. ter Haar Romeny (1982; 1984) showed that the recruitment of motor units in the human biceps depends on direction; units located more laterally were recruited for flexion while those more medially were recruited for supination. Herrmann and Flanders (1998) showed that the activity of motor units in the human biceps could be described by a cosine function of the task direction. The task direction of peak activity varied substantially across the population of motor units studied, and did not appear to depend on the recording location. What did not appear in any of these studies was a thorough analysis of the mechanical action of the units studied.

2.3.3 Potential differences in mechanical action among motor units in a muscle

The first dorsal interosseous (FDI) is a popular model muscle because if its accessibility from the skin surface. It is generally considered to be one muscle be-

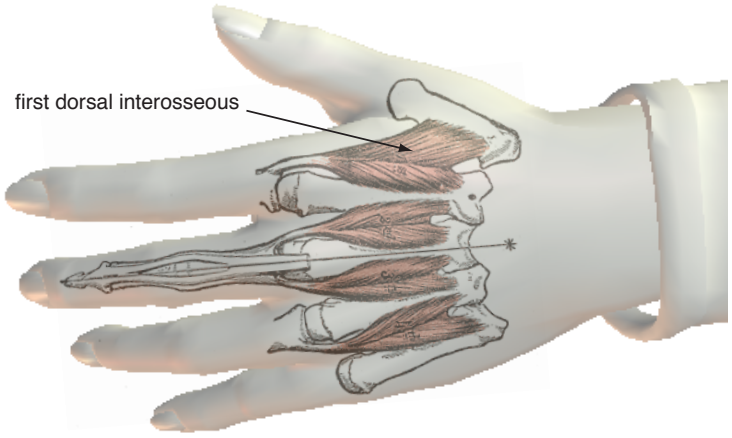

Figure 2.8: The human interossei muscles, reproduced from Gray's anatomy (public domain image).

cause of its anatomical structure (Figure 2.8), and evidence that different motor units in the FDI may receive some common inputs (Datta and Stephens, 1990; Deluca et al., 1993). It is know to exert abduction (away from the hand) torque about the metacarpophalangeal (MCP) joint of the index finger, as well as flexion (down toward the palm) torque about the same joint (An et al., 1983; Thomas et al., 1986). What is not known is whether different motor units within the FDI can generate mechanical action vectors having different directions.

Some preliminary support in favor of different mechanical action directions is provided by a careful analysis of spike-triggered averaging data (Thomas et al., 1986). This study estimated the relative force contribution of single FDI motor units to the abduction and flexion direction. The study presented this data on a log-log plot, which indicated a potential clustering of the estimates and a lack of different mechanical action directions among units (Figure 2.9a). However, when this data is re-plotted on linear axes as lines of action, a different picture emerges that suggests a 53° range of mechanical action directions among FDI motor units (Figure 2.9b).

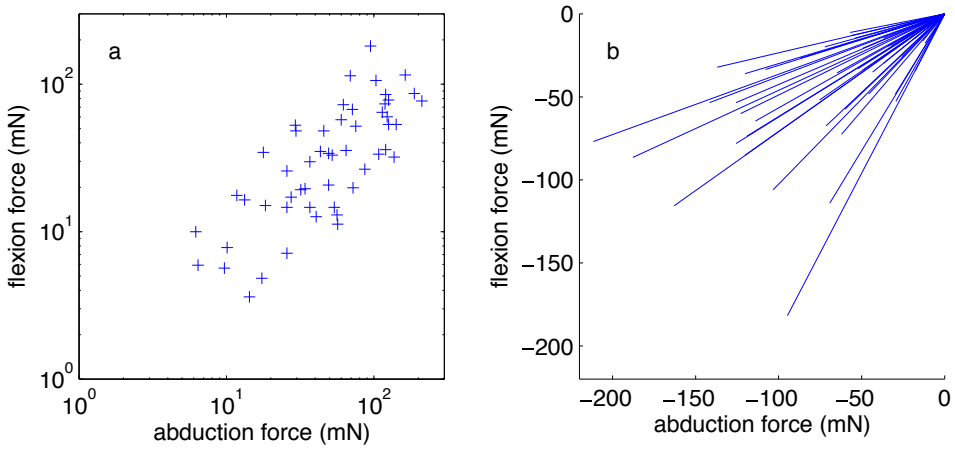

Figure 2.9: Mechanical action direction data from the FDI of Thomas et al. (1986) plotted in two ways. a. Data as presented in the article, which spike-triggered average estimated abduction and flexion force plotted on a log-log scale. b. The same data as in a, re-plotted as lines of action in a task plane with a linear scale.

If FDI motor units indeed have different action directions, it is conceivable that the CNS could set higher activity in a subset of the units with the most advantageous mechanical action.

2.3.4 Proposition: a direction principle of motor unit recruitment?

If motor units contained within a muscle exhibit differences in mechanical action direction, it is conceivable that the CNS might try and exploit these differences in an attempt to optimize motor function. The CNS could preferentially excite motor units that had mechanical action directions closer to the task direction (Figure 2.10). While the mechanical action direction of every motor unit would remain constant as the task changed, the effective mechanical action direction of the muscle as a whole would be expected to shift to align as closely as possible with the task direction. This work will examine movement unsteadiness looking for evidence of such a shift in muscle mechanical action direction.

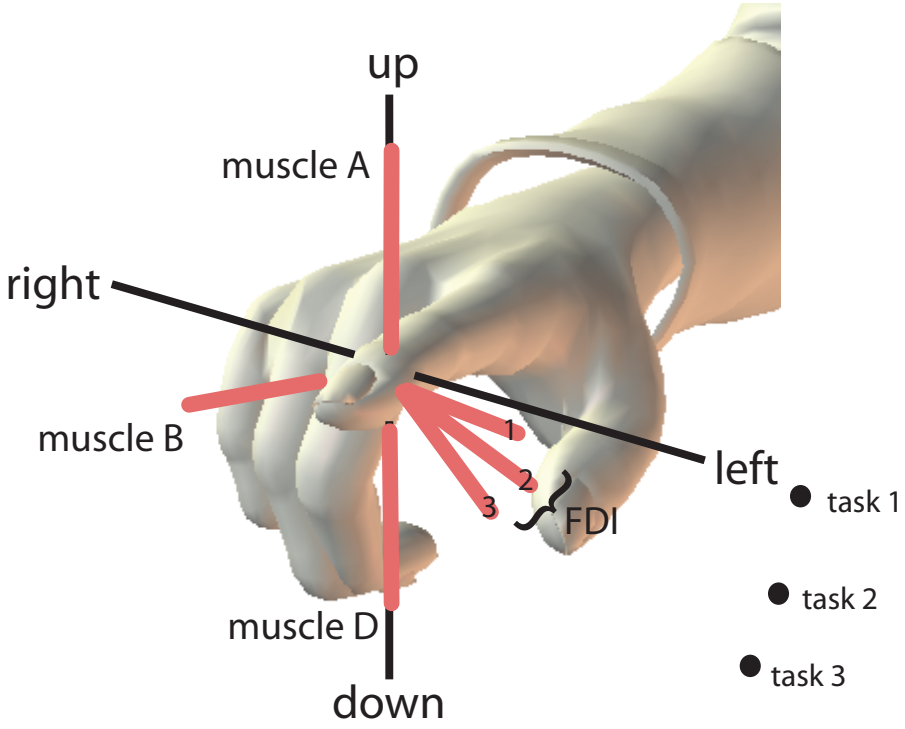

Figure 2.10: A direction principle of motor unit recruitment. If a muscle, such as the FDI, has motor units that have differences in mechanical action direction, then motor units similar to 1 might be preferentially active for task 1, motor units similar to 2 might be preferentially active for task 2, and motor units similar to 3 might be preferentially active for task 3. The effective mechanical action for the FDI would then be expected to shift as a function of task direction.

2.3.5 Proposition: nonlinear summation of force?

Another mechanism that could cause muscles not to be fixed vectors in task space is nonlinear summation of force. Nonlinear force summation can occur when application of one force deforms the structure used to transmit another force. To illustrate this concept, imagine a person pulling on an object with rigid rods in each hand versus elastic cords in each hand connected by a rigid rod (Figure 2.11). In the case of rigid rods, force exerted by one hand can not affect the direction of force exerted by the other. In the case of elastic rods, deformation in the structure induced by pulling with one hand will affect the direction of force exerted when the other

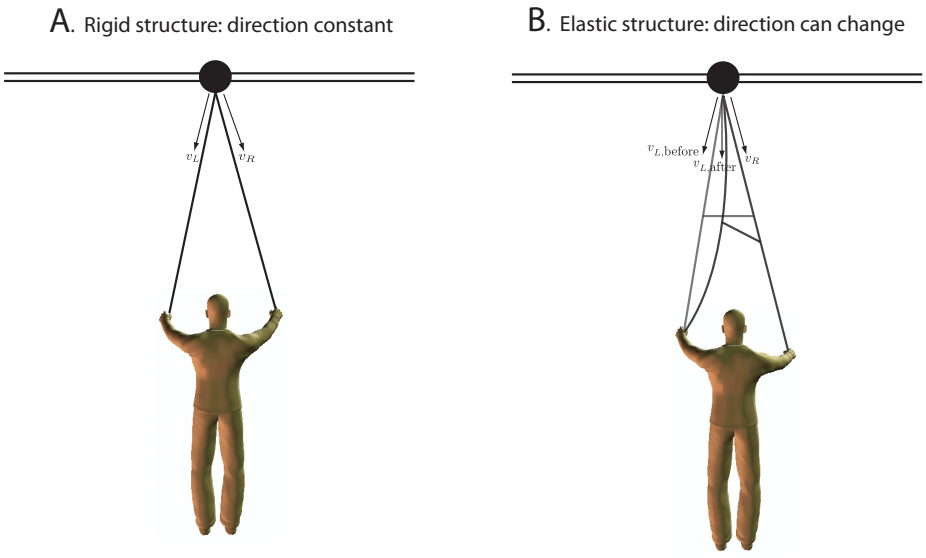

Figure 2.11: Principle of nonlinear force summation. Imagine a object (circle) that can slide in a track. A. If the person pulls on the object with two rigid links, the force exerted on the object by the left hand v_L can not affect the force vector exerted by the right hand v_R. B. Imagine that these links were not rigid, but could stretch but were connected by a rigid rod. Then the direction of force exerted by the left hand pulling $v_{L,\text{before}}$ could change direction to $v_{L,\text{after}}$ after the right link was pulled on and stretched.

hand pulls.

For many muscle systems, there may be compliant mechanisms in the transmission of muscle activity to endpoint force. One example is the finger extensor hood mechanism, which may be approximated by Winslow's tendinous rhombus (Winslow, 1732; Valero-Cuevas et al., 1998; Valero-Cuevas et al., 2007). With such a compliant network, activity of one muscle could affect the mechanical action directions of other muscles (Figure 2.12). Changes in activity among a group of muscles for changes in the task vector could then lead to muscle mechanical actions depending on the task vectors, i.e. not fixed vectors in task space. There are other mechanisms that could generate such effects, such as one muscle pulling on another (Sandercock, 2005).

Though this work will not deal with the exact biomechanical mechanisms, it will present evidence that the muscle mechanical action direction depends on task

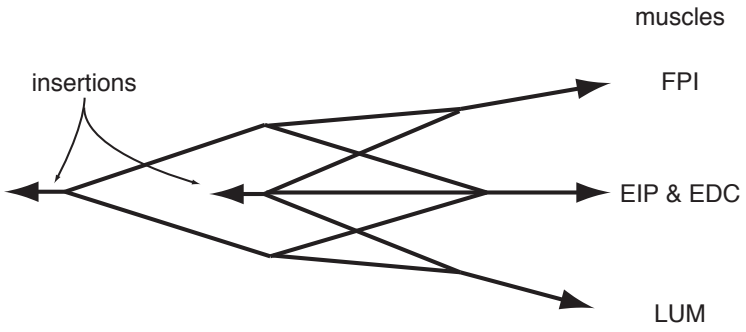

Figure 2.12: Winslow's tendinous rhombus - extensor hood model. Several index finger muscles insert into a compliant tendinous network, which transmits force to two insertion points on the index finger.

direction.

2.3.6 Example: using unsteadiness to determine muscle mechanical action

Unsteadiness in the net endpoint vector will lead to a trajectory in task space. If some measure of activity in a particular muscle is available, it can be used to extract sections of the net endpoint trajectory that likely contain a large contribution from the muscle. If these sections are averaged together, a mechanical action estimate can be constructed for the muscle of interest (Figure 2.13). This process is generally referred to a spike-triggered averaging (Buchthal and Schmalbruch, 1970; Stein et al., 1972). This dissertation will present rigorous equations describing this process, and then generalize to the case when muscle contributions are not considered discrete, yielding a process that is experimentally tractable for estimating muscle mechanical action for a variety of task vectors.

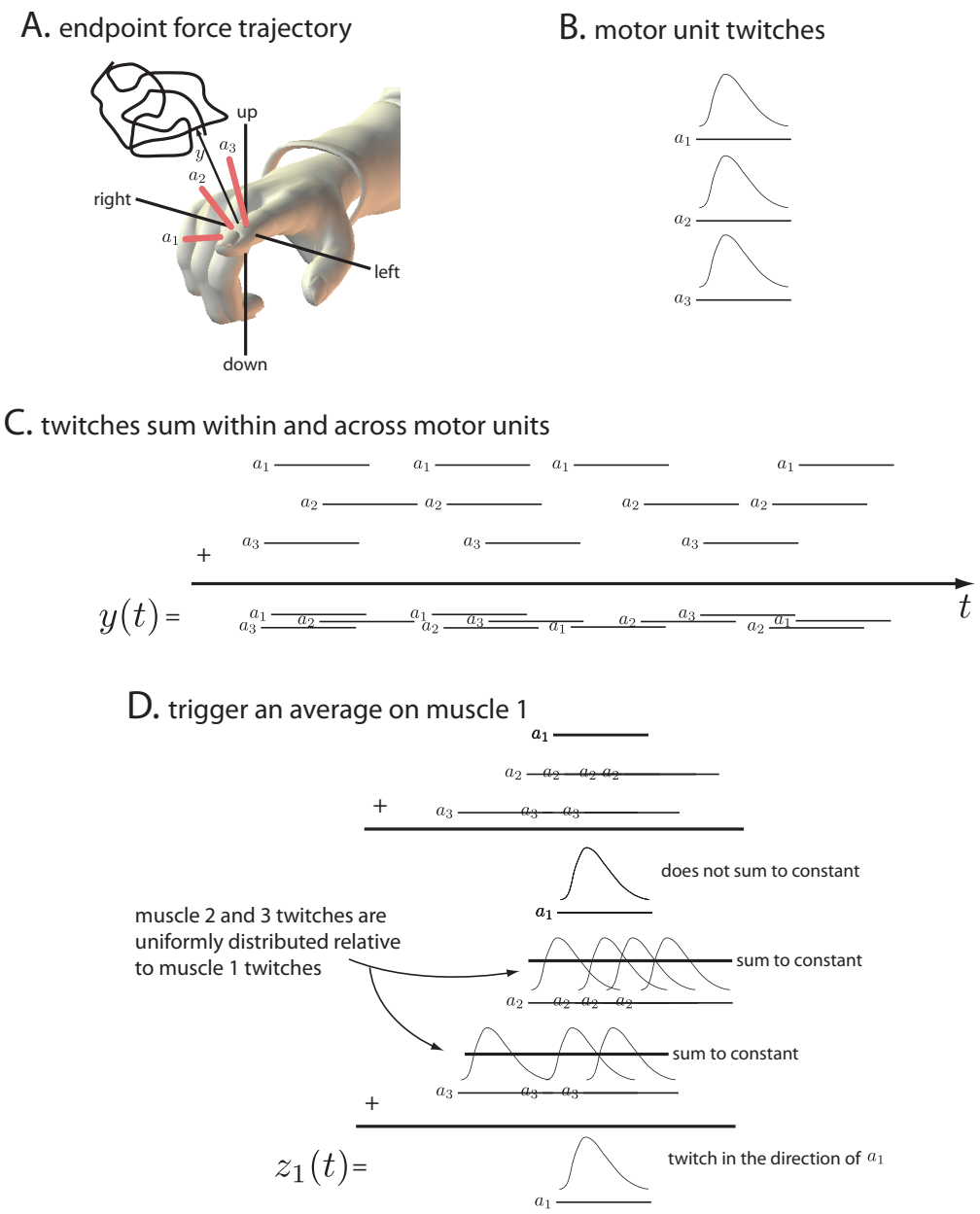

Figure 2.13: Example: using unsteadiness to determine muscle mechanical action. A. Three muscles are active for a particular task. Because of motor unsteadiness, the net endpoint vector Y moves along a random trajectory. B. When each muscle is active, it exerts a force with the time course shown in the direction of its mechanical action vector. C. Assume for simplicity that the contributions of the individual muscles sum to generate the net endpoint vector. D. Having knowledge of when muscle 1 is active, we can trigger an averaging process. Sections of $Y(t)$ are extracted around $a^{(1)}$ activity, and averaged. When the sections are added together, the contribution from $a^{(1)}$ is always in the same position, but contributions from other muscles may be distributed randomly around $a^{(1)}$. When the contributions are randomly distributed, they will sum to a constant. The resultant average, denoted $z^{(1)}(t)$ will have a time course the reflects the time course of muscle 1, and will a direction that reflects muscle 1's mechanical action.

2.4 Appendix

Here we show mathematically that muscle redundancy is a fundamental feature resulting from the fact that muscles only generate tension. We assume that the muscle mechanical action vectors are the columns of a matrix A, and that the net endpoint vector Y is generated by taking linear combinations of the columns of A: $Y = Au$.

Definition II.1. The nonnegative linear span of a linear transformation A is the set of vectors Au where $u \in R^m[0, \infty)$, and is denoted nlspan(A).

If the complete task space has dimension d, than nlspan$(A) = \mathbb{R}^d$ if all tasks in the space are doable. We need to determine the minimum number of muscles necessary to meet this condition. Clearly, d muscles are not enough, because muscles are constrained to only pull.

The next definition involves an important concept related to the nlspan of a transformation, and shows essentially when a set A will "open up" and span the space it lives in under nonnegative linear combinations.

Definition II.2. Let A be a set of $d + 1$ vectors in $\mathbb{R}^d$. Let $A^{(j)} = A - a^{(j)}$ (i.e. $A^{(j)}$ is a subset of A formed by removing the jth column). A is *noncollapsing* if $a^{(j)} \in$ nlspan$(-A^{(j)})$ for all j.

Lemma II.3. *If A is noncollapsing in $\mathbb{R}^d$, then* nlspan$(A) = \mathbb{R}^d$.

Proof. Since A is noncollapsing, then it must have d vectors $a^{(1)}, \ldots, a^{(d)}$ that are linearly independent in the standard sense. Furthermore, since A noncollapsing implies that

$$a^{(d+1)} = -(b_1 a^{(1)} + \cdots + b_d a^{(d)}) \tag{2.5}$$

with $b_j \in \mathbb{R}(0, \infty)$ for all $j = 1, \ldots, d$. This is equivalent to $a^{(n+1)} \in \text{nlspan}(-a^{(1)}, \ldots, -a^{(d)})$. Consider now a vector v such that $v \in \text{nlspan}(A)$. This means that

$$v = u_1 a^{(1)} + u_2 a^{(2)} + \cdots + u_d a^{(d)} + u_{d+1} a^{(d+1)} \tag{2.6}$$

We then substitute the expression for $a^{(d+1)}$ from Equation 2.5 into Equation 2.6 and find that

$$v = (u_1 - u_{d+1} b_1) a^{(1)} + \cdots + (u_d - u_{d+1} b_d) a^{(d)} \tag{2.7}$$

Let $g_j = u_j - u_{d+1} b_j$. The product $u_{d+1} b_j$ is a nonnegative number which is set for each j once u_{d+1} is chosen. However, we form g_j by adding a positive number *dvecuj* (that we can choose for each j to be as large as we like) to $u_{d+1} b_j$. It follows then that g_j can be controlled independently and all j. Therefore, since $a^{(1)}, \ldots, a^{(d)}$ are linearly independent in the standard sense, it follows that v can be any vector in $\mathbb{R}^d$. Since $v \in \text{nlspan}(A)$, it follows that $\text{nlspan}(A) = \mathbb{R}^d$. □

This shows that there is a set of $d + 1$ vectors that span $\mathbb{R}^d$ with nonnegative weighting coefficients. If the task space is d dimensional, it must have at least $d + 1$ muscle mechanical action vectors to make all tasks feasible, thus and task space chosen to be a subspace must have more muscles than dimensions.

CHAPTER III

Neuro-motor control strategies appear in endpoint force fluctuations

3.1 Abstract

How the nervous system activates multiple redundant muscles to achieve a specified task is a long-standing question in motor neuroscience. We used a novel approach to investigate this question by studying the net endpoint vector fluctuations during isometric force generation at a multi-degree-of-freedom joint: the metacarpophalangeal (MCP) joint of the human index finger. We made high-gain measurements of time-varying forces generated during ramp-and-hold tasks to different magnitudes and directions in the abduction-adduction/flexion-extension plane of the index finger. For each task, we calculated the force covariance between the abduction-adduction and flexion-extension components; this covariance could be visualized as an ellipse in the task plane with center at the magnitude and direction of the task. Two types of force covariance ellipses were observed: some task directions exhibited narrow ellipses with principal axis aligned to the task direction, while other task directions showed broad ellipses without clear directional alignment. Task directions containing narrow ellipses appeared to be aligned with estimated mechanical action directions of key muscles acting at the MCP joint. For example, an average of 90% of force variance was confined to the task direction when the direction was aligned with the

likely action direction of the first dorsal interosseous (FDI). It follows the FDI is likely a prime mover in this direction, and that at most 10% of the force variance could be explained by fixed coupling between the FDI and other muscles pulling in different directions. In contrast, other task directions exhibited broader ellipses that were not well-aligned with the task direction, with as little as 30% of force variance confined to the task direction. In these task directions, the cooperation of multiple muscles with distinct action directions is likely, and was supported by electromyographic recordings from relevant forearm and hand muscles. It follows that net endpoint vector fluctuations reveal multiple neural control strategies for muscle action at a multi-degree-of-freedom joint.

3.2 Introduction

When controlling multiple degrees-of-freedom (DOF) of the body, there are typically many different muscle combinations that the CNS can utilize to achieve a desired task (Bernstein, 1967). To simplify task control, it has been proposed that the CNS enforces fixed activation ratios (synergies) among multiple muscles acting at the involved DOF (d'Avella et al., 2003; Saltiel et al., 2001; Ting and Macpherson, 2005; Tresch et al., 2006). Alternatively, the CNS could tune muscle commands so that movement is optimized according to some suitable performance criteria (Buchanan and Shreeve, 1996; Harris and Wolpert, 1998; Todorov and Jordan, 2002).. It is also unclear whether some tasks are controlled by a "prime mover" muscle (Thomas et al., 1986), or whether all tasks involve the cooperation of multiple muscles (Buchanan et al., 1986; Keenan et al., 2006). These questions remain unresolved, in spite of multiple attempts to characterize muscle activation patterns across multiple DOF.

To date, most studies that have investigated muscle coordination across multiple

DOF have focused on the use of electromyographic (EMG) recordings. While such EMG recordings provide invaluable information about muscle activity, they offer significant disadvantages for studying muscle coordination in multiple muscle systems. First, EMG studies of muscle coordination require that recordings be made from each muscle that potentially contributes torque to the DOF of interest, a potentially difficult assignment. Second, the EMG-force relation remains undetermined at present for many muscles, since the relation depends critically on how mechanical and electrical motor unit properties are coupled (Zhou and Rymer, 2004). EMG assessments may either overestimate or underestimate muscle force (Zhou et al., 2007), which complicates the interpretation of muscle coordination studies based on EMG. Third, the identification of muscle-level synergies using EMG signals from multiple muscles may be complicated by the existence of biomechanical or neural constraints unrelated to muscle synergies (Saltiel et al., 2001).

An alternative approach to studying muscle coordination involves mapping isometric net endpoint vector variability for an array of tasks distributed uniformly across the task space. Stochastic effects may enter such tasks in several ways, but one of the most significant is signal-dependent noise, where isometric force variability increases with average isometric force. Such signal-dependent noise may arise from the properties of the motoneuron pool (Jones et al., 2002). If muscle force variability increases with average muscle force, then differing neuro-motor control strategies can generate different patterns of net endpoint vector variability. For example, one muscle acting alone will induce variability that not only increases with signal magnitude but is also directionally aligned with the muscles action direction in task space. Alternatively, cooperation among multiple muscles, each with different action directions, will induce net endpoint vector variability that reflects the multiple directions

of muscle pull. It follows that the overall net endpoint covariance caused by a muscle synergy will be composed of individual covariances from the constituent muscles, but will not be aligned with the covariance of any one muscle.

In light of these possibilities, the aim of the present study was to demonstrate, using multidirectional tasks performed by the human index finger, that the covariance of multidirectional isometric force exhibits significant differences as a function of task direction. Furthermore, we argue that such force covariance maps provide strong clues about the ways in which the nervous system controls muscle combinations or synergies, acting about multiple DOF.

3.3 Methods

We developed a method to use the variability of isometric forces exerted by the index finger as an indicator of underlying muscle coordination. The method uses the pattern of this force variability as a function of task direction and magnitude, termed the force covariance map, to quantify the relative amount of variability that occurs in the task direction itself, termed the task-directed variance fraction η. Muscle coordination strategies may constrain how η varies with the tasks direction. Below we describe the theoretical basis for the force covariance map, our means of experimentally measuring it, and the techniques used for relating the force covariance map to muscle action direction and activity.

3.3.1 Force covariance mapping (FCM)

The variability of the net endpoint vector will likely be influenced by how muscles are activated. In the present study, we define the task as the exertion of isometric forces by the tip of the index finger (i.e., the endpoint), with a specified direction and magnitude in the plane perpendicular to the finger. We define the axes of this

plane as flexion-extension and abduction-adduction, corresponding to vertical and horizontal forces, respectively, when the palm of the hand faces down. We define the force directions in this way purely for ease of reference, recognizing that the physical flexion-extension and abduction-adduction axes of the MCP joint are not orthogonal (Kamper et al., 2006). The relation between the pattern of net endpoint vector variability – the force covariance map – and hypothetical muscle coordination is based on three principles of muscle force production: linear superposition, signal-dependent noise, and at most modest correlation of forces among muscles. When these principles apply, the force covariance map may be used to study muscle coordination and muscle synergies.

Linear superposition provides a means to examine muscle coordination in task space. Superposition is the assumption that the net endpoint vector is the linear sum of individual contributions of force from each muscle. These individual contributions occur along directions in the task space, or muscle action directions (illustrated hypothetically in Figure 3.1A) that depend on the musculoskeletal geometry, for example the lengths of body segments and moment arms about the degrees of freedom of joints (Kuo, 1994; Kuo, 2000). Action directions have been empirically quantified for cat hindlimb muscles contributing to multidirectional ankle force (Lawrence et al., 1993), monkey forearm muscles contributing to multidirectional wrist force (Hoffman and Strick, 1999), and human thenar motor units contributing to thumb abduction and flexion (Westling et al., 1990). Superposition does not always apply, for example if a single muscle also pulls on neighboring muscles. However, these effects are usually small, even among motor units within a muscle (Sandercock, 2005), and are assumed negligible in the present study.

Signal-dependent noise will induce variability in endpoint forces, dependent on

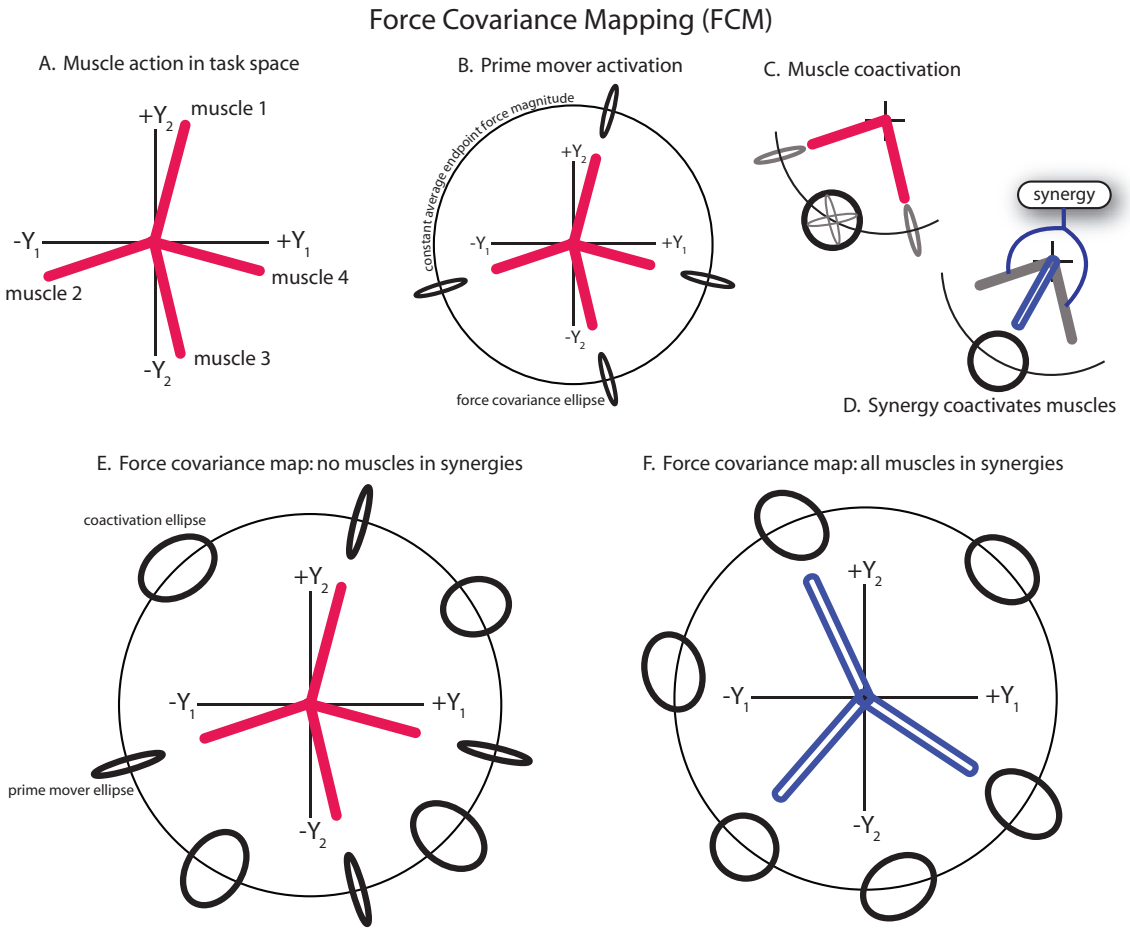

Figure 3.1: Conceptual basis for force covariance mapping. A. Muscles have biomechanical actions in task space, represented hypothetically as action directions in the task space of isometric abduction/adduction (Y_1) and flexion/extension (Y_2) forces exerted by the index finger. B. Activation of single muscles as prime movers will generated an average force vector in task space, with force covariance largely aligned with the muscles action direction. Four such covariances are illustrated. C. Two or more muscles may be coactivated, for example, to generate a force with direction between the individual muscle action directions. Coactivation produces a much broader covariance, representing the combined covariance of the individual muscles (see APPENDIX). D. If the average activations of multiple muscles are constrained by a synergy, a new effective synergy action direction is generated, but the corresponding covariance will be similar to the case of muscle coactivation. E-F. Constructing the force covariance map involves measuring the net endpoint vector covariance across an array of tasks around circles of constant average net endpoint magnitude. E. If muscles are not in fixed ratio synergies, both prime mover and coactivation force covariance ellipses may be observed. F. If all muscles are in fixed ratio synergies, only broad coactivation force covariance ellipses may be observed.

muscle action directions and how muscles are coordinated. We consider first the hypothetical case of muscles activated as prime movers, when the task direction is aligned with a particular muscles action direction. The endpoint force would be expected to fluctuate (e. g., (Galganski et al., 1993; Thomas et al., 1991)) with force variability increasing with activation magnitude (e. g., (Jones et al., 2002; Moritz et al., 2005)). The force covariance may be thought of as an ellipse, expected to align well with task direction (Figure 3.1B). We next consider the more typical case where muscles are activated together, for example to produce a force directed between the two individual muscle action directions. The individual muscle covariances then approximately add together to determine the total force covariance, provided that noise-like fluctuations in the individual muscle forces are relatively uncorrelated. The force covariance ellipse will then be aligned with neither muscle action (Figure 3.1C). A muscle synergy combines multiple muscles together (Figure 3.1D), and will therefore produce a covariance ellipse in the direction of synergy action that is the same covariance as the co-activation case.

The force covariance map is a set of force covariances measured at equally spaced points around a constant average net endpoint magnitude. A force covariance map when no muscles are in synergies may contain two types of force covariance ellipses: narrow ellipses aligned with the task direction in directions of muscle pull indicating muscles behaving as prime movers, and broad non-aligned ellipses in directions involving coactivation of multiple muscles with different action directions (Figure 3.1E). Alternatively, if all muscles are grouped into synergies with muscles having different action directions, only coactivation ellipses will be observed, because multiple muscles will always contribute in some fixed amount (Figure 3.1F).

Our analysis thus far is based on the assumption that muscles have uncorre-

lated force fluctuations. This assumption is a concern because, for instance, very highly correlated force fluctuations between two antagonistic muscles would cancel from the measurable net endpoint vector variance, hiding their activation from the force covariance map. Although we are not aware of any direct measurements of correlation in force between muscles, two lines of research support our assumption that correlation will not strongly affect inferences about muscle coordination made from the force covariance map. First, coherence between EMG pairs has been shown to be modest (¡10%) at low frequencies, with higher values (30-50%) only in upper frequencies of 15 30 Hz (Farmer et al., 2007; Fisher et al., 2002; Kilner et al., 1999). Second, joint force only contains significant signal in the 6-12 Hz range due to unfused motor unit twitches, but relatively little signal at higher frequencies due to the time course of muscle contraction (see (Galganski et al., 1993)). Therefore, even if there is significant coherence in muscle electrical activity, it occurs at frequencies unlikely to produce significant muscle forces. We will return to the potential effects of muscle force correlation in the DISCUSSION.

3.3.2 Experimental methods

We experimentally measured the force covariance map for endpoint forces produced by the metacarpophalangeal joint of the human index finger. We also measured surface EMG from three muscles to compare with the force covariances and also to form rough estimates of muscle recruitment curves and action directions. Seven unimpaired subjects (2 female, 5 male) participated in the study. All subjects were right-handed, and used their dominant index finger to produce isometric forces in different directions and magnitudes in the flexion-extension/abduction-adduction (FEAA) task space. The Northwestern University Institutional Review Board approved the study protocol, and informed consent was obtained from each subject

prior to participation.

The experimental apparatus was designed to mechanically isolate the index finger (Figure 3.2). Subjects were seated upright in an adjustable chair with the shoulder abducted approximately 15° with the elbow resting on a padded support. The elbow joint was flexed to 90°, and the forearm was casted and secured in a plastic orthosis, in a pronated position with the palm facing down. The index finger was casted and placed in a fixed cylindrical tube, so that forces were exerted against the inside of the tube and about an "endpoint" just distal to the DIP joint. These forces were transmitted to the tube by 3 screws 120° apart that centered the finger in the tube. The screws were gently pushed into the cast while it hardened, making a secure but comfortable connection with the index finger. One subject repeated the experiment with the screws rotated to different positions relative to the finger, and it was found that the screw positions did not affect the results. This setup maintained both interphalangeal joints extended and approximately aligned the MCP extension axis with the vertical load cell axis. Digits 3-5 were secured in a resting position that was slightly adducted away from the index finger. The thumb was abducted to 50° and casted with the wrist. One Velcro strap was placed around the subjects waist, and two Velcro straps were placed in a criss-cross fashion over each shoulder to restrain the subject and to minimize shoulder movement.

Isometric index finger forces in the FEAA plane were measured using a sensitive 6 axis load cell (JR3, Woodland, CA, Model 20E12A-I25 9N.5). The index finger exerted forces on one end of the tube, and the other end transmitted and amplified these forces to the load cell. The length of the tube (10 cm) was designed to amplify potentially small endpoint forces, and to allowed them to be recorded by both translational forces and rotational moments on the load cell. We estimated the load

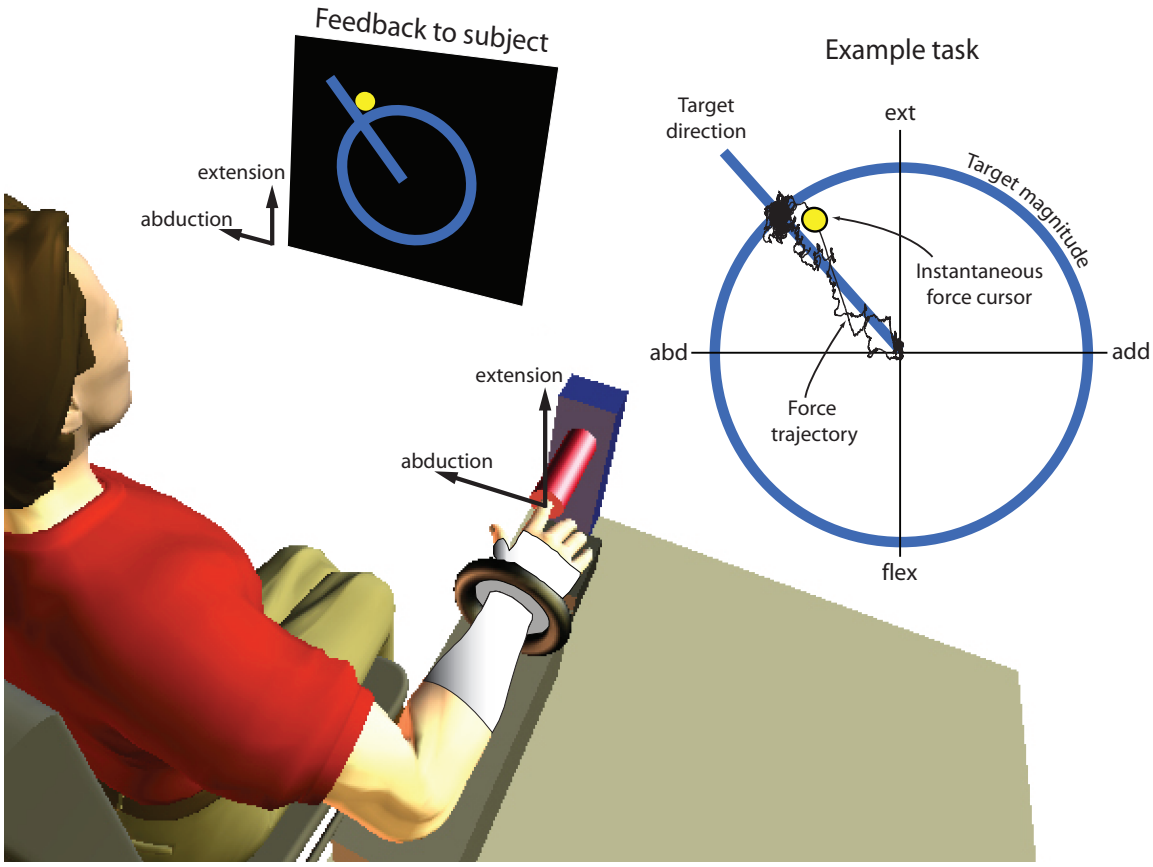

Figure 3.2: Experimental setup for measuring isometric forces exerted by the index finger. The subject is configured with the shoulder abducted approximately 15°, and the elbow flexed to 90° and positioned in full pronation. The wrist is immobilized with rigid casting tape and secured within a fixture. The right index finger is similarly immobilized and secured just distally to the distal interphalangeal joint, connected to a 6 degree-of-freedom load cell through a rigid tube. Visual feedback of abduction-adduction (left-right direction) and flexion-extension (down-up) forces is displayed to the subject on a computer screen, with instantaneous force and the task direction and magnitude displayed in polar coordinates. The subject exerts forces to move the cursor towards the target force. The example shows the force trace recorded over a trial.

cell's resolution (smallest measurable force) to be 1 mN. These forces were also presented visually to subjects in real time. We displayed a dynamic cursor representing the instantaneous two-dimensional force in the FEAA plane (see 3.2) on a computer screen. Forces were recorded at 1000 Hz.

We also recorded surface electromyograms (EMG) from several finger muscles, so that EMG activity regions could be compared with force covariances. EMGs were recorded using miniature electrode/preamplifiers (DELSYS, Boston, MA) with 2 silver recording surfaces, 5 mm long and 10 mm apart. The preamplifiers have bandwidth 20-450 Hz for surface recordings, with gains set to 100. EMG electrodes were placed according to standard anatomical landmarks and verified with the recommended test maneuvers (Perotto, 2005). EMG signals were sampled at 2000 Hz.

EMGs were recorded from the first dorsal interosseus (FDI), extensor digitorum communis (EDC), and extensor indicis proprius (EIP), but not in all subjects. EMG activity was recorded from the FDI in six subjects. Additional activity was recorded from the EDC in three of these subjects, and the EIP from the other three. We used the EMGs to estimate recruitment curves as a function of task direction and to estimate muscle action directions. These were then compared qualitatively to force covariance results. We found the small number of subjects acceptable for such qualitative comparisons. The experimental protocol called for the exertion of endpoint forces in 24 different directions and at 3 different magnitudes. The directions were generally distributed equally over the plane at 15° increments. One subject performed a slightly different protocol, with tighter distribution between pure abduction and pure flexion, but the same number of directions overall. A rest trial was collected for each subject to establish EMG baseline levels. For each trial, the subject viewed the desired force as a target on the visual display (Figure 3.2), represented in polar

coordinates by a static ray for target direction, and a static circle for target magnitude. The subject was instructed to gradually exert force in the target direction, and then to hold the target force as precisely as possible for about 10-20 seconds. The experimenter examined the time-domain force traces on-line. Trials were repeated if forces were found not to be approximately constant. The force feedback display was zeroed, with the subject at rest, before each set of trials. Subjects were asked to rest for at least ten seconds between each trial, and at least one minute after each group of ten trials.

The force magnitudes were also equally distributed at three levels, chosen to require very minimal effort for all subjects. Because these magnitudes were at discrete levels, we refer to them as task levels 1 - 3. These task levels were distributed at equal intervals, with the highest magnitude level, task level 3, at approximately 2 N in magnitude.

3.3.3 Data analysis

The experimental data were analyzed to quantify net endpoint vector variability, to determine regions of activity in task space for key muscles, and to estimate the action direction of these muscles.

Quantifying force variability

We used measured forces to compute force covariance maps. We first cropped each trial to isolate relatively constant forces of at least 10 sec duration (Figure 3.3A). The time series forces, Y_{AA} in the adduction-abduction direction and Y_{FE} in the flexion-extension direction, were combined in a vector time series Y. The empirical task force vector Y_{T} was defined to be equal to the average force vector $\bar{Y}$, with $\hat{Y_{\mathrm{T}}}$ defined as the unit vector in that direction. Task direction can also be expressed as an angle

θ in task space, measured counter-clockwise from the adduction axis. To reduce the voluntary contribution to force variability, we filtered both force components (Figure 3.3B) with a zero-phase-lag 8th order Butterworth band-pass filter with -3 dB cut-offs at 5 and 30 Hz (Filter Design and Analysis Toolbox of MATLAB, Mathworks, Natick MA). We found substantial voluntary contribution below 5 Hz, and non-physiological noise above 30 Hz. Experimentation with cutoff frequencies showed that they did not qualitatively change the results. Filtered force data $\tilde{Y}$ were then used to compute the force covariance (Figure 3.3C-E). The covariances, plotted as ellipses centered at the mean task force for each trial, comprise the force covariance map (Figure 3.3F).

To determine if net endpoint vector variability could be used as an indicator of muscle activity, we examined net endpoint magnitude variability for signal-dependent noise. Signal-dependent noise should manifest itself in recordings of multidirectional force variability as a scaling of variability as a function of task magnitude level (see APPENDIX). We tested this hypothesis by computing the total variance of force as the trace of the force covariance matrix. The total variance was averaged across all task directions for each task level and subject. Within each subject, the total variance was normalized by dividing by the total variance of task level 1. A linear regression analysis was performed (regress in MATLAB) using the equation Normalized total variance $= a * (\text{Task level}) + b$, where a and b were coefficients to be determined. We quantified the degree to which the covariance for each trial was aligned with that trial's task direction. The task-directed variance fraction η was defined as the fraction of the total variance (in both force components) that occurs in the task direction (Figure 3.3G). η is 100% if force fluctuates only in the task direction, 50% if it fluctuates equally in all directions, and 0% if it fluctuates entirely

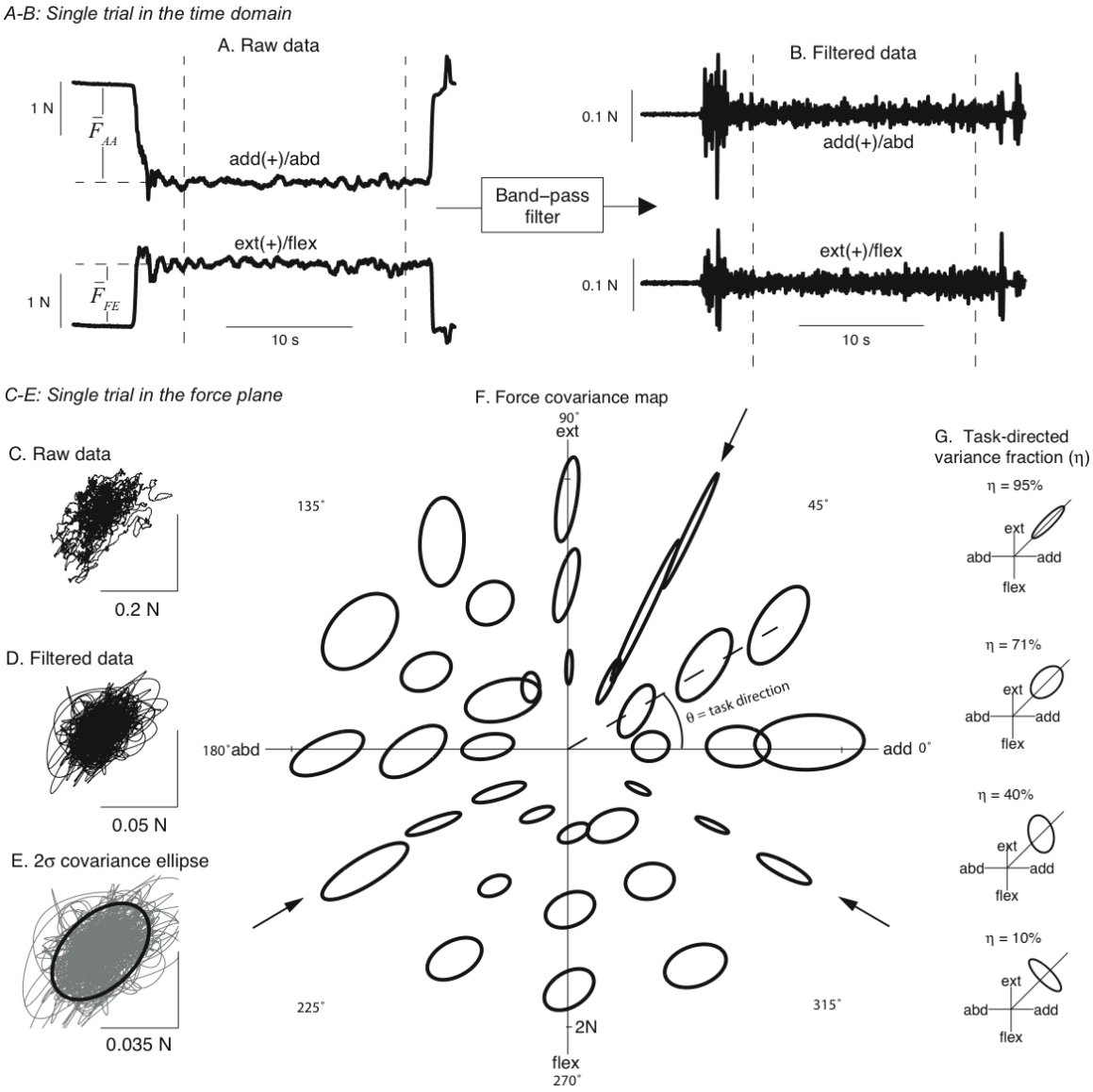

Figure 3.3: Construction of force covariance map with representative data. A. Raw force traces in abduction/adduction and flexion/extension. Subjects produced ramp-and-hold forces to a specified magnitude and direction, holding for between 10 and 20 seconds. B. Noise-like fluctuations were emphasized by filtering data (passband 5 - 30 Hz) to de-emphasize both high-frequency noise and low-frequency oscillations associated with voluntary drive. C. Raw force fluctuations, plotted in the abduction-adduction/flexion-extension plane. D. Band-pass filtered force fluctuations. E. Covariance of force variability, plotted as a two standard deviation ellipse, representing the data covariance matrix. Note that data are plotted in an expanded scale relative to D. F. Covariance ellipses plotted for every trial from one representative subject. The center of the ellipse indicates the average force vector produced during the trial; the task direction θ is the angle between the average force vector direction and the adduction axis. The ellipses are magnified by a factor of 25 for visualization. G. Alignment between ellipse and task direction is quantified using the task-confined variance fraction *eta*, the fraction of total variance that occurs in the direction of the task. Various hypothetical force covariance ellipses are shown along with the corresponding η value, where the diagonal ray indicates the task direction.

in a direction orthogonal to the task. We refer to the covariance matrix of filtered data as $\mathrm{cov}[\tilde{Y}]$, and define η as

$$\eta = \frac{\hat{Y_{\mathrm{T}}}^{T} \mathrm{cov}[\tilde{Y}] \hat{Y_{\mathrm{T}}}}{\mathrm{Trace}\left(\mathrm{cov}[\tilde{\mathrm{Y}}]\right)} \tag{3.1}$$

Assuming that correlation between forces generated by different muscles is modest, and that the dependence of force noise on signal is similar for different muscles, the task-directed variance fraction can be used as a bound on synergistic behavior among muscles. Suppose that the force covariance map exhibits task directed variance in a muscle A's action direction. If $\eta = 0.90$ in this task direction, then at most 10% of the force variance is generated by the combined effect of muscles acting in different directions than muscle A. Such a relatively low contribution to force variability from muscles in other direction would suggest that muscle A is not strongly synergistically linked to muscles that act in different directions. $1 - \eta$ is an upper bound on synergistic behavior because muscle A may contain motor units with slightly different mechanical actions, thereby generating variance outside the task direction without any synergistic coupling with other muscles. Statistical regularities in the force covariance map were quantified using a one-way ANOVA of the task-directed variance fraction using task direction as the factor. Task direction θ, was a continuous variable. In order to make it a discrete factor for ANOVA analysis, task direction was put into 15° bins. 15° bins were the natural choice for discretization because it was the increment of target directions presented to the subject. A post-hoc multi-comparison test with Bonferroni correction was performed to determine which groups exhibited significant differences. Task directions with statistically significant peaks in η were determined using the post-hoc test. The post-hoc test then revealed contiguous task direction sets for which η was significantly less than the peak η values. This analysis

revealed regions of task space that did not contain task-directed variance, and these regions were compared with regions of coactivation between muscles with distinct action directions.

Regions of muscle activity in task space

Muscle recruitment curves were computed from EMG data and plotted as a function of task direction. Raw EMG traces were first rectified and averaged across the hold period of each trial and the corresponding rest period, with the difference between the two serving as the net EMG. We fitted a cosine tuning curve (Hoffman and Strick, 1999; Todorov, 2002) to net EMG data within each subject and task level (24 values for each task level), minimizing the sum-squared error. The EMG data for each task level and subject were then normalized to the maximum of the fit, thus avoiding normalization to a spurious maximum in the data. Once the EMG data were normalized, comparisons of directional tuning could be made across task levels and subjects. A single cosine tuning curve was fit to the normalized data grouped across subject to produce a single curve representing a region of muscle activity in task space for each muscle studied. These curves were compared with features of the force covariance map.

Estimates of muscle action direction

Muscle action directions specific to our experimental setup were estimated with a cross-correlation of force and EMG data. This is a generalization of the spike-triggered averaging method, normally applied to single motor unit EMGs, to surface EMGs. Spike-triggered averaging correlates intramuscular EMGs to a single motor unit's spike waveform to yield spike times, and then correlates spike times with endpoint force yielding an estimate of a single motor unit's mechanical action. Our

method correlates surface EMGs directly with endpoint force to yield an estimate of a muscle's action direction. Referring to muscle i's EMG time series (normalized to its mean) as $E_i[n]$ with n for discrete time, the cross-correlation $z^{(i)}[n]$ is defined as

$$z^{(i)}[n] = \sum_j Y[j+n]E_i[j] \tag{3.2}$$

where the sum was computed across the hold period of each trial. The action direction estimate α_i was derived by computing the direction of the average vector $\overline{z^{(i)}[n]}$ over a range of time shifts between force and EMG (EMG and force simultaneous to EMG leading force by 100 milliseconds). α_i is the direction of change for isometric force when the rectified EMG in muscle i is increasing, averaged across the hold period. When $E_i[n]$ is a spike train, the above process reduces to spike-triggered averaging. We have recently shown on theoretical grounds that the direction of α_i may accurately represent muscle mechanical action despite the fact that $z^{(i)}[n]$ may not accurately represent the muscle activation magnitude or time course (Kutch et al., 2007).

Action direction estimates, specific to our experimental setup, were constructed as follows for the first dorsal interosseous (FDI), extensor digitorum communis (EDC), and extensor indicis proprius (EIP). For each muscle i, a polar histogram of α_i was constructed across all subjects and task directions in 15° bins. The peak of this distribution was taken as the action direction estimate for muscle i. For muscles that we did not record EMG from, we estimated action directions from moment arm data in the literature. We used published data for index finger muscles derived from MRI data (Fowler et al., 2001), for finger postures that corresponded to the posture used in the present study. The literature estimates were: flexor digitorum profundus (FDP) 296.5°, flexor digitorum superficialis (FDS) 292.7°, first lumbrical (LUM) 247.9°, and first palmar interosseous (FPI) 347.5°.

3.4 Results

A representative force covariance map measured from a single subject during a single session is shown in Figure 3.3F. Though the force covariance ellipse structure varies smoothly as task direction changes, the ellipses fall into roughly two categories. Certain task directions (indicated by arrows in Figure 3.3F) exhibit force covariance ellipses that are relatively narrow and have their principal axes relatively well-aligned with the task direction. We will refer to these as task-directed ellipses, because they have high task-directed variance fractions (η). Based on the theoretical framework for force covariance mapping developed in Section 3.3, we suspect that task-directed ellipses reflect control by a prime mover muscle. In contrast, intermediate task directions exhibit broad covariance ellipses without clear directional alignment. We will refer to these as non-task-directed ellipses, because they have lower η-values. Based on our theoretical framework, we suspect that non-task-directed ellipses are reflective of cooperation among multiple muscles with different action directions.

We wanted to determine if η varied significantly as a function of task direction, if similar force covariance map features were consistently found in multiple subjects, and if the covariance map features could be related to estimates of muscle activity and action direction. Task directions having task-directed ellipses should correspond to directions of muscle action if these covariance ellipses reflect control by a prime mover muscle. Task directions non-task-directed ellipses should correspond to directions where the cooperation of multiple muscles can be supported by EMG data. We first define the activity and action direction for 3 key muscles likely contributing force to the endpoint, and then show how these relate to the force covariance map.

3.4.1 Regions of muscle activity and directions of muscle action

The goal of our EMG analysis was to determine likely task direction ranges of significant activity for the FDI, EIP, and EDC, and to also make an estimate of the action direction for these muscles that was specific to our experimental setup. We fit cosine tuning curves to normalized EMG data grouped across subjects and task levels (Figure 3.4). The FDI was most active in the left half of the task plane, with significant activity extending as far as extension and flexion. The EIP was most active in the top half of the task plane, with significant activity extending as far as abduction and adduction. The EDC activity appeared to be concentrated on the 2nd quadrant, which is interesting because the EIP and EDC have similar action directions in the FEAA plane, but different activity tuning curves.

Based on the regions of significant activity described above, histograms across all tasks in these active ranges were made of the action direction estimate (Figure 3.4). These histograms indicated that action direction estimates for each muscle tended to cluster along particular directions. The average action direction estimate was taken as the likely action direction for these muscles (average $\pm$ standard deviation across subjects): FDI pulled in $196^\circ \pm 7^\circ$ (abduction with some flexion), EIP pulled in $75^\circ \pm 3^\circ$ (extension with some adduction), and EDC pulled in $91^\circ \pm 9^\circ$ (almost pure extension).

The muscle activity ranges and likely action directions were then compared to the force covariance map in the following section.

3.4.2 Force covariance map relates to muscle activity and muscle action directions

Force covariance ellipse geometry, as described by η, was significantly non-uniform as a function of task direction (ANOVA, $p < 0.001$). η as a function of task direc-

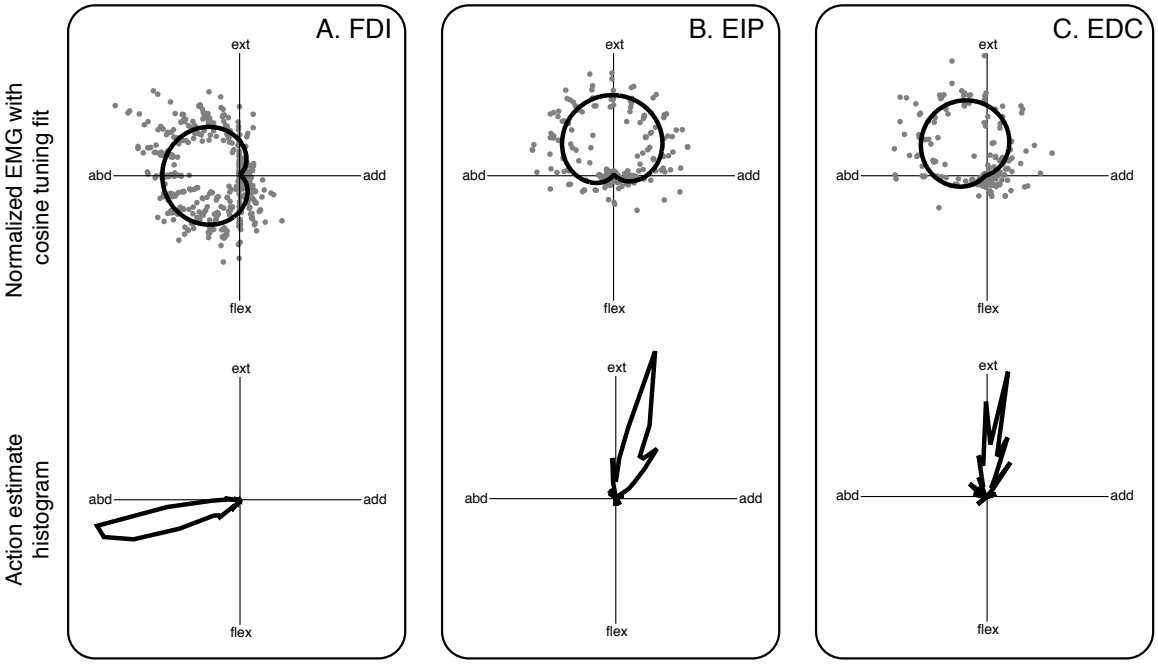

Figure 3.4: Task regions of muscle activity and muscle action direction estimates. Normalized EMG data from each muscle were fit with cosine tuning curves. Top panels show EMG data grouped across subjects from the three muscles studied plotted in polar coordinates along with the best-fit cosine tuning curve. Bottom panels show polar histograms of action direction estimates from each muscle studied. A. The FDI was most active in the second and third quadrants between extension and flexion, and had an average action direction estimate of 196°. B. The EIP was most active in quadrants 1 and 2 between adduction and abduction, and had an average action direction estimate of 75°. C. The EDC was most active in quadrant 2 between extension and abduction, and had an average action direction estimate of 91°.

tion, was consistent across subjects, having a standard deviation across subjects averaged across task directions of 0.099. The variation in η across task directions averaged across subjects was 0.53. Thus, inter-subject variability was small compared to inter-task-direction variability, leading to a cloud of data points with consistent features when η was plotted as a polar function of task direction (Figure 3.5A). We consistently found 3 distinct task directions with high η values, indicating that force covariance ellipses were largely task-directed in these directions (marked η peak in Figure 3.5A). These η-peak directions were 195°, 75°, and 330°. We grouped η data into 15° task direction bins, and between η-peak directions, we consistently found "non-task-directed ranges" where η was significantly ($p < 0.05$) lower than the nearest η-peak, and thus force covariance ellipses were relatively non-task-directed. These task direction ranges were 0°-45°, 105°-180°, and 225°-300° (illustrated as shaded regions in Figure 3.5B).

We found that η-peak directions corresponded closely to muscle action directions (Figure 3.5B). The η-peak direction of 195° was closely matched by the FDI action direction estimate of 196°. The η-peak direction of 75° was closely matched by the EIP action direction estimate of 75°. The η-peak direction of 330° was less well matched by the 347.5° FPI action direction estimate, though this might be expected since the FPI estimate was not produced by our recording setup or exact posture.

Based on cadaveric data, we would expect that slight increases in the MCP flexion angle would cause the FPI to have a greater flexion moment arm while having the abduction moment arm remain unchanged (An et al., 1983), thus reducing the discrepancy between the η-peak direction and the FPI action direction estimate. The close alignment between directions of task-directed ellipses and muscle action directions suggests that these muscles may act as prime movers for tasks in their action

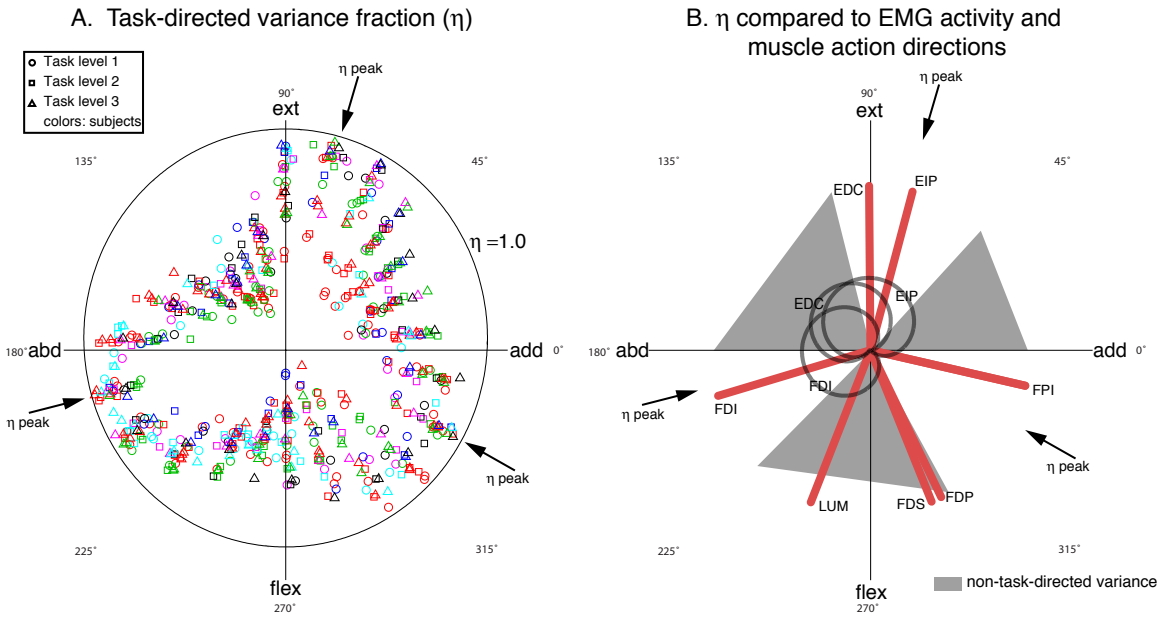

Figure 3.5: Force covariance map relates to muscle activity and action direction. A. Relation between force covariance ellipses and the task direction, as quantified by the task-directed variance fraction (η). Each point represents a task, with direction given by the task direction, and magnitude given by η. Different task magnitude levels are represented by different symbols, while different subjects are represented by different colors. The subject population consistently showed relative peaks in η at 195°, 75°, and 330°, marked with arrows. These peaks correspond to narrow, task direction-aligned covariance ellipses in these task direction. B. η data were grouped by 15° task direction bins, and task-direction regions with average η significantly less than the closest peak average η are shown as shaded regions. These regions contain covariance ellipses that are either broad or not task-aligned. Cosine tuning curves derived from normalized EMG data are shown, and action direction estimates are shown as lines (see text for abbreviations). Notice that EMG data and action direction estimates suggest coactivation of muscles with different action directions in regions of non-task-directed variance.

direction.

For all non-task-directed ranges of task directions, which exhibit non-task-directed ellipses, there is clear EMG evidence of cooperation among multiple muscles with different action directions (Figure 3.5B). For the second quadrant non-task-directed range (105°-180°), there was significant EMG activity in the FDI, EDC, and EIP, so there were muscles with different action directions active throughout this region of task directions. For the non-task-directed range in quadrants 3 and 4 (225°-300°), there was significant EMG activity in the FDI. Since the FDI action direction is

not in this range, there must have been significant force contributions from other muscles with different action directions to achieve the tasks. Likewise, for the non-task-directed range in quadrant 1 (0°-45°), there was significant EMG activity in the EIP, and since the range did not contain the EIP action direction, other muscles with different action directions had to have been active to achieve the tasks. Thus, task directions exhibiting force covariance ellipses are relatively non-task-directed, correspond to task directions where EMG data indicates cooperation of multiple muscles.

3.4.3 Signal-dependent noise generates the force covariance map

The force covariance map produces inferences about the average amount of force produced by a muscle based on variability in the net endpoint vector; thus, force covariance mapping requires a scaling of muscle force variability with mean muscle force. We indeed observed that the total endpoint force variance significantly ($p < 0.001$) scales with task level (Figure 3.6), which may be interpreted as the average, across active muscles, of the scaling relation between individual muscle force variance and individual muscle average force (APPENDIX).

3.5 Discussion

We have introduced force covariance mapping (FCM) as a novel approach using variability in human index finger forces for studying muscle coordination at the metacarpophalangeal joint of the index finger in the hand. We have shown that this force covariance map offers several significant insights. In particular, we found that net endpoint vector covariance depends critically on task direction. We further showed that non-uniformities in the force covariance map could plausibly be related to action directions of contributing muscles, based on analysis of the EMG activity

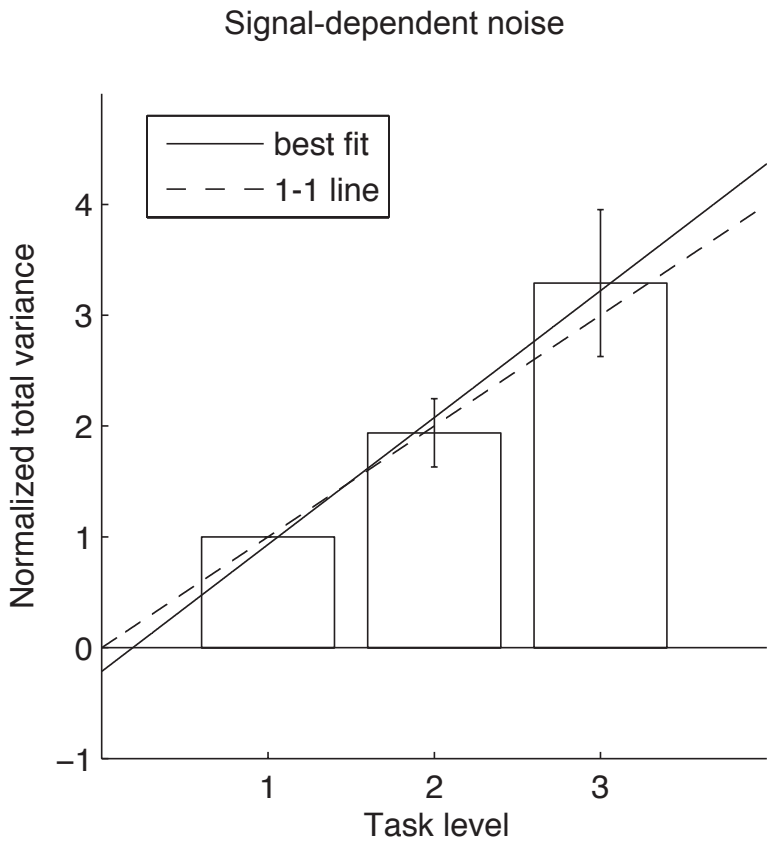

Figure 3.6: Endpoint force variability exhibits signal-dependent noise. Total force variance, normalized to the lowest task level, plotted versus task magnitude level. Variance increased with task level, as would be expected with signal-dependent noise. Error bars indicate 95% confidence intervals, and the best fit line shows results of a regression analysis indicating that the increase in total variance as a function of task level was significant ($p < 0.001$).

of the contributing muscle.

To integrate these findings into current motor control thinking, we first discuss the relevance of our results to theories of muscle coordination, including the muscle synergy hypothesis, prime mover activation, and optimization. We then further discuss the FCM technique, contrasting it to uncontrolled manifold analyses and showing how it complements dimensionality analyses of EMG data and stimulation of anatomical structures. We conclude with a discussion of potential limitations of FCM and of this study.

3.5.1 Muscle coordination: FCM and the muscle synergy hypothesis

We interpret the existence of task-direction-confined (TDC) covariance ellipses in directions of likely muscle action as evidence that these particular muscles are not strongly coupled, in fixed ratio synergies, to other muscles with different action directions. As an example of non-synergistic behavior, we found a high TDC variance fraction for force production in the action direction of first dorsal interosseous (FDI), with approximately 90% of the force variance confined to the task direction.

Recent muscle synergy descriptions have defined individual synergies as a fixed set of weights for activating a set of muscles, with overall motor coordination achieved by appropriate activation of multiple synergies (e.g. (Ting and Macpherson, 2005)). If such a synergy involving the FDI had significant weights for muscles with different action directions than the FDI, FDI activation would automatically incur activation in the other muscles of the synergy. This muscle coactivation would be expected to generate non-TDC covariance ellipses for any task for which the synergy was active. Thus, based on our results, we suspect that many index finger muscles do not exhibit fixed synergistic behavior.

3.5.2 Muscle coordination: FCM and prime movers versus cooperating muscles

Alternatively we sought to establish whether a given task could be executed using a prime mover muscle, or whether multiple muscles with different action directions could be played off against each other. The results of our study suggest that both situations may occur, depending on the desired direction of the task.

For example, the FDI is often assumed to be a prime mover for MCP abduction (Flament et al., 1993; Semmler and Nordstrom, 1998; Thomas et al., 1986). This assumption has recently been challenged because of the finding of relatively large

amounts of extensor EMG activity during finger abduction (Keenan et al., 2006). Our results support this latter finding (see Figure 3.5B). However, the FDI is also known to generate flexion torque about the MCP joint in addition to abduction torque (An et al., 1983; Thomas et al., 1986). We found that the EMG activity in both EDC and EIP dropped off sharply as the task direction changed from pure abduction toward the FDI action direction. Our results suggest that the MCP joint torque may be more governed by the FDI alone for tasks directed in the FDI action direction.

As a converse to prime mover activation, there is clear evidence in the force covariance map for sets of task directions controlled by multiple muscles with different action directions. This type of coordination strategy was particularly apparent for tasks between pure extension and pure abduction, a range for that contains the unique action directions of no muscles.

If muscle activity does indeed exhibit cosine tuning with the task direction based on an optimization principle (Herrmann and Flanders, 1998; Hoffman and Strick, 1999; Todorov, 2002), we would predict that some muscles might appear as prime movers in their action direction and others would not. Cosine tuning predicts that muscle activity should drop to baseline levels 90° away from the muscle preferred direction.

Assuming that muscle activity is cosine tuned, and that the preferred directions correspond approximately to the action directions, we can make some interesting predictions. The extensor action directions are greater than 90° from the FDI and FPI, whereas the flexor action directions have other muscles within 90° on both sides (Figure 5B). According to the assumptions put forth here, we would expect that the extensors, FDI and FPI might appear as prime movers for tasks in their

action directions, whereas the flexors would not because coactivation of the FDI and FPI (within 90°) would produce smaller errors (Todorov, 2002). We found force covariance ellipses consistent with this expectation, as well as significant FDI EMG activity in the flexor action direction.

3.5.3 Technique: FCM and uncontrolled manifold analyses

Our approach is superficially similar to the evaluation of the uncontrolled manifold (UCM) hypothesis, in that we also seek to use motor variability as a window into CNS organization (Latash et al., 2002). However, whereas UCM studies seek to exploit a mismatch between kinematic and feedback degrees-of-freedom, we seek to provide complete feedback about the involved kinematic degrees-of-freedom while observing residual variability in isometric force. For instance, when visual feedback is provided to a subject about the total vertical force generated by the index and middle fingers, force is distributed among the fingers to stabilize moments about a point between the fingers, at the expense of stabilizing total force (Latash et al., 2001). This approach provides important information about how the CNS coordinates kinematic degrees-of-freedom by exploiting a mismatch between the number of kinematic degrees-of-freedom (two) and the number of feedback dimensions (one). If feedback were given to the subject showing both force and moment, and the subject was instructed to hold a specified force and moment, forces exerted by the kinematic degrees-of-freedom would still fluctuate because of fluctuations in muscle force. We are interested in this latter form of motor variability, namely variability that arises even if the subject has feedback about all relevant kinematic degrees-of-freedom.

Technique: FCM and dimensionality analysis

We introduced force covariance mapping in a largely intuitive fashion, and then demonstrated that there is significant experimental information available in this new

approach. In this section, we illustrate with a simple computational model that the force covariance map likely contains information about muscle coordination beyond traditional dimensionality analysis (see APPENDIX for mathematical details).

We begin with a set of muscle action directions from cadaveric estimates (An et al., 1983) (Figure 3.7A). We then consider two, of many possible, activation strategies that the CNS could use to activate these redundant muscles to achieve isometric force tasks of constant magnitude. These are examined in 5° direction increments in the flexion-extension/abduction-adduction plane (the task set). One possible activation strategy is to reduce the degrees of freedom in muscle activity by introducing muscle synergies (Figure 3.7B). We choose three synergies here, because it is the minimum necessary to generate force in all directions of the task plane. Activation of the three chosen synergies is dictated by the task commands so that the desired magnitude and direction of force is achieved for each task. As one possible alternative that does not contain explicit neural coupling between muscles, is that each muscles activity is a cosine function of the task direction (Herrmann and Flanders, 1998; Hoffman and Strick, 1999; Todorov, 2002) (Figure 3.7C). Each muscle has a force specified for each task in the task set. The set of forces across muscles are subjected to principal components across the task set. The set of muscle forces exhibits low dimensionality for both synergy activation (Figure 3.7D) and cosine tuning activation (Figure 3.7E).

Muscle activity dimensionality is unable to distinguish between these activation strategies because the underlying dimensionality of the task demands is low in both cases. The same set of muscle forces used to compute dimensionality is used to compute the expected force covariance map. The task-directed variance fraction η was calculated as a function of task direction for the synergy activation (Figure 3.7F) and the cosine tuning activation (Figure 3.7G). It is evident that the force covariance map

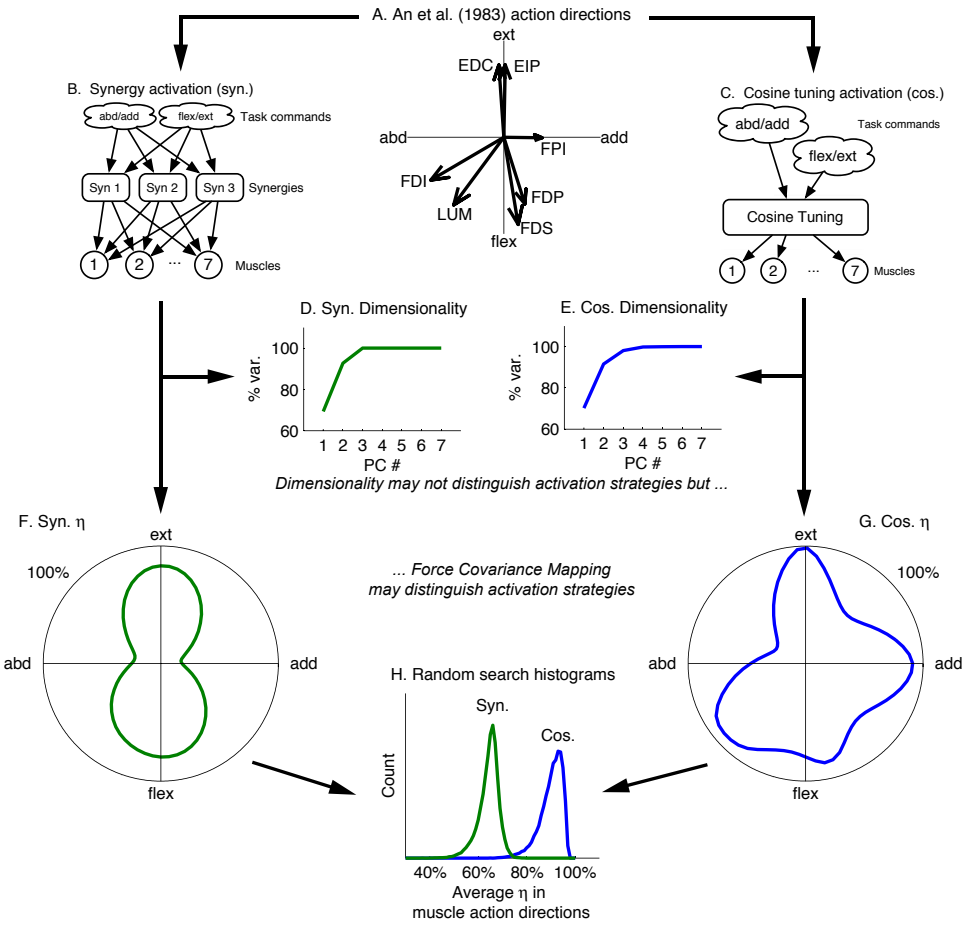

Figure 3.7: Comparison of dimensionality analysis with force covariance mapping, for two hypothetical muscle recruitment strategies. A. Action directions in the task space of isometric forces for seven index finger muscles, estimated from cadaveric data (An et al., 1983). B. The synergy hypothesis combines muscles into a relatively small number of fixed, synergistic groups. Here muscle redundancy is eliminated because three synergies are sufficient to produce any desired force in task space. C. Another hypothesis is that muscles are activated according to a cosine tuning function rather than fixed groupings. Model simulations produce hypothetical results for the two strategies and the two types of analysis. Simulations were performed for a random selection of parameter values for synergy weightings, signal-dependent noise coefficients, and muscle force correlations (see APPENDIX). D. Simulation results of principal component analysis for synergy hypothesis, plotted as average % variance versus number of principal components. E. Simulation results of principal component analysis for cosine tuning hypothesis are similar, with two to three principal components accounting for the majority of the variance. F. Average task-confined variance fraction (η) as a function of task direction for synergy hypothesis, and G. for cosine tuning hypothesis. H. Histograms of the average η for tasks aligned with a muscles action direction, for the two simulated hypotheses. The cosine tuning strategy predicts that high values of η will be produced, whereas the synergy hypothesis predicts lower values. Principal components analysis, applied to this simple model, cannot distinguish whether low dimensionality is due to the task or due to muscle synergies. In contrast, force covariance mapping can indicate lack of synergistic behavior even for low-dimensional tasks.

is very different for the two activation strategies, with synergy activation producing non-specific peaks in η along the skew of the muscle action direction distribution, and cosine tuning activation producing η peaks in muscle action directions (Figure 3.7H).

3.5.4 Technique: FCM and the stimulation of anatomical structures

If the dimensionality reduction observed experimentally in EMG signals indeed occurs at the level of task planning, one implication is that low dimensionality will be observed among muscle control signals even if there are no neural constraints among muscles. More direct support for the muscle synergy hypothesis comes from techniques involving stimulation of anatomical structures along with the measurement of resulting EMG dimensionality. For example, when NMDA microstimulation is applied to a large number of frog spinal cord regions, a large percentage of EMG variance in 12 muscles is accounted for using 7 muscle synergies (Saltiel et al., 2001). The stimulation paradigm for examining muscle synergies may show that low dimension in muscle activation across muscles is unlikely to result only from low dimensionality in task planning during natural movements. However, the stimulation paradigm may not reveal the full repertoire of coupling between muscles available to the CNS. It is highly desirable then to have an experimental approach, complementary to CNS stimulation, that can examine muscle synergies during natural behavior but does not rely on estimating the dimension of EMG activity among a set of muscles. Force covariance mapping, as described in the present study, is one such experimental approach.

3.5.5 Technique: FCM compared to EMG studies

EMG studies of muscle coordination clearly have the advantage of having a measurement of neural input for all relevant muscles. However, EMG assessments may either overestimate or underestimate muscle force (Zhou et al., 2007), which complicates the interpretation of muscle coordination studies based on EMG. Furthermore, for many muscles, it may be difficult to estimate the EMG-force relation because it may be impossible to have a particular muscle active in isolation. FCM relies on a different relation: the relation between average muscle force and muscle force variability. While FCM, as applied in this study, can not directly determine which muscles are contributing to a particular task, the average force-force variability can be directly estimated from the scaling of endpoint force variability with average endpoint force (see APPENDIX) as is shown in Figure 6.

3.5.6 Technique: Inferring muscle forces from FCM

The results presented in this study largely focused on classifying force covariance ellipses into task-directed and non-task-directed. This binary classification separates tasks that are performed using cooperation among muscles and those performed by muscles functioning as prime movers. However, the specific geometry of the covariance ellipse may actually allow the exact force contribution of multiple muscles to be estimated. For a 2-dimensional task plane, the ellipse carries 5 pieces of information. Two come from the Cartesian coordinate of the ellipse center. Three come from the covariance matrix (which is symmetric and thus only has 3 free parameters). If the muscle action directions are known, and the constant of proportionality between average muscle force and force variance can be estimated, then the ellipse uniquely specifies the activity of up to 5 muscles. Further study is required to deter-

mine if FCM can appropriately estimate the activity in muscles having known action directions.

3.5.7 Limitations: FCM and correlation

Force varies mainly in the task direction when the task aligns with the action direction of certain index finger muscles. This observation is possibly because the muscle (and possibly others with similar action directions) is preferentially activated relative to muscles with different action directions. As an example, we found a high TDC variance fraction for force production in the action direction of FDI, with more than 90% of the force variance confined to the task direction.

An alternative explanation is that the same result could be produced by muscles that are coactivated, but with highly correlated noise-like force fluctuations. We can assess the likelihood of this possibility using a simple thought experiment. Suppose that muscle E pulls 90° from the FDI toward extension and muscle F pulls 90° from the FDI toward flexion, and all three muscles have mechanical actions of equal magnitude. Neglecting the lumbrical muscle, this fictive muscle system could be considered an approximation to the cadaveric estimates for the action directions of muscles likely to be active in the left half of the task plane (Figure 3.7A).

Activating the FDI, muscle E, and muscle F equally would generate a net average endpoint vector in the direction of the FDI. We would be concerned that a large task-confined variance fraction might be observed if muscles E and F had correlated force fluctuations. Assume that the correlation coefficient between the time-varying forces generated by muscle E and F is 0.5, which is the largest peak coherence value between pairs of surface EMG signals from different muscles that we are aware of in the literature (Kilner et al., 1999). If we measured the task confined variance fraction for this system and task, we would find that $\eta = 0.5$ (see APPENDIX), much less

than the observed 0.90. Therefore, correlated force fluctuations would be unlikely to solely produce task-directed variance fractions for tasks in the FDI action direction as high as were observed in this study. However, the usefulness of $1 - \eta$ as a upper bound on synergistic activity with other muscles having distinct action directions may be affected by the presence of muscle force correlation, an issue that will require further investigation.

3.5.8 Limitations: Proving prime mover activity

We hypothesized that task-directed variance was generated by prime mover activity, while non-task-directed variance was generated by muscle coactivation. Using EMG data from muscles with different action directions, we directly showed that low task-directed variance fractions were associated with muscle coactivation. We used EMG-based and MRI estimates of muscle action direction to establish the plausibility of high task-directed variance fractions being generated by prime mover activity, as we showed that high task-directed variance fractions were found in directions of muscle action. However, further study is required to establish that EMG for muscles other than the prime mover was actually low in these directions. Nonetheless, we can claim that the high task-directed variance fractions observed in the FDI action directions are unlikely to result from mechanisms other than the FDI behaving as a prime mover. The previous section showed that correlation is not a likely candidate for explaining our results. We also note that extensor activity was not significant in the FDI action direction (Figure 3.5B). Therefore based on the action directions of the relevant muscles (Figure 3.5B), if the FDI were not also significantly more active than the other muscles not recorded from in this study, forces would not balance correctly to generate a net endpoint vector in the FDI action direction.

3.6 Conclusion

The detailed structure of multidirectional net endpoint vector variability likely contains a significant amount of information about how muscles are coordinated to achieve tasks. Force variability patterns are consistent with the CNS using different types of muscle coordination strategies for tasks in different directions, but many index finger muscles are not likely to couple into fixed ratio synergies with other muscles acting in different directions. The CNS may recruit primarily one muscle for tasks in the action direction of the muscle, or may recruit multiple muscles when appropriate. Further study of the detailed multidirectional structure of human motor variability will hopefully provide additional insights into how the CNS coordinates multiple redundant muscles.

3.7 Acknowledgements

We would like to thank M. Chardon and Dr. N. Suresh for technical assistance and helpful discussions. This work was supported by NIH NRSA training grant 1F31NS057855-01 to JJK and WZR, and also NSF grants DMS-0604307 and CMS-0408542 to AMB.

3.8 Appendix

Force covariance mapping (FCM) was introduced in METHODS in a largely intuitive fashion. Here, we illustrate the most important equations underlying the use of signal-dependent noise for studying muscle coordination, and describe how these equations were used to show that FCM may reveal more about muscle coordination than dimensionality analysis when the inherent task dimension is low (Figure 3.7).

Assuming that the endpoint forces generated by different muscles sum linearly to

generate the observed time-varying net endpoint vector $Y(t)$, then

$$Y(t) = \sum_{i=1}^{m} F^{(i)}(t) \tag{3.3}$$

where $F^{(i)}(t)$ is the force vector exerted by the ith muscle. The statistics we compute will be over multiple samples through time, so t will not explicitly appear in our equations for simplicity. The average net endpoint vector $\bar{Y}$ (i.e. the covariance ellipse center) is then simply

$$\bar{Y} = \sum_{i=1}^{m} \bar{F^{(i)}} \tag{3.4}$$

The covariance matrix of Y, denoted $\mathrm{cov}[Y]$, can be expressed as $\mathrm{cov}[Y] = E[YY^T] - \bar{Y}\bar{Y}^T$, where $E[X]$ is the average (expected value) of X. Assuming, for the moment, that forces exerted by different muscles are uncorrelated, then the observed force covariance is simply the sum of the covariance of the force vectors exerted by all muscles

$$\mathrm{cov}[Y] = \sum_{i=1}^{m} \mathrm{cov}[F^{(i)}] \tag{3.5}$$

How does signal-dependent noise in the net endpoint vector reflect how variability in individual muscle force vectors contains information about muscle activation? The trace of a covariance matrix of a random vector indicates the total variance induced by that vector. We denote total variance by var_T, and note that $\mathrm{var}_T[a] = \mathrm{tr}(\mathrm{cov}[a])$ for any vector a. Returning to Equation 3.5, we see that

$$\frac{1}{m}\,\mathrm{var}_T[Y](\|\bar{Y}\|) = \frac{1}{m}\sum_{i=1}^{m} \mathrm{var}_T[F^{(i)}](\|\bar{Y}\|) \tag{3.6}$$

Thus, up to a potentially unknown constant (the number of muscles), the measurable left-hand side of Equation 3.6 shows that total force variance scales with average force magnitude the same as individual muscles do, on average across the set of active muscles.

How will the net endpoint vector covariance matrix differ if different control strategies are used? If muscle 1 is a prime mover, $\|\bar{F^{(1)}}\| \gg \|\bar{F^{(i)}}\|$ for all i other than 1. Thus, by Equation 3.5, $\mathrm{cov}[Y] \approx \mathrm{cov}[\bar{F^{(1)}}]$. If we assume that the action of any muscle i can be described by a vector $a^{(i)}$, then $F^{(i)} = u_i a^{(i)}$, the product of a scalar weighting u_i and the muscle action vector $a^{(i)}$. We then find

$$\mathrm{cov}[Y] = \mathrm{cov}(F^{(1)}) = E[F^{(1)}{F^{(1)}}^T] - \bar{F^{(1)}}{\bar{F^{(1)}}}^T = \mathrm{var}[u_1]a^{(1)}{a^{(1)}}^T \tag{3.7}$$

Such a covariance matrix has one zero eigenvalue and one non-zero eigenvalue corresponding to an eigenvector in the direction of $a^{(1)}$. Thus, the force covariance ellipse is highly elongated along the direction of $a^{(1)}$. Now, suppose that a task is performed by coordinated action of two muscles: $\mathrm{cov}[Y] = \mathrm{cov}[F^{(1)}] + \mathrm{cov}[F^{(2)}]$. Suppose that $a^{(1)}$ and $a^{(2)}$ are orthogonal vectors of equal length, and that scalar weightings satisfy $u_1 = u_2$. Without loss of generality, $a^{(1)} = [1, 0]^T$ and $a^{(2)} = [0, 1]^T$. Then

$$\mathrm{cov}[Y] = \mathrm{var}[u_1]\left(\begin{bmatrix} 1 & 0 \\ 0 & 0 \end{bmatrix} + \begin{bmatrix} 0 & 0 \\ 0 & 1 \end{bmatrix}\right) \tag{3.8}$$

$$= \mathrm{var}[u_1]I_2 \tag{3.9}$$

where I_2 is the 2×2 identity matrix. $\mathrm{cov}[Y]$ therefore has eigenvalues $\lambda_1 = \lambda_2 = \mathrm{var}[u_1]$, and the corresponding covariance ellipse will be a circle. Many intermediate covariance ellipse types are possible, but based on these simple calculations, we expect tasks performed by prime mover muscles to have narrow covariance ellipses elongated along the task direction, and tasks performed by coordinated activity of muscles with very different action directions to have broad covariance ellipses.

How do fixed ratio muscle synergies affect the force covariance map? If the CNS enforces a rigid constraint between two muscle force vectors, such that $F^{(2)}(t) = wF^{(1)}(t)$ for all tasks and some constant w, then the synergy will appear to FCM to

be just another muscle. A more interesting case to consider is what would appear in FCM if only average force vectors were constrained across tasks, $\|\bar{F^{(2)}}\| = w\|\bar{F^{(1)}}\|$. In this case, muscles retain some element of uncorrelated noise that we can seek to exploit. In accord with our experimental findings, we assume that covariance matrix scales linearly with average net endpoint force vector magnitude. Using this assumption, we can express the covariance of a particular muscle force vector as the product of the muscle force vector magnitude and some covariance matrix for unit excitation: $\mathrm{cov}[F^{(i)}] = \|\bar{F^{(i)}}\|\,\mathrm{cov}_1[F^{(i)}]$. Using Equation 3.5, we find

$$\mathrm{cov}[Y] = \|\bar{F^{(1)}}\|(\mathrm{cov}_1[F^{(1)}] + w\,\mathrm{cov}_1[F^{(2)}]) + \sum_{i=3}^{m} \mathrm{cov}[F^{(i)}] \tag{3.10}$$

For simplicity, we consider muscle 1 and muscle 2 to have orthogonal action directions. In this case, the covariance matrix associated with the synergy S can be expressed as

$$\mathrm{cov}[S] = \|\bar{F^{(1)}}\| \begin{bmatrix} 1 & 0 \\ 0 & w \end{bmatrix} \tag{3.11}$$

$\mathrm{cov}[S]$ has eigenvalues $\lambda_1 = 1$ and $\lambda_2 = w$. If the fixed ratio synergy strongly couples muscles 1 and 2, $w \approx 1$. In this case, the covariance ellipse associated with the synergy is a circle, whenever the synergy is active. This constraint makes impossible the observation of narrow task-aligned ellipses in the action directions of either muscles 1 or 2.

How can more general forms of these equations be used to simulate the force covariance map? We began with estimates of muscle action directions made from cadaver measurements of all 7 muscles that could contribute abduction-adduction/flexion-extension force to the human index finger (An et al., 1983). The goal of each simulation was to activate the muscles to generate task vectors distributed at 5° increments

around the unit circle. All simulations were performed by random search (50000 iterations) over parameters with unknown values. For each iteration, a vector k was generated with 7 elements selected uniformly between 0.05 and 1.0. For muscle i with mean scalar weighting $\bar{u_i}$ for a given task, the standard deviation of u_i was $\sigma_i = k_i \bar{u_i}$. A random correlation matrix ρ was generated for each iteration using standard methods (Marsaglia and Olkin, 1984). The cross-correlation values in the correlation matrix were selected uniformly between 0 and 0.2, which seemed to be reasonable values maximal coherence values for the pairs FDI/EDC and FDI/FDS (flexor digitorum superficialis) as reported in the literature (Fisher et al., 2002).

Average muscle forces were simulated according to two strategies. The synergy activation strategy couples muscles and thereby reduces the number of variables that need to be controlled (e.g. (Macpherson, 1991)). Since we worked with muscles acting in the plane, the biomechanical system requires 3 muscle synergies. The measured 2-dimensional muscle action vectors were placed as columns in a 2×7 matrix A. During each iteration of the random search, random 7×3 synergy coupling matrices W were generated with elements between 0 and 1 until the synergy mechanical actions $A_{\text{syn}} = AW$ formed a biomechanically feasible set (i.e. vectors in the columns of A_{syn} span the plane with positive coefficients). Once a suitable coupling matrix W was identified, there was an obvious choice to activate the synergies: activate the two synergies surrounding the given desired task vector and deactivate the other synergy. This procedure produced a vector of average muscle scalar weightings $\bar{u_i}^{(s)}$ for the synergy strategy.

The cosine tuning activation strategy activates muscles as a function of the angular difference between the desired force direction and the "preferred" force direction of the muscle. To implement cosine tuning, we choose to minimize total net endpoint

vector variance (Todorov, 2002) as it was consistent with instructing our subjects to be as precise as possible. For simplicity, we use the notation that $x \overset{*}{\cdot} y$ denotes a matrix whose ijth element is the product of the ijth elements of x and y. We used quadratic programming (*quadprog* in MATLAB) to choose a vector of average muscle weightings that minimized $u^T H u$ subject to $\bar{Y} = Au$ and $u \geq 0$ where $H = kk^T \overset{*}{\cdot} \rho \overset{*}{\cdot} A^T A$. This procedure produced a vector of average scalar weightings $\bar{u_i}^{(c)}$ for the cosine tuning strategy.

For each iteration, the net endpoint vector covariance matrix was computed using Equation 3.12.

$$\text{cov}[Y] = A(kk^T \overset{*}{\cdot} \rho \overset{*}{\cdot} \bar{u}\bar{u}^T)A^T \tag{3.12}$$

where u could be generated either by the synergy or cosine tuning strategy. The task-directed variance fraction was then computed as a function of task according to

$$\eta = \frac{\hat{\bar{Y}}^T \text{cov}[Y] \hat{\bar{Y}}}{\text{tr}(\text{cov}[Y])} \tag{3.13}$$

where $\hat{\bar{Y}}$ denotes a unit vector in the direction of $\bar{Y}$.

We used principal components analysis (PCA) to estimate the dimensionality of the average muscle scalar weighting vectors across all tasks for each iteration. For the muscle activation strategies considered, we would expect the average muscle weighting vectors to occupy linear subspaces of 7 dimensional Euclidian space. Though PCA vectors will not describe the synergies themselves (Tresch et al., 2006), it is an appropriate technique to put an upper bound on the dimension of the subspace containing the average muscle force vectors, as any non-linear dimensionality reducing structure should be contained within the linear PCA subspace containing the majority of the data.

CHAPTER IV

Analysis of the effects of firing rate and synchronization on spike-triggered averaging of multidirectional motor unit torque[1]

4.1 Abstract

Spike-triggered averaging (STA) of muscle force transients has often been used to estimate motor unit contractile properties, using the discharge of a motor unit within the muscle as the triggering stimulus. For motor units that exert torque about multiple degrees-of-freedom, STA has also been used to estimate motor unit action direction. It is well known that motor unit firing rate and weak synchronization of motor unit discharges with other motor units in the muscle can distort STA estimates for contractile properties, but the distortion of STA estimates for motor unit action direction has not been thoroughly evaluated. Here, we derive exact equations that predict that STA decouples firing rate and synchronization distortion when used to estimate motor unit action direction. We derive a framework for analyzing synchronization, consider whether the distortion due to synchronization can be removed from STA estimates of action direction, and show that there are distributions of motor unit action directions for which the STA is insensitive to synchronization. We conclude that STA may give insight into how motoneuronal

[1]This chapter is based on the publication: Kutch J, Suresh N, Bloch A, Rymer W (2007) Analysis of the effects of firing rate and synchronization on spike-triggered averaging of multidirectional motor unit torque. Journal of Computational Neuroscience 22:347-361.

synchronization is organized with respect to motor unit action direction.

4.2 Introduction

Spike-triggered averaging (STA) is one of the most widely used system identification techniques in motor neuroscience. When estimating motor unit properties, STA involves extracting sections of joint torque based on the timing of discharges of a single motor unit, and then averaging the sections together (Buchthal and Schmalbruch, 1970). While the resulting torque transient is reflective of the magnitude and time course of the motor unit twitch, it has also been shown in numerous experimental and theoretical studies that STA of joint torque based on motor unit discharge times is strongly influenced by both mean motor unit firing rate (Calancie and Bawa, 1986; Nordstrom et al., 1989) and by synchronization (Taylor et al., 2002; Keen and Fuglevand, 2004b). Synchronization refers to the increased probability of simultaneous discharge between a pair of motor units relative to chance, and has been studied in many muscles (Datta and Stephens, 1990; Deluca et al., 1993; Farmer et al., 1997; Semmler, 2002). The distortion of the twitch waveform by firing rate is well understood (Andreassen and Baron, 1983; Lim et al., 1995), but the distortion due to motor unit synchronization is less well understood. For example, it has been observed that increases in motor unit firing rate decrease estimates of motor unit peak force, whereas increases in population synchronization likely increase estimates of motor unit peak force (Thomas et al., 1990a; Taylor et al., 2002; Keen and Fuglevand, 2004b). Clearly, such confounding distortions make the interpretation of STA estimates for motor unit contractile properties difficult.

Motor unit action direction is a very different property. Action direction is an angle that specifies the relative torque contribution of a motor unit to the various

components of torque output. For example, Keen and Fuglevand (2004b) evaluated the action direction of motor units in the extensor digitorum communis, a large digital extensor muscle on the dorsal side of the forearm. The action direction described the relative amounts of torque generated on each of the digits subsequent to a discharge in a particular motor unit. Thomas et al. (1990b) evaluated the action direction of thenar motor units. In this case, the action direction specified the relative amounts of torque generated in thumb abduction and flexion subsequent to a discharge in a particular motor unit.

Many other experimental studies have sought to determine the range of action directions for the motor units within a muscle or a related group of muscles. We show that whether synchronization distorts STA results is likely to depend on the action directions of the weakly synchronized motor units. In particular, STA distortion may occur if weakly synchronized motor units have action directions spanning a larger range than the desired directional accuracy of the study. Throughout the paper, motor units that pull in a range of directions greater than the desired accuracy are said to have different action directions, while motor units that pull in a range of directions less than the desired accuracy are said to have similar action directions.

Here, we develop a framework for analyzing the effects of motor unit firing rate and population synchronization on STA estimates of motor unit action direction. We show that when multiple torque components are recorded and simultaneously averaged based on a single motor unit spike train, firing rate distorts all components equally and the correct action direction is recovered in the absence of synchronization. Therefore, any distortion of the STA estimate for action direction is likely to result from motor unit population synchronization. In other words, STA performed on multidirectional motor unit torque decouples firing rate and synchronization dis-

tortion.

We further develop the analysis of synchronization to show that if the set of weakly synchronized motor units all pull in the same direction, STA will still correctly identify the action direction of any sampled motor unit. Alternatively, if several motor units with very different action directions are even weakly synchronized, STA estimates of action direction will be profoundly distorted, with each sampled motor unit producing roughly the same STA estimate for action direction. We consider whether synchronization-induced distortion of STA estimates for motor unit action direction can be removed. We show, both in the case of uniform synchronization applied to a population of motor units and also in a simple case of non-uniform synchronization motivated by the experiments of Keen and Fuglevand, that the distortion of STA estimates for action direction can be removed. It has been shown that pairs of motor units between muscles with very different action directions can be weakly synchronized (Bremner et al., 1991a; Bremner et al., 1991c; Bremner et al., 1991b); we therefore show that there are distributions of motor unit action directions for which STA is insensitive to synchronization.

4.3 Methods

The theoretical framework and assumptions are illustrated in Figure 4.1. The key assumptions of this model were that

1. Motor unit force sums linearly among units, and
2. Force within a single motor unit can be described by the superposition of impulse responses (twitches), though the impulse response gain can vary through time in a stochastic or nonlinear way.

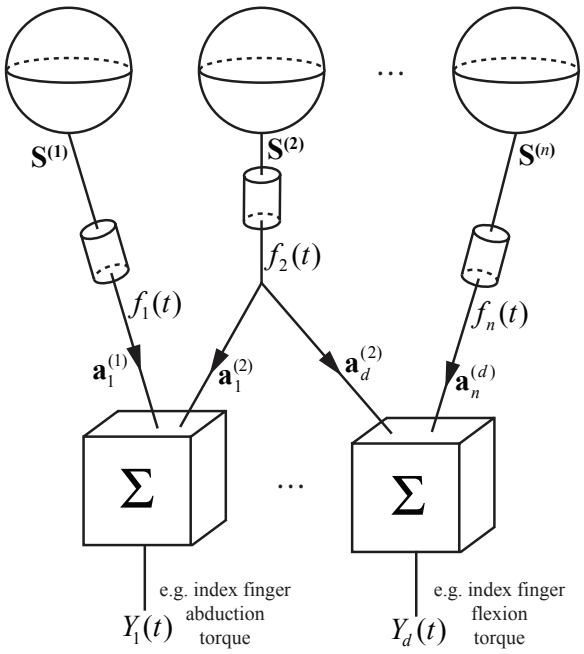

Figure 4.1: The modeling framework for spike-triggered averaging. A population of m active motor units generates spike trains $S^{(1)}, \ldots, S^{(n)}$. These spike trains generate continuous-time joint torques $Y_1(t), \ldots, Y_d(t)$. The spike trains are transformed into continuous-time motor unit forces $u_1(t), \ldots, u_m(t)$ by time-varying linear transformations. The effect of $u_t(t)$ for some motor unit i may be confined to a single torque dimension, such as motor units 1 and m, or may span multiple torque dimensions such as motor unit 2. This information is encoded in the motor unit's "action direction" which is a multidimensional vector $a^{(i)}$ whose components specify the relative contributions made by motor unit i to the different dimensions of torque output. The motor unit "action direction" α_i for motor unit i is the direction of $a^{(i)}$.

With regard to the first assumption, nonlinear summation of motor unit force is most easily observed in otherwise passive muscle, and does not appear to be as significant when large portions of muscle are active (see (Sandercock, 2005) for review). Westling et al. (1990) found that individual thenar motor units have straight force trajectories in the flexion/abduction plane of the thumb when activated by intraneural stimulation, suggesting that motor unit action across multiple degrees-of-freedom can be approximated by a single vector.

With regard to the second assumption, experiments have shown that the frequency response of motor units is consistent with a second-order, critically-damped linear model (Stein et al., 1972; Mannard and Stein, 1973). However, the steady state force

versus firing rate curve is nonlinear and similar for most motor units when firing rate is normalized to the twitch time course (Kernell et al., 1983), suggesting that the motor unit twitch gain is firing-rate dependent (Fuglevand et al., 1993).

The analytical predictions were compared to the numerical model of Fuglevand et al. (1993) for a motor unit population. This model specifies the contractile properties of the set of motor units, as well as the dependence of motor unit firing rate on these properties and on the global level of excitation applied to the motor unit population. 200 seconds of simulated data were generated, which typically produced 1600-3000 spikes on which to perform STA. Motor unit spike trains were generated independently with a constant coefficient of variation in their inter-spike interval of 20% (Fuglevand et al., 1993). Synchronization was then applied using the algorithm of Yao et al. (2000). Spikes selected for synchronization by this algorithm were shifted into exact alignment plus a normal random variable with mean zero and standard deviation of 1.67 ms (Taylor et al., 2002). Under these conditions, the expected width of synchronization peaks was approximately 6 ms. Imposing weak motor unit synchronzation using the algorithm of Yao et al. requires two input parameters: the fraction of reference spikes that would be used to apply synchronization, and the fraction of "alternate" motor units that would have spikes synchronized to the selected reference spike. The actual amount of synchronization was measured between all active motor unit pairs using the synchronization index (described below). Since the parameters of the algorithm of Yao et al. are not experimentally measurable, they were adjusted by trial-and-error until the average synchronization index across all active motor unit pairs was set to a level that could be compared with experimental measures.

The synchronization index was computed as follows. Given a pair of motor units $_{\text{test}}$ and $_{\text{alt}}$, with unit $_{\text{test}}$ serving as the reference, let the synchronization probability p be the fraction of spikes discharged by unit $_{\text{test}}$ for which there is a spike in unit i within the synchronization peak. The synchronization index s was the difference between the actual synchronization probability and the synchronization probability when the spike trains were independent. Thus, $s = p_{\text{actual}} - p_{\text{independent}}$. This synchronization index s was the same as the "extra spikes per trigger" used by Binder and Powers (2001) and the synchronization index of Deluca et al. (1993). We chose to use this synchronization measure for two reasons. First, it has been measured experimentally from several muscles and can be computed directly from the crosscorrelogram (Deluca et al., 1993). Second, unlike the Common Input Strength (CIS), the synchronization index that we used does not depend on reference motor unit firing rate. In the theoretical analysis of synchronization derived below, the synchronization index that we used arises naturally in the equations. STA depends critically on the fraction of synchronized spikes, but not how fast they occur, which would be measured by the CIS.

For some simulations, the synchronization index was varied over the physiological range measured by (Deluca et al., 1993), which was 0-25%. In other simulations, the average synchronization index was set to 0.08, which was the average synchronization index measured from the FDI by Deluca et al. (1993). In some simulations, synchronization is applied uniformly across all motor unit pairs, while in other simulations synchronization is limited to motor units with similar action directions. When we refer to uniform synchronization, we are referring to uniform with respect to action direction. Synchronization is not uniform with respect to motor unit recruitment threshold (Schmied et al., 1994; Datta and Stephens, 1990). We did not model

the dependence of synchronization on recruitment threshold as we were interested in the effects of synchronization on STA estimates for action direction. Thomas et al. (1990b) did not find a clear relation between motor unit peak force and action direction. Therefore in our model, peak force, and consequently recruitment threshold, was distributed uniformly with respect to action direction.

We were interested in how STA would perform when multidirectional torque is averaged based on a single reference spike train. Therefore, a two-dimensional action vector additionally described each motor unit. The action vector of motor unit i is labeled $a^{(i)}$, and is a vector of that specifies the relative contribution of motor unit i to the two torque outputs. Motor unit i exerted force $u_i(t)$ along the action vector $a^{(i)}$ so that the total torque output was the linear sum

$$Y(t) = \sum_{i=1}^{m} u_i(t) a^{(i)} \tag{4.1}$$

We derive general equations and analyses that apply to an arbitrary distribution of action vectors. In order to compare simple analytical predictions with numerical simulations, we were interested in how STA would perform in identifying motor unit action vectors if simultaneously active motor units had action vectors spanning a broad range; thus the direction vectors during simulation were assumed to continuously span a range of 90°. A broad, continuous range of action vectors was observed from human thenar motor units using intraneural stimulation (Thomas et al., 1990b); a broad range is also possible for human first dorsal interosseous motor units (Thomas et al., 1986).

To investigate the possibility of action vector distributions for which STA would be insensitive to synchronization, a separate set of simulations were performed that involved the simulation of simultaneously active muscles. The action vectors (moment arms) for the 7 muscles that contribute torque to human metacarpophalangeal

(MCP) joint torque were estimated from cadaver measurements by An et al. (1983). These muscles were the first dorsal interosseous (FDI), first palmar interosseous (FPI), first lumbrical (LUM), extensor indicis proprius (EIP), extensor digitorum communis (EDC), flexor digitorum profundus (FDP), and flexor digitorum superficialis (FDS). We used the moment arms that corresponded to a joint flexion angle of 0° and a joint adduction angle of 0°. For these simulations, each motor unit within a muscle was assumed to have the same action vector. Since, to our knowledge, no models exists for the recruitment and rate-coding schedule for muscles other than the FDI, we assumed that each muscle had the same schedule as does the FDI model (Fuglevand et al., 1993).

To find the proper excitation for each muscle to achieve the desired force in each muscle, a calibration curve was derived by using various levels of excitation with a model with one-dimensional force output and measuring the resultant average force level. In the case where activating each muscle generated no net torque, we solved for the required average force level of each muscle using quadratic programming (quadprog in MATLAB) so that the minimum total squared force was exerted subject to the constraint that there was no net torque and all muscles were active. Each muscle was given a (potentially) different excitation command, independent spike trains were generated for all motor units in all muscles, weak synchronization was applied using the algorithm of Yao et al. (2000) as above to to all pairs of active motor units both within and across muscles, and finally the force for each muscle was computed, multiplied by the moment arm vector, and summed to generate net joint torque. Bremner et al. (1991a; 1991c; 1991b) estimated the level of synchronization between the FDI and the second dorsal interosseous to be roughly half of the level between motor unit pairs within the FDI. Since the synchronization index

of Deluca et al. (1993) was the same as the one that we used, and they found an average synchronization index of 0.08 between FDI motor units, we applied synchronization between motor unit pairs within and across muscles so that the average synchronization index was 0.08. We reasoned that this would provide a worst-case simulation of the distorting effects of synchronization on STA when synchronization spanned multiple muscles.

4.4 Results

General Equations

It is possible to use the assumptions of Figure 4.1 to derive general equations that describe the STA process. Assuming that the motor units in Figure 1 generate torque in parallel, it is possible to write

$$Y(t) = \sum_{i=1}^{m} u_i(t) a^{(i)} + \epsilon(t) \tag{4.2}$$

where $\epsilon(t)$ is a mean-zero independent and identically distributed random vector associated with the measurement uncertainty inherent in observing the output torque vector $Y(t) = [Y_1(t), \ldots, Y_d(t)]$. Using assumption 2 for motor unit force generation, we can write

$$u_i(t) = \sum_{j=1}^{N_i} g_j^{(i)} T_i(t - S_j^{(i)}) \tag{4.3}$$

where $S_j^{(i)}$ is the time of the jth spike in the ith motor unit, and $g_j^{(i)}$ is the impulse response gain in the force of the ith motor unit at the time of the jth spike, $T_i(t)$ is the unpotentiated twitch waveform of motor unit i, and N_i is the number of spikes in motor unit i. The twitch gain $g_j^{(i)}$, which can vary from discharge to discharge, was included to model the nonlinear dependence of twitch gain on firing rate (Fuglevand et al., 1993). Inserting Equation 4.3 into Equation 4.2, we obtain

an equation describing the output torque vector

$$Y(t) = \sum_{i=1}^{m} a^{(i)} \sum_{j=1}^{N_i} g_j^{(i)} T_i(t - S_j^{(i)}) + \epsilon(t) \tag{4.4}$$

STA involves knowing the spike times $S^{(\text{test})}$ from a reference motor unit test, and then averaging the torque based on these spike times. Applying this process to Equation 4.4, we find that the STA trajectory $z^{(\text{test})}(t)$ based on motor unit test is

$$\begin{aligned} z^{(\text{test})}(t) &= \frac{1}{N_{\text{test}}} \sum_{k=1}^{N_{\text{test}}} Y(t + S_k^{(r)}) \\ &= \sum_{\text{alt}=1}^{m} a^{(\text{alt})} \underbrace{\frac{1}{N_{\text{test}}} \sum_{k=1}^{N_{\text{test}}} \sum_{j=1}^{N_{\text{alt}}} g_j^{(\text{alt})} T_{\text{alt}}(t + S_k^{(\text{test})} - S_j^{(\text{alt})})}_{C_{\text{test,alt}}(t)} \\ &\quad + \frac{1}{N_{\text{test}}} \sum_{k=1}^{N_{\text{test}}} \epsilon(t + S_k^{(\text{test})}) \\ &= \sum_{\text{alt}=1}^{m} C_{\text{test,alt}}(t) a^{(\text{alt})} + \frac{1}{N_{\text{test}}} \sum_{k=1}^{N_{\text{test}}} \epsilon(t + S_k^{(r)}) \end{aligned} \tag{4.5}$$

We are interested in the behavior of the STA process as N_{test} gets very large, and it is clear by the Law of Large Numbers that the second term in Equation 4.5 approaches zero as $N_{\text{test}} \to \infty$. The first term of Equation 4.5 shows that STA is composed of weighted averages of the action vectors, the weighting functions we will refer to as contribution functions. Contribution functions can be expressed as

$$C_{\text{test,alt}}(t) = \frac{1}{N_{\text{test}}} \sum_{k=1}^{N_{\text{test}}} \sum_{j=1}^{N_{\text{alt}}} \underbrace{g_j^{(\text{alt})}}_{\text{random gain}} T_{\text{alt}}(t + \underbrace{S_k^{(\text{test})} - S_j^{(\text{alt})}}_{\text{random shift}}) \tag{4.6}$$

Equation 4.6 shows that the contribution function is an average of a function of two random variables, a random gain and a random shift, over the duration of the STA. We denote the random gain g and the random shift x. For a given motor unit pair $(\text{test}, \text{alt})$, there is a map $(k, j) \to (x, g)$ generating a locus of $N_{\text{test}} N_{\text{alt}}$ points in the (x, g)-plane. We convert Equation 4.6 into an integral by letting $f_{\text{test,alt}}(x, g)$ denote

the fraction of shift-gain pairs per unit area from the spike trains of motor units test and alt observed in the rectangle with lower left corner at (x, g), horizontal side length Δx , and vertical side length Δg. The integral expression for $C_{\text{test,alt}}(t)$ is

$$C_{\text{test,alt}}(t) = N_{\text{alt}} \int_0^\infty \int_{-\infty}^\infty g T_{\text{alt}}(t+x) f_{\text{test,alt}}(x, g) dx dg \tag{4.7}$$

We first note that Equation 4.7 predicts that, if the spike trains of all motor unit pairs in the population are independent, STA will accurately identify the action direction α_{test} without being able to accurately identify either the magnitude or time-course of the reference motor unit twitch $T_{\text{test}}(t)$. To show this fact, we note that if the spike trains of motor units test and alt are independent, then $f_{\text{test,alt}}(x, g) = f_{\text{test,alt},X}(x) f_{\text{test,alt},G}(g)$ where $f_{\text{test,alt},X}(x)$ and $f_{\text{test,alt},G}(g)$ are marginals of the density $f_{\text{test,alt}}(x, g)$. $f_{\text{test,alt},X}(x)$ is the crosscorrelogram between the spike trains in motor units test and alt , with motor unit test serving as the reference. Since we assume no correlation between the spike trains of motor units test and alt, $f_{\text{test,alt},X}(x)$ is a constant function (for some region surrounding $x = 0$ that becomes arbitrarily large as $N_{\text{test}} \to \infty$) if alt $\neq$ test. Therefore, if alt $\neq$ test,

$$C_{\text{test,alt}}(t) = N_{\text{alt}} \int_0^\infty g f_{\text{testalt},G}(g) dg \int_{-\infty}^\infty T_{\text{alt}}(t+x) f_{\text{test,alt},X}(x) dx \tag{4.8}$$

Since $f_{\text{test,alt},X}(x)dx$ is a constant function, the integral in x is the same value regardless of t. Thus, $C_{\text{test,alt}}(t)$ is a constant function of t if alt $\neq$ test. Returning to Equation 4.5, we can see that

$$z^{\text{test}}(t) = C_{\text{test,test}}(t) a^{(\text{test})} + c \tag{4.9}$$

$C_{\text{test,test}}(t)$ does not necessarily have the same magnitude or time-course as $T_{\text{test}}(t)$, but nonetheless points in the direction of $a^{(\text{test})}$.

Figure 4.2 illustrates the convergence of motor unit action estimate (MUAE) direction (STA trajectory direction) to the action direction in the absence of synchronization for the simulated Fuglevand model. MUAE is computed as the direction of the best fit line to the STA trajectory. Figure 4.2A shows simulation results at 5% maximum as an increasing number of spikes are used for STA. The MUAE direction converges to the actual motor unit action direction, but neither the time course (time to STA trajectory peak) nor the magnitude (peak STA trajectory magnitude) converges to the corresponding properties of the twitch waveform. Figure 4.2B-C shows simulation results at 15% maximum after 1500 spikes have been used for STA. The angular error in the MUAE direction is shown across all 75 active motor units. Figure 4.2B shows results for the standard distribution of peak forces across the motor units; motor units that discharge more rapidly also have smaller peak forces. Equation 4.9 predicts that increased firing rate can not distort the MUAE direction, so Figure 4.2C shows results from a modified model in which all motor units have the same peak force. Notice that the MUAE direction now converges to the correct action direction for all motor units, indicating that increased firing rate is not the source of distortion seen during increased excitation. Equation 4.8 predicts the distortion of STA for low force motor units when higher force motor units are simultaneously active. If $N_{\text{test}} < \infty$, there will be residual non-uniformity in the crosscorrelogram between motor unit pairs. If unit $_{\text{alt}}$ is a higher force motor unit and unit $_{\text{test}}$ is a lower force motor unit, the convolution in the computation of $C_{\text{test,test}}(t)$ will amplify the non-uniformity of the crosscorrelogram $f_{\text{test,alt},X}(x)$ because the convolution depends on the twitch waveform $T_{\text{alt}}(t)$ of the larger force motor unit.

Even weak synchrony between motor unit pairs may significantly complicate the use of STA, so the remainder of the paper is devoted to analytical tools for predicting

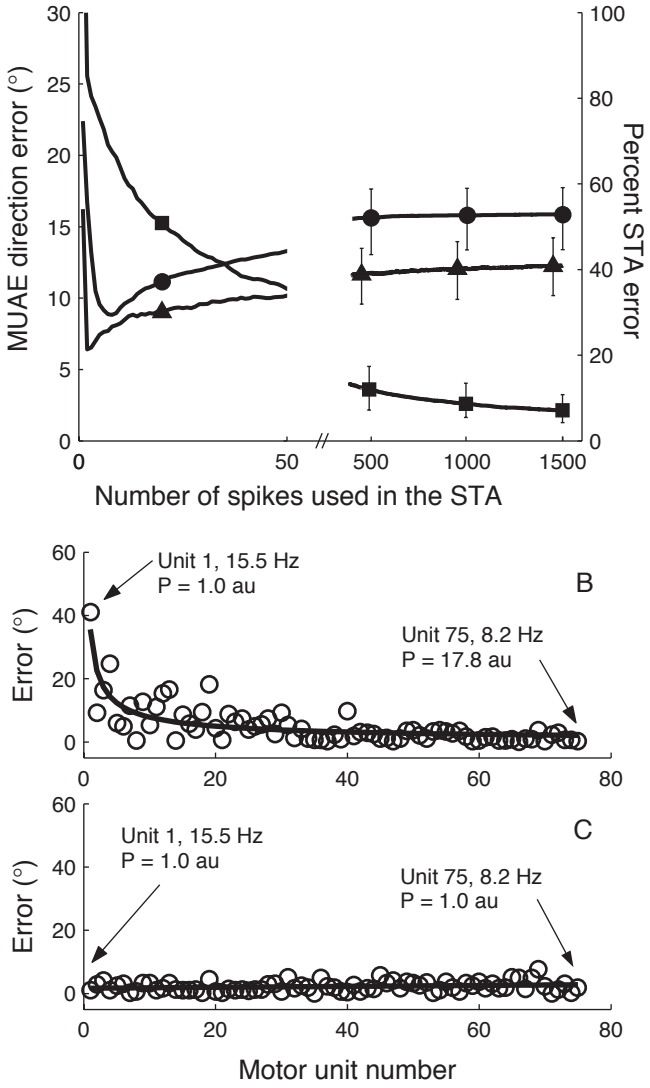

Figure 4.2: Motor unit action estimate (MUAE) direction (STA trajectory direction) converge to motor unit action direction in the absence of synchronization whereas estimates of contractile properties do not. A. STA error as a function of the number of number of spikes in the average for a 90° range of action directions and an excitation of 5% maximum. Square curve corresponds to the left vertical axis and shows the angular error in degrees between the line of best fit to the STA trajectory and the true motor unit action direction. Triangle curve corresponds to the right vertical axis and shows the error in percent between the actual contraction time and the average time to peak of the STA waveforms for both torque components. Circle curve corresponds to the right vertical axis and shows the error in percent between the actual peak force and the peak magnitude of the STA trajectory. Error bars indicate best and worst performance over the population of active motor units. B, C. Simulations performed at 15% maximum. Each plot shows the angular error in degrees as a function of motor unit number. B. The standard model that contains motor units with peak forces ranging from $P = 1$ arbitrary unit (au) to $P = 17.8$ au. Notice that lower force motor units that are firing at a faster rate have more error than the larger units firing at a slower rate. C. Modified model that contains motor units all having peak force $P = 1$. Notice that STA identifies the correct action direction for all motor units independent of firing rate.

the effects of synchronization on MUAE direction. When considering the entire set of active motor units, STA should be viewed as a time-varying linear map from the distribution of action vectors to the distribution of STA trajectories. This linear map can be visualized by the following matrix

$$\begin{bmatrix} z^{(1)}(t) \\ z^{(2)}(t) \\ \vdots \\ z^{(m)}(t) \end{bmatrix} = \begin{bmatrix} C_{1,1}(t) & C_{1,2}(t) & \cdots & C_{1,m}(t) \\ C_{2,1}(t) & C_{2,2}(t) & \cdots & C_{1,m}(t) \\ \vdots & \vdots & \ddots & \vdots \\ C_{m,1}(t) & C_{m,2}(t) & \cdots & C_{m,m}(t) \end{bmatrix} \begin{bmatrix} a^{(1)} \\ a^{(2)} \\ \vdots \\ a^{(m)} \end{bmatrix} \tag{4.10}$$

We can write this equation compactly as $z(t) = C(t)A^T$. If the motor unit population torque $Y(t)$ is d-dimensional, then A is a $m \times d$ matrix with the ith row equal to $a^{(i)}$ (represented as a row vector). $Z(t)$ is also a $m \times d$ matrix with the $z^{(i)}(t)$ trajectory represented as the ith row of $Z(t)$. We call $C(t)$ the contribution matrix, A the distribution of action vectors, and $Z(t)$ the distribution of STA trajectories.

From the general equations, we are able to make some hypotheses about the effects of synchronization on STA. Note that all terms in the integral expression for $C_{\text{test,alt}}(t)$ (Equation 4.7) are positive. Therefore, the set $Z(t)$ are linear combinations of the set A with positive coefficients, so $Z(t)$ must be in the interior of A. Thus, the range of MUAE directions can only underestimate the range of action directions.

Next, consider a population of motor units, potentially expressing weak synchronization, that all have the same action direction a. The STA trajectory for motor unit can be written

$$z^{(\text{test})}(t) = \left(\sum_{\text{alt}=1}^{m} C_{\text{test,alt}}(t) \right) a \tag{4.11}$$

for which the MUAE direction is correct regardless of synchronization. Therefore synchronization-induced distortion of MUAE directions will depend critically on how

synchronization is organized with respect to action directions. Finally, we would expect that if many motor units with very different action directions were synchronized, the effects of synchronization would compound and profoundly distort the distribution of MUAE directions relative to independent spike trains.

We tested these hypotheses by simulating the Fuglevand model and the results are shown in Figure 4.3. Figure 4.3 shows that the distribution of MUAE directions represents the underlying distribution of action directions when spike trains are independent, the distribution MUAE directions is profoundly altered when synchronization is uniform with respect to action direction, and that the distortion is limited if synchronization occurs between motor units with similar action directions.

Homogenous Approximation for Synchronization Analysis

The purpose of this section is to show that, under certain conditions, synchronization can be analyzed using linear algebra. The conditions underlying this analysis are that the set of active motoneurons can be approximated as homogenous in discharge statistics and that there is one impulse response $T(t)$ common to all motor units. By comparison to the Fuglevand motor unit population model, we will show that the homogenous approximation well describes STA applied to the full system in which motor units can have different firing rates and motor unit twitch properties are different among the population of motor units. Presumably, the quality of approximation comes from the fact that differences in motor unit properties are averaged out in the STA process. The homogenous approximation retains the synchronization structure of the motor unit pairs, and generates a simple framework for analyzing different synchronization configurations.

The simulation of contribution functions strongly suggests the linear scaling of contribution function magnitude by the synchronization index: $C_{\text{test,alt}}(t) \approx sC_{\text{test,test}}(t)+$

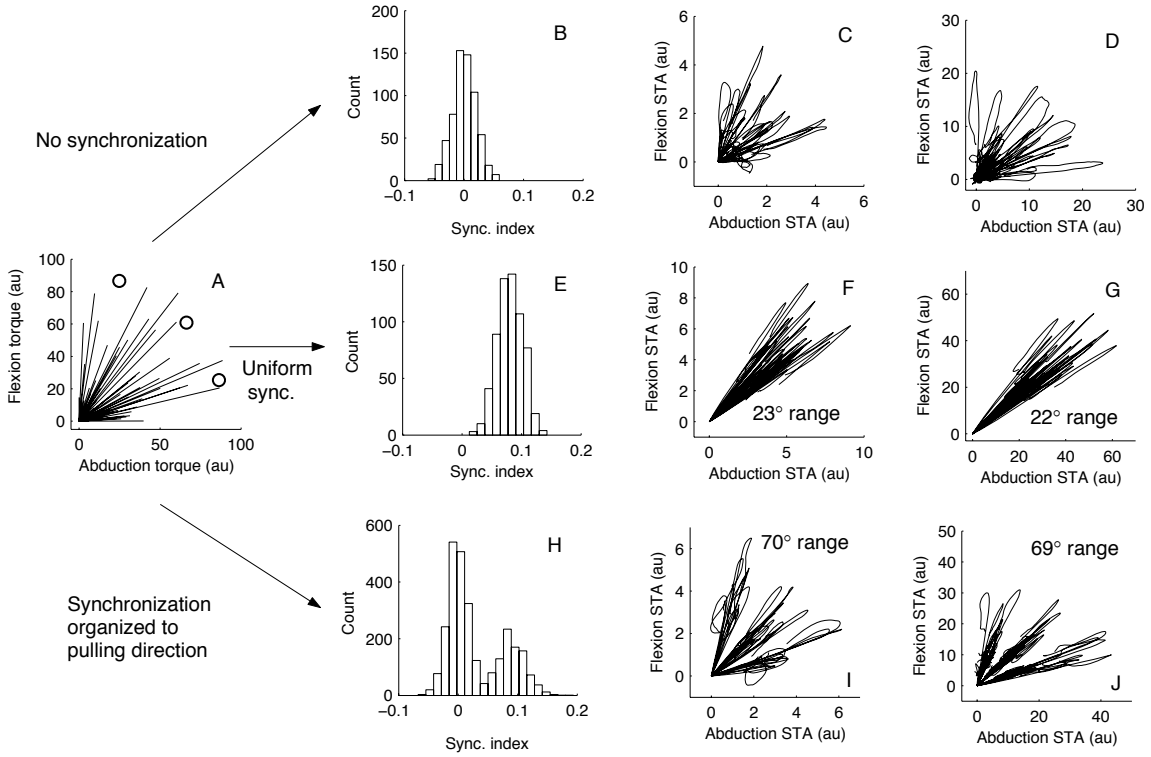

Figure 4.3: The effect of synchronization on STA estimates for motor unit action direction. A. The assumed underlying distribution of action directions for the set of potentially active motor units. Circles become relevant in H-J. B-D. Evaluation of STA trajectories without motor unit synchronization. B. Distribution of synchronization indices between all active motor unit pairs (shown for 5% of maximum; distribution at 15% maximum was similar). C. The STA trajectory from 0 to 100 ms post-spike for each active motor unit at 5% of maximum. D. The STA trajectory for from 0 to 100 ms post-spike for each active motor unit at 15% of maximum. E-G. Evaluation of STA trajectories with synchronization applied uniformly to all motor unit pairs. E. Distribution of synchronization indices between all active motor unit pairs (shown at 5% of maximum; distribution at 15% maximum was similar), with a mean of 0.08 consistent with the measurements of Deluca et al. (1993) from the FDI muscle. F. The STA trajectory from 0 to 100 ms post-spike for each active motor unit at 5% of maximum with uniform synchronization. G. The STA trajectory from 0 to 100 ms post-spike for each active motor unit at 15% of maximum with uniform synchronization. H-J. Evaluation of STA trajectories with non-uniform synchronization. Three groups of motor units were formed by finding the set of active motor units with active directions closest to each of the three directions indicated by the circles in A. Synchronization was only permitted within the motor unit groups, resulting in synchronization organized with respect to motor unit action direction. H. Distribution of synchronization indices between all active motor unit pairs (shown at 15% of maximum; distribution at 5% maximum was similar), showing peaks corresponding to intra- and inter- group synchronization. I. The STA trajectory from 0 to 100 ms post-spike for each active motor unit at 5% of maximum with non-uniform synchronization. J. The STA trajectory from 0 to 100 ms post-spike for each active motor unit at 15% of maximum with non-uniform synchronization.

c, where c is an arbitrary constant. Figure 4.4 compares $C_{\text{test,alt}}(t)$ and $C_{\text{test,test}}(t)$ both in an example (A), and across a range of synchronization indices and firing rates (B). The results of these simulations suggest that $C_{\text{test,alt}}(t) \approx sC_{\text{test,test}}(t) + c$ is an appropriate approximation for a pair of motor units with identical properties under the conditions of relatively low variability in the discharge statistics (i.e. inter-spike interval coefficient of variation ≈ 0.2).

The homogenous approximation allows the contribution function matrix to be represented by the product of a single function of time $C(t)$, and a symmetric time independent matrix C_H (H for homogenous):

$$\begin{bmatrix} z^{(1)}(t) \\ z^{(2)}(t) \\ \vdots \\ z^{(m)}(t) \end{bmatrix} = C(t) \underbrace{\begin{bmatrix} 1 & s_{1,2} & \cdots & s_{1,m} \\ s_{1,2} & 1 & \cdots & s_{2,m} \\ \vdots & \vdots & \ddots & \vdots \\ s_{1,m} & s_{2,m} & \cdots & 1 \end{bmatrix}}_{C_H} \begin{bmatrix} a^{(1)} \\ a^{(2)} \\ \vdots \\ a^{(m)} \end{bmatrix} \tag{4.12}$$

where $s_{\text{test,alt}}$ is the synchronization index between the motor unit pair $(\text{test}, \text{alt})$. In this case we will write $Z = C_H A$, because $C(t)$ is common to all components of Z, and is thus no longer relevant to the direction of the STA trajectories (MUAE direction). Thus, the homogenous approximation maps the changes in STA induced by synchronization into the structure of a matrix. The special case of particular interest that we analyzed is that of a homogenous set of motor units with uniform synchronization index s applied between all motor unit pairs and a uniform distribution of two-dimensional action vectors A. The homogenous contribution matrix C_H has $s_{\text{test,alt}} = s$ for $\text{alt} \neq \text{test}$, so we will denote it $C_H^{(s)}$. Suppose that a set of m active motor units have a set of 2-dimensional action vectors that span an angular

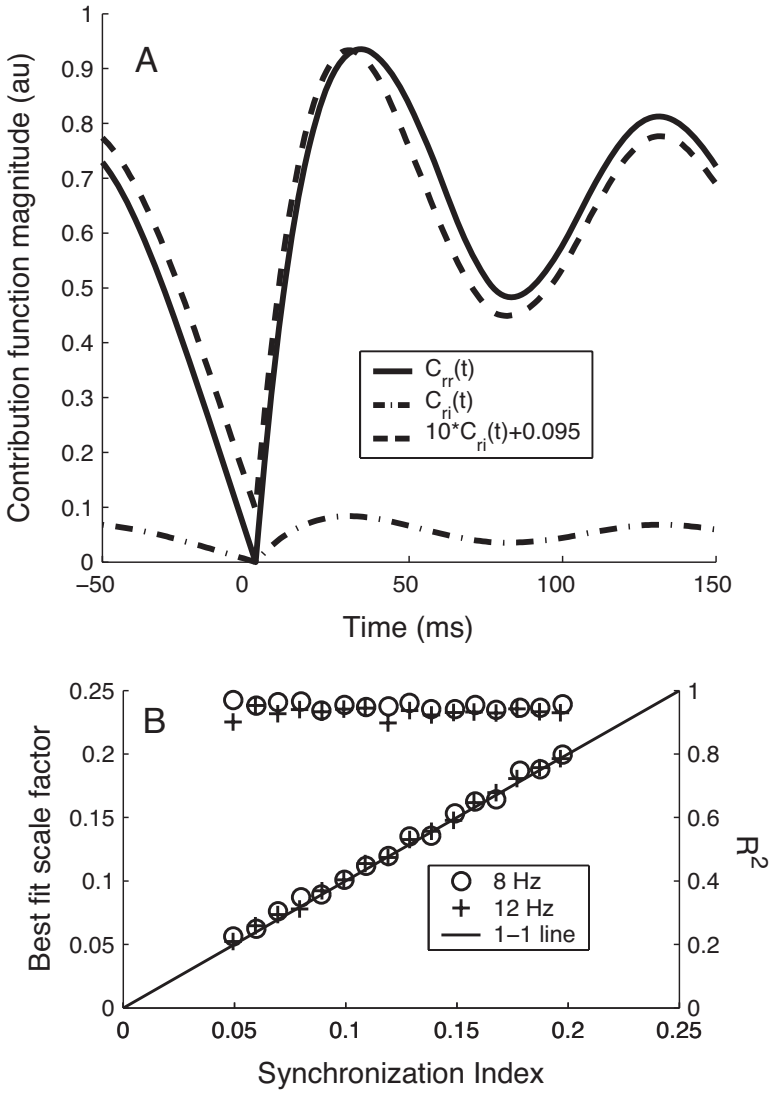

Figure 4.4: Contribution functions scale linearly with synchronization. A. Example of contribution functions derived from a pair of simulated motor units discharging at 10 Hz, inter-spike interval coefficient of variation 0.2, peak force 1 arbitrary unit (au), contraction time 50 ms, with a 10% synchronization index. Notice that $C_{\text{test,test}}(t)$ is 10 times $C_{\text{test,alt}}(t)$ (alternatively $C_{\text{test,alt}}(t)$ is 0.1 times $C_{\text{test,test}}(t)$. B. Empirical evaluation of the proposed relation $C_{\text{test,alt}}(t) \approx sC_{\text{test,test}}(t) + c$ over a range of synchronization indices for discharge rates of 8 and 12 Hz, which is a typical range of rates for STA experiments. The goodness of the approximation is evaluated by least-squares fitting $C_{\text{test,alt}}(t)$ to a linear function of $C_{\text{test,test}}(t)$. The scale factors are shown with the left axis and conform very well to the 1-1 line. The goodness of fit is evaluated using the R^2 coefficient as shown by the right axis; the R^2 values are greater than 0.9 indicating a good similarity in shape between $C_{\text{test,alt}}(t)$ and $C_{\text{test,test}}(t)$.

range of θ_r. The angular range of STA trajectory directions θ'_r is given by

$$\tan\frac{\theta'_r}{2} = \frac{1-s}{1-s+ms}\tan\frac{\theta_r}{2} \tag{4.13}$$

which is derived in the Appendix.

To investigate the usefulness of the homogenous approximation, we simulated the Fuglevand motor unit population model and compared the range of STA trajectory directions to that predicted by Equation 4.13. The results of this comparison are shown in Figure 4.5. Both the full model and the homogenous approximation predict a rapid collapse in the range of STA directions relative to the range of action directions in the presence of synchronization applied uniformly across motor units with different action directions. Equation 4.13 makes an accurate approximation when there are 36 active motor units, and a slightly less accurate by reasonable prediction when 75 motor units are active. Presumably, the homogenous approximation provides a good "rule-of-thumb" because the STA process averages out differences in firing rate, peak force, and contraction time among motor units.

STA Invertibility

The collapse of STA trajectories illustrated in Figure 5 provides a worst-case scenario for the corrupting effects of synchronization. If synchronization is limited to pairs of motor units with similar action directions, the distribution of STA trajectories will be much less distorted with respect to the distribution of action directions. Nonetheless, it is logical to ask whether or not the synchronization effects on STA can be inverted: that is, given a set of STA trajectories and the structure of the contribution matrix, can the underlying distribution of action directions be recovered? This question is equivalent to determining whether or not the contribution matrix is invertible.

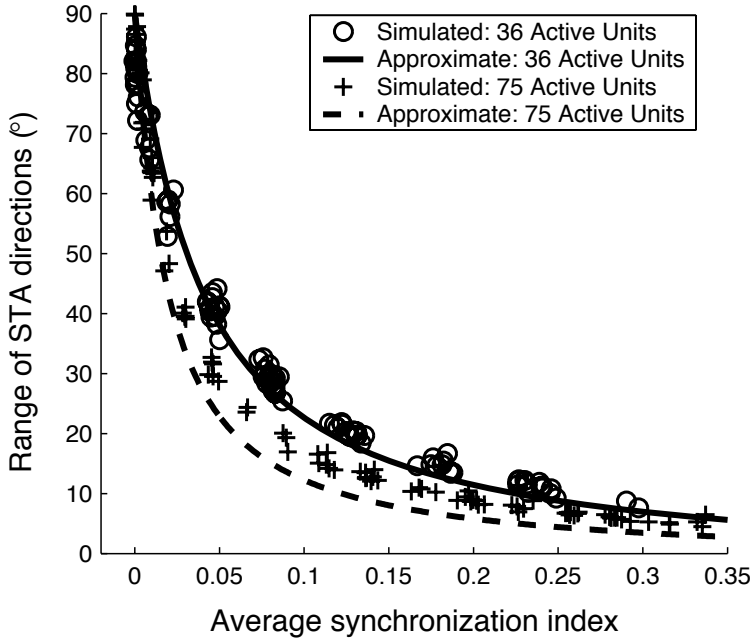

Figure 4.5: Range of STA directions for the simulated Fuglevand motor unit model and homogenous approximation with uniform synchronization. At 5% of maximum, the model predicts 36 active motor units, firing rate ranging from 8.07 Hz to 9.82 Hz, peak force ranging from 1.03 arbitrary units (au) to 3.98 au, and contraction time ranging from 64 ms to 89 ms. At 15% of maximum, the model predicts 75 active motor units, firing rate ranging from 8.17 Hz to 15.5 Hz, peak force ranging from 1.03 au to 17.78 au, and contraction time ranging from 45 ms to 89 ms. Uniform synchronization was applied at various levels, and STA was performed on the two-dimensional torque based on the spike times from all active units. Notice the sharp collapse in the range of STA trajectories relative to the 90° range of action directions as synchronization increases. The approximate curves shown were derived from Equation 4.13. Notice that both the full model and the homogenous approximation predict a sharp collapse of STA trajectories with increasing synchronization. The homogenous approximation with uniform synchronization makes very accurate predictions at 5% maximum, and slight less accurate but acceptable predictions at 15% maximum, which is a reasonable limit to the level at which STA would be performed experimentally at present.

Again, we consider a synchronization index s applied uniformly to all motor unit pairs. In this case, we can explicitly write down the eigenvalues of the contribution matrix:

$$\lambda_1 = (m-1)s + 1 \quad \text{and} \quad \lambda_2, \ldots, \lambda_n = 1 - s \tag{4.14}$$

Notice that since the synchronization index satisfies $0 \leq s \leq 1$, all eigenvalues are positive unless all pairs are perfectly synchronized and $s = 1$. Physiological synchronization is never this large across a population of motor units, and therefore the contribution matrix is invertible in this case. The range of STA trajectories θ' can be directly inverted to the range of action directions θ using Equation 4.13.

Keen and Fuglevand (2004b; 2004a) described non-uniform synchronization with respect to action direction in a population of motor units. They showed that motor unit pairs in different compartments of the extensor digitorum communis muscle expressed different levels of synchronization. Motor unit pairs within a compartment expressed the highest synchronization levels, while pairs in adjacent compartments expressed less but significant synchronization (Keen and Fuglevand, 2004a). They also showed that while intraneural stimulation of motor units produced force on a single finger, STA gave the impression that motor units generated force on multiple fingers (Keen and Fuglevand, 2004b).

We consider whether the effect of synchronization can be removed in this case of non-uniform synchronization. We suppose that there are two compartments of motor units; one group only exerts torque on the index finger while the second group only exerts torque on the middle finger. Motor unit pairs in this population express synchronization index s_{within} within the same compartment, while the motor unit pairs express synchronization index s_{between} between compartments. If we make the homogenous approximation for this system, the STA system can be expressed with

block contribution matrix as

(4.15)

$$Z = \left[\begin{array}{ccc|ccc} 1 & & \boxed{s_{\text{within}}} & & & \\ & \ddots & & & \boxed{s_{\text{between}}} & \\ \boxed{s_{\text{within}}} & & 1 & & & \\ \hline & & & 1 & & \boxed{s_{\text{within}}} \\ & \boxed{s_{\text{between}}} & & & \ddots & \\ & & & \boxed{s_{\text{within}}} & & 1 \end{array}\right] \left[\begin{array}{c} a^{(1)} \\ \vdots \\ a^{(1)} \\ a^{(2)} \\ \vdots \\ a^{(2)} \end{array}\right]$$

where $a^{(1)}$ is the action vector of compartment 1 motor units and $a^{(2)}$ is the action vector of compartment 2 motor units. If we assume that each compartment has m active motor units, a contribution function matrix of this form has $2m-2$ eigenvalues $\lambda_1 = 1 - s_{\text{within}}$ and 2 eigenvalues $\lambda_2 = (m-1)s_{\text{within}} + 1 + ms_{\text{between}}$ and $\lambda_3 = (m-1)s_{\text{within}} + 1 - ms_{\text{between}}$. λ_1 and λ_2 are clearly greater than zero because s_{within} is not near 1 (synchronization is weak). λ_3 can be rewritten as $\lambda_3 = m(s_{\text{within}} - s_{\text{between}}) + 1 - s_{\text{within}}$ which is greater than 0 under the experimental observation that $s_w > s_b$. Therefore, the contribution matrix for this simple non-uniform synchronization configuration has no eigenvalues equal to zero, and is therefore invertible.

Synchronization-insensitive direction vector distributions

The previous section highlighted the finding that if synchronization is known, its effects may be inverted without the need for a specific linear model. Although there are experimental examples of non-uniform synchronization where the synchronization structure is known (Keen and Fuglevand, 2004a), in general, the structure of synchronization with respect to direction vectors may not be known. Therefore, it is appropriate to ask whether there are special action direction distributions A_{SI} for which MUAE direction is synchronization insensitive (SI). For simplicity, we ask this

question in the case of the homogenous approximation with synchronization index s applied uniformly to all motor unit pairs acting in two dimensions of torque output, though this analysis can be readily extended to more complicated synchronization configurations and higher dimensional torque outputs. We conclude the section by studying a specific example of muscle action vectors measured experimentally by An et al. (1983), and show that, if the muscles are appropriately activated to produce zero net torque, STA may be synchronization-insensitive for these action vectors.

To look for action vector sets for which MUAE direction is synchronization insensitive, we need to look at the fixed point structure of the contribution matrix $C_H^{(s)}$. That is, does there exist a set of direction vectors A for which $C_H^{(s)}A = \lambda A$. The application of $C_H^{(s)}$ to the cth column of A results in the cth column of the STA trajectory matrix Z. In order for a direction vector set A to be insensitive to synchronization, the columns of A must be linear combinations of the eigenvectors of $C_H^{(s)}$ with common eigenvalues. Interestingly, $C_H^{(s)}$ has $m-1$ repeated eigenvalues (see Equation 4.14). Linear combinations of eigenvectors with the same eigenvalue are also eigenvectors, so a synchronization-insensitive matrix A of action vectors must have columns in the span of the eigenvectors of $C_H^{(s)}$ that are associated with $\lambda_2, \ldots, \lambda_n$. This set of eigenvectors can be represented as the columns of matrix V. As an example, if the torque vector $Y(t)$ is two-dimensional, we can generate an action direction distribution for which MUAE directions are synchronization insensitive by taking two linear combinations of the columns of V. If these two linear combinations are labelled $v^{(1)}$ and $v^{(2)}$, then we form the action vector distribution A_{SI} for which STA is synchronization insensitive by looking at the *rows* of the following

matrix

$$A_{\mathrm{SI}} = \begin{bmatrix} | & | \\ v^{(1)} & v^{(2)} \\ | & | \end{bmatrix} \tag{4.16}$$

Since any two linear combinations of the eigenvectors in V yields a valid A_{SI}, STA may be insensitive to synchronization for many action vector distributions. Therefore, it is useful to ask if, given an action vector distribution A, is it possible to compute the "nearest" A_{SI} for which STA would be insensitive to synchronization? For simplicity, we consider this question in the context of the homogenous approximation with uniform synchronization. Given a contribution matrix $C_H^{(s)}$ and a action vector distribution A, we first compute the eigenvalue matrix V as above. For any non-zero matrix M, $A_{\mathrm{SI}} = VM$ is guaranteed to produce STA directions that are synchronization-insensitive. We would like to find M such that the overdetermined system $A = VM$ is solved in a least-squares sense. The resultant $A_{\mathrm{SI}} = VM$ will have STA directions insensitive to synchronization and will be the nearest possible distribution to the starting distribution A in the least squares sense. An example of A_{SI} computed in this way for A measured experimentally by An et al. (1983) assuming equal force generated by each muscle is shown in Figure 6G-H.

Figure 4.6 shows simulation results for the muscle action vectors measured by An et al. (1983). All graphs except Figure 4.6D have the same axes and units, which is shown in the upper left of the figure to be the four directions of torque production at the MCP joint with arbitrary units. Figure 4.6A shows the measured action vectors. Figure 4.6B shows the predicted distribution of MUAE directions using the homogenous approximation with uniform synchronization (index=0.08) assuming that all muscles generate the same force. Figure 4.6C shows the simulated STA trajectories

with each muscle contributing 5% of its maximum force. Figure 4.6D shows the distribution of synchronization indices for this simulation across all active motor units (within and between muscles). Figure 4.6E shows the predicted STA directions using the homogenous approximation with uniform synchronization (index=0.08) assuming that muscles are appropriately activated to generate no net torque. Figure 4.6F shows the simulated STA trajectories with each muscle contributing an appropriate force level to achieve no net torque (the average contribution was 5% of each muscle's maximum). Notice that the homogenous approximation with uniform synchronization accurately predicts the simulated STA trajectory direction when each muscle is generating the same force, but does not accurately predict the synchronization-insensitivity under conditions of no net torque. Figure 4.6G shows the nearest distribution (in the least-squares sense) of action vectors to the vectors in Figure 4.6A for which STA is insensitive to synchronization when all muscles contribute equal amounts of force. Figure 4.6H shows simulated STA trajectories for the distribution of action vectors shown in Figure 4.6G. These results suggest that synchronization-insensitive STA might be successfully applied experimentally if the subject were required to co-contract to generate zero net torque.

4.5 Discussion

This paper presents a simple framework for the analysis of the effects of firing rate and synchronization on the STA of joint torque based on motor unit discharge. If the joint torque output is multidirectional, and motor units discharge independently, STA trajectories are unaffected by firing rate and correctly represent the action direction of the motor unit being studied. This observation is significant because it decouples the effects of firing rate and synchronization on STA. When STA is

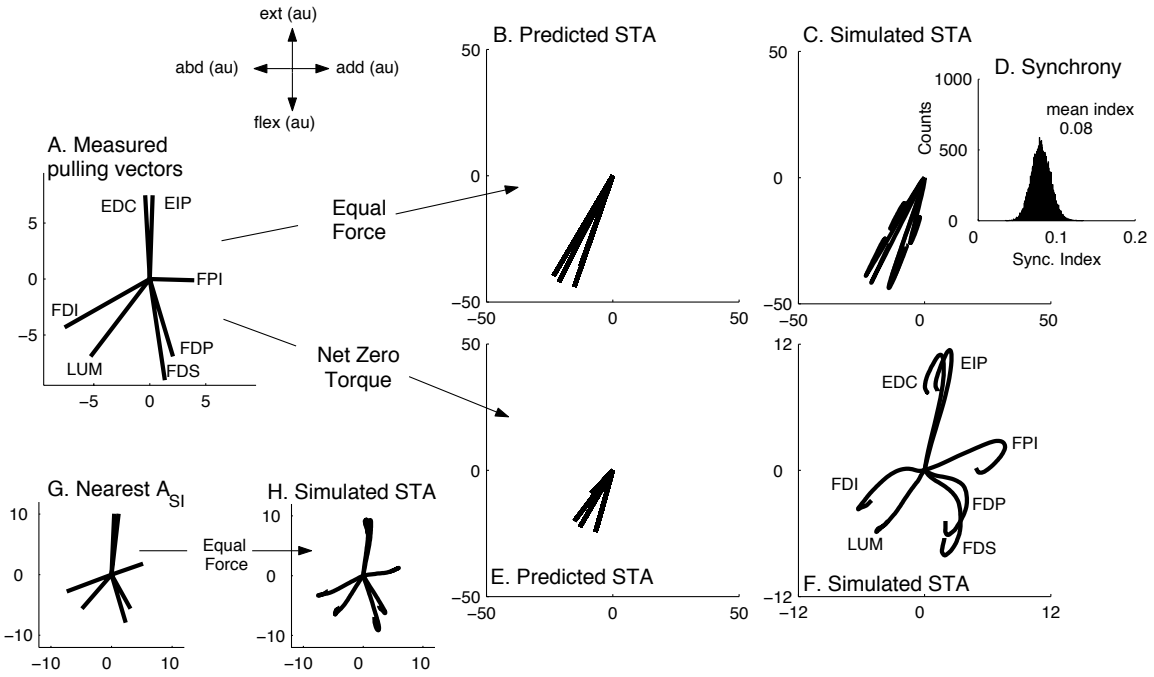

Figure 4.6: Analysis of STA synchronization insensitivity of the muscle action directions measured by An et al. (1983). Each plot (with the exception of D) has the same axes and same arbitrary units (au), shown in the upper left. A. Moment arms measured by An et al. (1983) for muscles controlling the human second metacarpophalangeal (MCP) joint (see text for abbreviations used). B-D: STA results assuming equal force generated by each muscle and uniform weak synchronization between all motor unit pairs with synchronization index of 0.08. B. STA directions predicted by the homogenous approximation with uniform synchronization for the case of equal force exerted by all muscles. C. Numerical simulation results of STA trajectories for all active motor units for the case of equal force exerted by all muscles. D. The distribution of the synchronization index across all active motor unit pairs had a mean of 0.08, which we expect to be an overestimate for the synchronization that can occur between motor units in different muscles. E-F: STA results assuming muscle forces are chosen so that the net torque about the MCP joint is zero. Muscles forces were chosen using quadratic programming to minimize total squared muscle force while requiring that the force in each muscle was larger than a small positive amount. E. STA directions predicted by the homogenous approximation with uniform synchronization. F. Numerical simulation results of STA trajectories for net zero torque. The distribution of the synchronization index between motor unit pairs during the net zero torque simulation was identical to the distribution shown in D. G-H: Analysis of the least-squares nearest distribution of action vectors to those measured by An et al. for which STA is insensitive to synchronization assuming equal force in all muscles. G. The nearest distribution of action vectors to the vectors in A for which STA is synchronization insensitive assuming equal force in all muscles. H. Simulated STA trajectories for the equal activation of muscles with the action vectors shown in G. The net zero torque case examined had an average excitation of 5% maximum, so 5% maximum was also used for the case of equal force.

applied to estimate motor unit twitch contractile properties, firing rate leads to the underestimation of peak force while synchronization leads to the overestimation of peak force (Thomas et al., 1990a; Keen and Fuglevand, 2004b). These competing effects make the interpretation of STA waveforms difficult. However, our analysis framework would suggest that any distortion of the direction of STA trajectories from averaging multiple dimensions of joint torque would result from synchronization, not firing rate.

We analyzed the effects of synchronization on STA estimates of motor unit action direction and showed that even weak synchronization applied to motor units with different action directions could significantly alter STA estimates of action direction. We constructed our synchronization analysis based on an approximation that motor units were homogenous in contractile properties and firing statistics. This approximation is only justified by comparison to the simulation of the Fuglevand motor unit population model with non-homogenous motor units. Even under conditions of weak uniform synchronization across motor units with different action directions, STA would indicate that all motor units act in approximately the same direction. We showed that synchronization-induced distortion could be removed both for uniform synchronization and a specific case of non-uniform synchronization. Lim et al. (1995) considered whether firing-rate distortion of STA estimates of contractile properties could be removed. Removal of firing rate distortion requires the assumption of a particular model for the twitch waveform. The removal of synchronization-induced distortion does not require a specific twitch waveform because its effects are common to the multiple dimensions of torque output. Finally, we showed that there are distributions of motor unit action directions for which STA is insensitive to synchronization.

Our analysis may also be applicable to STA of postsynaptic membrane potential based on extracelluar spike recording Komatsu et al. (1988); Matsumura et al. (1996) or STA of muscle activity based on cortical spikes (Fetz and Cheney, 1980). The framework that we developed is based on the assumptions illustrated in Figure 1. If post-synaptic potentials combine under approximately linear spatio-temporal summation, then the same equations apply. If the time-varying postsynaptic potentials from two neurons were simultaneously recorded, it may be appropriate to denote these variables $y_1(t)$ and $y_2(t)$ as in Figure 1. If these potentials were simultaneously averaged based on the spike train $\mathbf{S}_r$ from a reference neuron r, "action vector" $\mathbf{a}_r$ would have the interpretation as the relative actions of neuron r on the output neurons 1 and 2. Our analysis would be useful in predicting the effects of synchronized inputs on the estimation of $\mathbf{a}_r$.

Keen and Fuglevand (2004b) compared STA of multiple dimensions of joint torque based on spikes from extensor digitorum communis (EDC) motor units with intraneural stimulation of EDC motor units. They found that intraneural stimulation produced torque on primarily one finger while STA showed torque on multiple fingers. The authors conclude, based on previous work (Keen and Fuglevand, 2004a), that synchronization was the primary cause of the distortion. Our results agree with this conclusion. However, STA would not have been distorted relative to the underlying distribution of action directions unless there were synchronizing pathways between motor units that had very different action directions. Binder and Powers (2001) showed that common input to a pair of motoneurons may need to be quite strong to produce experimentally-observed levels of synchronization. It remains to be seen whether these common inputs are strong enough to prevent the central nervous system from exploiting the differences in action directions that exists

among motor units within the EDC.

The strong effect of relatively weak synchronization seen in Figures 3 and 5 cautions against STA being used as a direct measure of motor unit action direction. However, STA can be very useful in more subtle ways. Preliminary observations from our laboratory suggest that the first dorsal interosseous (FDI), which contributes torque to both abduction and flexion of the index finger about the MCP joint, may have a 53° range of STA trajectory directions in the abduction/flexion torque plane. Using Equation 4.13 and assuming that the muscle has between 36 and 75 active units when STA measurements were made, we predict that the FDI could have had a 90° range of action directions with a 0.027 uniform synchronization index, or a 60° range of action directions with 0.005 uniform synchronization index, or perhaps anything in between. However, these synchronization indices are much less than literature values for the FDI. Deluca et al. (1993) observed an average 0.08 synchronization index from the FDI, which is smaller than values reported elsewhere (Datta and Stephens, 1990). Given a 90° range of action directions with a synchronization index of 0.08 and 5% MVC activation (36 active units), we would predict a range of STA directions of 27°. Given the same conditions with 15% MVC activation (75 active units), we would predict a range of 15°. If the range of action directions is smaller than 90° and the synchronization index was uniform at 0.08, the range of STA directions would likely be even smaller.

The most direct explanation of this discrepancy is that synchronization is not uniform with respect to action direction. If motor units with similar action directions are more likely to synchronize than units with different action directions, the collapse of STA trajectory directions will not be nearly as dramatic (see Figure 3 H-J). STA is simultaneously indicating that FDI motor units may both span a sizable range of

action directions, and motor units with different action directions may receive less common input than those with similar action directions.

STA is potentially useful for studying how motor unit synchronization is organized with respect to motor output. The framework developed in this paper demonstrates how STA trajectories are generated by an interaction between motor unit action directions and crosscorrelograms between motor unit pairs. Since performing STA in a multidirectional setting removes firing rate distortion, it allows the direct examination of how synchronization is organized with respect to action direction. A broad distribution of STA trajectories observed from a motor unit system implies both that the active motor units have a broad distribution of action directions, and that there is very limited synchronization between motor units with different action directions. This analysis may aid in the interpretation of STA studies, and may give significant clues about how descending pathways are organized to control movement.

In Chapter V, the theoretical work of this chapter will be extended to construct a method capable of estimating muscle mechanical action. The extension is straightforward: suppose the discharge times in each and every active motor unit are known, but not which motor unit was associated with each discharge. Suppose these discharge times are merged into a single spike train. If STA is performed on this spike train, the associativity of addition would produce the average STA trajectory across the set of active motor units, which might be considered a reasonable estimate for the action of the muscle. In general, finding the discharge times of all motor units within a muscle is experimentally prohibitive, but the surface EMG signal retains qualitatively similar information because the electrical potential generated at the skin surface by a motor unit discharge is relatively brief. Chapter V will show how a surface EMG signal can be coupled with fluctuations in the net endpoint force vector

to construct a muscle action estimate, in analogy with how, in this chapter, a motor unit spike train was coupled with fluctuations in the net endpoint force vector to construct a motor unit action estimate

4.6 Acknowledgements

We would like to thank Dr. C.J. Heckman and Dr. A.D. Kuo for helpful discussions. This work was supported by NSF grants DMS-0305837 and DMS-0604307 to AMB and a NICHD R24 grant to WZR.

4.7 Appendix

Here we derive Equation 4.13, which relates the angular range of STA trajectories to the angular range of two-dimensional action directions using the homogenous approximation with uniform synchronization. We suppose that n active motor units, each pair of motor units being uniformly synchronized with synchronization index s, exhibit a range of action directions θ_r. Given the homogenous contribution function matrix with uniform synchronization

$$Z = \begin{bmatrix} 1 & s & \cdots & s \\ s & 1 & \cdots & s \\ \vdots & \vdots & \ddots & \vdots \\ s & s & \cdots & 1 \end{bmatrix} A \tag{4.17}$$

we need to determine what angular range θ_r' is exhibited by the rows of Z given that the rows of A exhibit a range of θ_r. We observed in computer simulations that the same range of θ_r' was observed regardless of whether A had m rows with directions uniformly distributed over a range of θ, or $m/2$ rows at one angle and the other $m/2$ rows at an angle of θ from the first set. We visualize this transformation from action

direction to STA direction as:

$$\begin{bmatrix} z^{(1)} \\ \vdots \\ z^{(\frac{m}{2})} \\ z^{(\frac{m}{2}+1)} \\ \vdots \\ z^{(m)} \end{bmatrix} = \left[\begin{array}{ccc|ccc} 1 & & s & & & \\ & \ddots & & & s & \\ s & & 1 & & & \\ \hline & & & 1 & & s \\ & s & & & \ddots & \\ & & & s & & 1 \end{array}\right] \begin{bmatrix} a^{(1)} \\ \vdots \\ a^{(\frac{m}{2})} \\ a^{(\frac{m}{2}+1)} \\ \vdots \\ a^{(m)} \end{bmatrix} \tag{4.18}$$

Given that

$$\begin{aligned} a^{(1)}, \ldots, a^{(\frac{m}{2})} &= \begin{bmatrix} \cos\frac{\theta_r}{2} & \sin\frac{\theta_r}{2} \end{bmatrix} \text{ and} \\ a^{(\frac{m}{2}+1)}, \ldots, a^{(m)} &= \begin{bmatrix} \cos\frac{\theta}{2} & -\sin\frac{\theta}{2} \end{bmatrix} \end{aligned} \tag{4.19}$$

it is clear that

$$z^{(1)}, \ldots, z^{(\frac{m}{2})} = u^{(1)} \quad \text{and} \quad z^{(\frac{m}{2}+1)}, \ldots, z^{(m)} = u^{(2)} \tag{4.20}$$

where $u^{(1)}$ and $u^{(2)}$ are single two-dimensional vectors. The angular range θ_r' of the STA directions will be the angle between $u^{(1)}$ and $u^{(2)}$. We can write down $u^{(1)}$ and $u^{(2)}$ explicitly as

$$\begin{aligned} u_1^{(1)} &= \cos\frac{\theta_r}{2} + s\left(\frac{m}{2}-1\right)\cos\frac{\theta_r}{2} + s\frac{m}{2}\cos\frac{\theta_r}{2} \\ u_2^{(1)} &= \sin\frac{\theta_r}{2} + s\left(\frac{m}{2}-1\right)\sin\frac{\theta_r}{2} - s\frac{m}{2}\sin\frac{\theta_r}{2} \\ u_1^{(2)} &= \cos\frac{\theta_r}{2} + s\left(\frac{m}{2}-1\right)\cos\frac{\theta_r}{2} + s\frac{m}{2}\cos\frac{\theta_r}{2} \\ u_2^{(2)} &= -\sin\frac{\theta_r}{2} - s\left(\frac{m}{2}-1\right)\sin\frac{\theta_r}{2} + s\frac{m}{2}\sin\frac{\theta_r}{2} \end{aligned} \tag{4.21}$$

Vectors $u^{(1)}$ and $u^{(2)}$ are of the form $u^{(1)} = [\alpha, \beta]$ and $u^{(2)} = [\alpha, -\beta]$ where

$$\begin{aligned} \alpha &= (1 - s + ms)\cos\frac{\theta_r}{2} \\ \beta &= (1-s)\sin\frac{\theta_r}{2} \end{aligned} \tag{4.22}$$

We also have

$$\tan \frac{\theta'_r}{2} = \frac{\beta}{\alpha} \tag{4.23}$$

Substituting Equation 4.22 into Equation 4.23 gives the desired result.

$$\tan \frac{\theta'_r}{2} = \frac{1-s}{1-s+ms} \tan \frac{\theta}{2} \tag{4.24}$$

CHAPTER V

Does muscle mechanical action change depending on the task direction?

5.1 Abstract

An individual muscle's mechanical action - its contribution to the net force produced in extrinsic task space - may be described as a vector whose magnitude is scaled by the muscle activity and whose direction is determined by musculoskeletal geometry. The direction of this action is usually assumed constant for a specific posture, independent of the task being performed. But some muscles' motor units are differentially recruited based on task direction (e.g. (Herrmann and Flanders, 1998)); given broad enough insertions these muscles could then potentially produce different actions. Deformable tendon networks in the finger can also cause one muscle to alter the mechanical action of another (e.g. (Valero-Cuevas et al., 2007)). Both possibilities lead to the hypothesis that the direction of muscle action may change with task. We propose a new method for estimating muscle mechanical action *in vivo*, termed EMG-weighted averaging, based on cross-correlation of endpoint forces and surface electromyograms (EMGs). We examined endpoint forces exerted by the distal end of the human index finger in 24 different task directions, keeping posture fixed. These were cross-correlated against EMGs from the first dorsal interosseous (FDI) and the extensor indicis proprius (EIP) to estimate their direction of mechan-

ical action. We found that, while mechanical action directions tended to point along known directions derived from anatomical studies, they also shifted systematically in the direction of endpoint force. The FDI action changed at a rate of 0.13 degrees per degree of task direction change, and the EIP's at 0.36 degrees per degree (both $p < 0.0001$). These results indicate that muscle mechanical action can vary with task, even for isometric tasks at fixed posture. The CNS might therefore compensate for or exploit these changes when coordinating muscles. EMG-weighted averaging may also be useful for estimating mechanical action for cases where no anatomical data is available.

5.2 Introduction: Can muscle action change?

The action produced by a muscle in task space is often characterized as a single vector that remains invariant as long as posture is fixed. Sometimes referred to as muscle pulling direction, muscle action likely depends on musculoskeletal geometry, for example the lengths of body segments and moment arms about the degrees of freedom of joints (Kuo, 1994; Kuo, 2000). Actions have been empirically quantified for cat hindlimb muscles contributing to multidirectional ankle force (Lawrence et al., 1993), monkey forearm muscles contributing to multidirectional wrist force (Hoffman and Strick, 1999), and human thenar motor units contributing to thumb abduction and flexion (Westling et al., 1990).

The assumption of constant mechanical action has become very pervasive in models of neural coordination of muscle. For example, Fagg et al. (2002) attempted to predict the spatial tuning properties of wrist muscles observed by Hoffman and Strick (1999) based on the observed muscle action directions and an optimization criterion. Haruno and Wolpert (2005) used constant muscle action directions to

predict the spatio-temporal activation from the same data set. Todorov (2002) developed a optimal control theory for muscle tuning that assumed constant muscle action vectors.

Extensive work has been done to understand changes in muscle action as posture changes. Changes in muscle action have been investigated in musculoskeletal models (Murray et al., 1995), using MRI images (Fowler et al., 2001), and by applying electrical stimulation (Kamper et al., 2006; Hoffman and Strick, 1999). The distribution of muscle action across the set of involved muscles can change substantially as posture changes, and these action change likely give rise to changes in how muscles are coordinated by the CNS.

Much less work has been done to understand mechanisms that could change muscle action for constant posture tasks, but evidence for such mechanisms exists. Perhaps the simplest example would be a highly compartmentalized muscle. The cat biceps femoris has 3 neuromuscular compartments that have different mechanical actions (Chanaud et al., 1991) and different tuning curves as a function of movement direction (Chanaud and Macpherson, 1991). While the action of each compartment may be constant across a range of directional tasks, if the biceps femoris were considered as a whole, its direction would be characterized as shifting as a function of task because of the tuned activity in the compartments. The activity of single motor units within human muscle have been shown to exhibit activity tuned to task direction (ter Haar Romeny et al., 1982; ter Haar Romeny et al., 1984), with the tuning perhaps not having a clear relation to recording location (Herrmann and Flanders, 1998). This tuning, when coupled with differences in mechanical action for different motor units, could produce changes in muscle action. Also, muscle action could be altered by nonlinear force summation.

For example, different muscles transmit force to the human finger through an elastic tendon network; the direction of torque produced about the finger joints generated by one muscle can be changed substantially by the ratio of forces provided by a set of muscles deforming the tendon network (Valero-Cuevas et al., 2007). An *in vivo* case where muscle force ratios can change dramatically is varying the task direction.

The purpose of this work was to introduce a new method for estimating muscle action for human muscles under conditions of natural excitation, and to determine if this method provided any evidence for muscle action changes during constant posture tasks.

5.3 Methods: How is muscle action estimated *in vivo*?

Muscle mechanical action (henceforth: muscle action) can be characterized using a number of different methods. Cadaveric estimates are useful because they provide a direct measure of mechanical output when tension is applied to various tendons (An et al., 1983), but are limited because it is difficult to maintain the tissue in a relatively intact state and it is also difficult to coordinate multiple muscles in a similar way to the CNS. Estimates based on MRI data provide a unique view of muscloskeletal geometry (Fowler et al., 2001), but are limited by image quality and inability to study active contraction. Electrical stimulation can be used to study muscle action over a wide range of intact postures (Kamper et al., 2006), but it would be useful to have a complementary method that could examine muscle action under conditions of natural excitation by the CNS.

Isometric net endpoint vector variability likely contains a great deal of information about muscle action, and when coupled with electromyographic data, can be used to construct a muscle action estimate. The concept of this approach is first explained,

and followed by a description of the experimental methods.

5.3.1 Concept of EMG-weighted averaging (EWA)

The technique of spike-triggered averaging (STA) (Buchthal and Schmalbruch, 1970; Stein et al., 1972) can be used to investigate the mechanical properties of single motor units. Briefly, STA extracts sections of endpoint force or joint torque subsequent to discharges in a motor unit of interest, and then averages the sections together. The principle behind STA is that, by triggering the averaging based on a particular motor unit, the mechanical output due to that motor unit will always be in a "rising phase", whereas mechanical output from other motor units will be in a random phase. Thus, mechanical output contributions from other motor units will average out, while mechanical output contributions from the motor unit of interest will average to a function relating to the magnitude and time course of the mechanical contribution. Of course, any time correlation among motor unit discharges will adversely affect this process (Taylor et al., 2002), can generate misleading results (Keen and Fuglevand, 2004a; Keen and Fuglevand, 2004b), and will be the limiting factor for determining motor unit action direction (Kutch et al., 2007). Nonetheless, the STA principle can be a powerful tool for gaining insight into motor unit action, if its limitations are carefully considered.

EMG-weighted averaging (EWA) is a natural extension of the STA principle in an attempt to estimate muscle action. The set of active muscles will generate a random net endpoint (force) trajectory (Figure 5.1A). Sections of the net endpoint trajectory, usually 100 ms in duration, are extracted from the force trace. Whereas when performing STA only those segments following a motor unit discharge are used, EWA uses all possible 100 ms long segments, but weights the segment by the amplitude of the surface EMG signal from a muscle being tested at the beginning of the segment

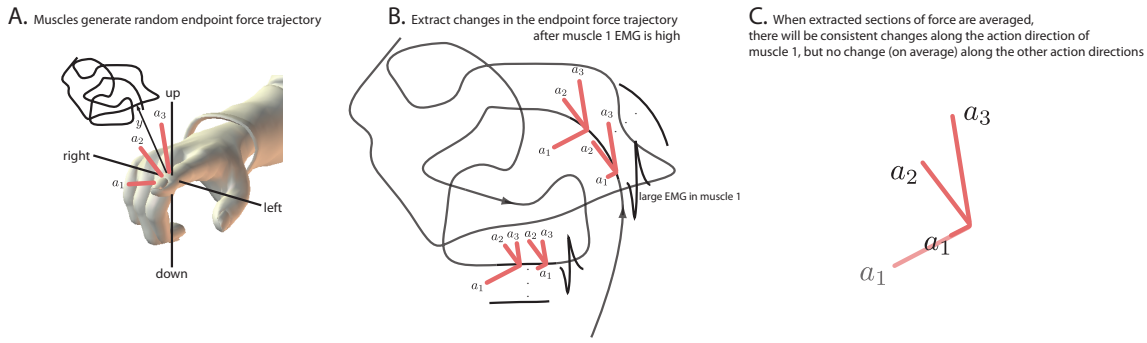

Figure 5.1: Conceptual basis for EMG-weighted averaging (EWA). A. Fluctuation in the tension generated by the set of active muscles will generate a random trajectory for the endpoint force vector. B. Segments are extracted and weighted by the surface EMG from a muscle of interest, muscle 1 in this example. Segments of high weight will signal the imminent development of force in muscle 1, but are likely not to reflect any consistent changes in the other muscles. C. When the weighted force trajectory segments are averaged together, all variation in time will likely be along the action direction of muscle 1.

(Figure 5.1B). In this way, sections of high weight will signal imminent increases in the net endpoint trajectory along the action direction for the reference muscle. If the activity in the muscles is sufficiently uncorrelated, large EMG in the test muscle will not signal any consistent changes in endpoint force generated by the other muscles. Thus, when the weighted-sections are averaged together, all time variation will be along the action direction for the test muscle, whereas the contributions of the other muscles will average to constant vectors and may be subtracted out (Figure 5.1C).

5.3.2 Experimental Methods

This section describes the experimental procedure to acquire the data necessary for EWA. Net endpoint trajectories were measured during the hold period of ramp-and-hold contractions produced by the metacarpophalangeal joint of the human index finger. Surface EMG data from two muscles with distinct action directions were also measured so that EWA could be performed. Five unimpaired male subjects participated in the study. All subjects were right-handed, and used their dominant

index finger to produce isometric forces in different directions and magnitudes in the flexion-extension/abduction-adduction (FEAA) task space. The Northwestern University Institutional Review Board approved the study protocol, and informed consent was obtained from each subject prior to participation.

The experimental apparatus has been described previously (Chapter III). Briefly, subjects were seated with the index finger was casted and placed in a fixed cylindrical tube, so that forces were exerted against the inside of the tube and at an "endpoint" just distal to the DIP joint. This setup maintained both interphalangeal joints extended and approximately aligned the MCP extension axis with the vertical load cell axis. Isometric index finger forces in the FEAA plane were measured using a sensitive 6 axis load cell (JR3, Woodland, CA, Model 20E12A-I25 9N.5). The load cell's resolution (smallest measurable force) was estimated to be 1 mN. These forces were also presented visually to subjects in real time. We displayed a dynamic cursor representing the instantaneous two-dimensional force in the FEAA plane on a computer screen. Forces were recorded at 1000 Hz.

Surface electromyograms (EMG) were recorded from the first dorsal interossesous (FDI) and extensor indicius proprius (EIP). EMGs were recorded using miniature electrode/preamplifiers (DELSYS, Boston, MA) with 2 silver recording surfaces, 5 mm long and 10 mm apart. The preamplifiers have bandwidth 20-450 Hz for surface recordings, with gains set to 100. EMG electrodes were placed according to standard anatomical landmarks and verified with the recommended test maneuvers (Perotto, 2005). EMG signals were sampled at 2000 Hz.

The experimental protocol called for the exertion of endpoint forces in 24 different directions and at 3 different magnitudes. The directions were distributed equally over the plane at 15° increments. A rest trial was collected for each subject to establish

baseline EMG signals. For each trial, the subject viewed the desired force as a target on the visual display, represented in polar coordinates by a static ray for target direction, and a static circle for target magnitude. The subject was instructed to gradually exert force in the target direction, and then to hold the target force as precisely as possible for about 10-20 seconds. The experimenter examined the time-domain force traces on-line. Trials were repeated if forces were found not to be approximately constant. The force feedback display was zeroed, with the subject was at rest, before each set of trials. Subjects were asked to rest for at least ten seconds between each trial, and at least one minute after each group of ten trials.

The force magnitudes were also equally distributed at three levels, chosen to require very minimal effort for all subjects. Because these magnitudes were at discrete levels, we refer to them as task levels 1 - 3. These task levels were distributed at equal intervals, with the highest magnitude level, task level 3, at approximately 2 N in magnitude.

5.3.3 Analytical computations of EWA

EMG-weighted averaging (EWA) is performed by cross-correlating the time-varying net endpoint vector with EMG. Let n denote discrete time, $Y[n]$ denote the endpoint force trajectory, and $E_{\text{test}}[n]$ denote the (processed) EMG in a muscle test. The EWA trajectory for muscle test, denoted $z^{(\text{test})}[n]$, can be computed using the following equation

$$z^{(\text{test})}[n] = \sum_j Y[j+n]E_{\text{test}}[j] \tag{5.1}$$

where the sum is computed over the hold period of the ramp-and-hold contraction. This process is illustrated with representative data in Figure 5.2. We begin with EMG signals $E_{\text{FDI}}[n]$ and $E_{\text{EIP}}[n]$ collected simultaneously from a single subject

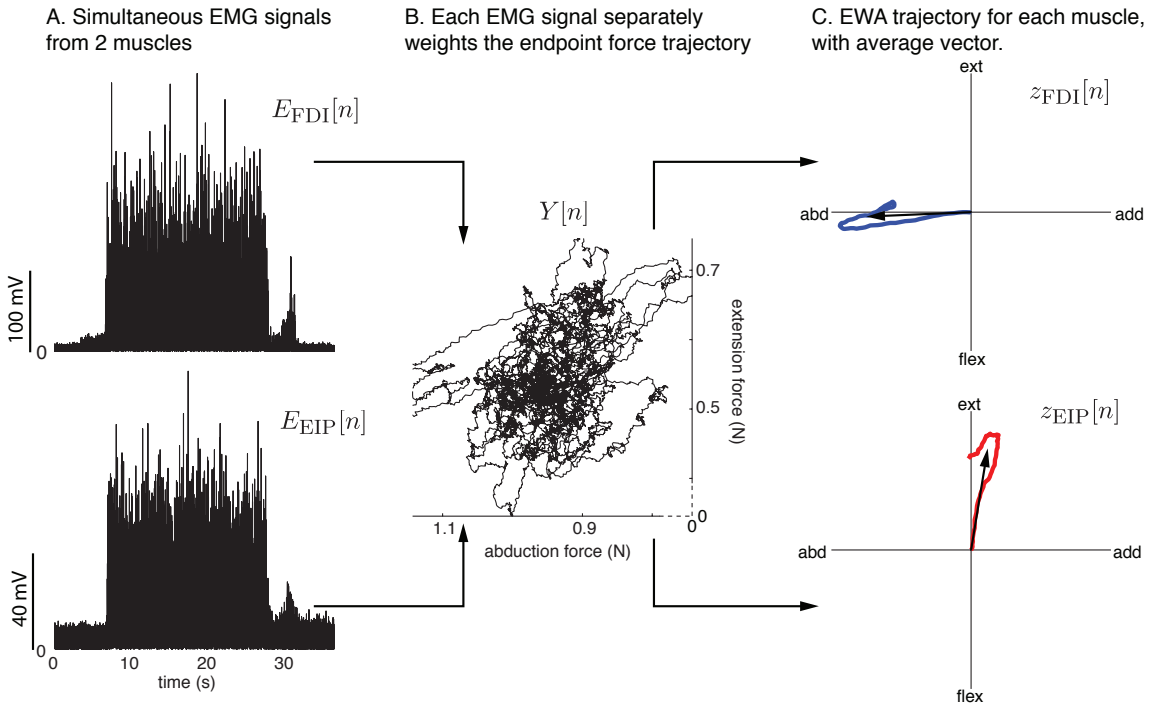

Figure 5.2: Representative EWA data from a single subject during a single task. A. EMG data collected simultaneously from the first dorsal interoesseous (FDI) and extensor indicis proprius (EIP). B. The force trajectory in steady state generated by the action of these (and potentially other) muscles. EMG-weighted averaging (EWA) is performed separately on this force trajectory using the FDI and EIP EMG signals. C. The average trajectory produced by EWA for the FDI and EIP over a 100 ms period. The trajectory is averaged across time to generate a single EWA vector, which serves as the mechanical action estimate (MAE) for these muscles.

during a single trial (Figure 5.2A). These signals are used, in conjunction with the hold period endpoint force trajectory $Y[n]$ (Figure 5.2B), to generate two EWA trajectories (Figure 5.2C). A muscle action estimate (MAE) was formed by averaging the trajectory over its 100 ms duration, and can be represented as a vector with magnitude and direction (Figure 5.2C). The vector magnitude was normalized to the EWA vector magnitude computed for the subject's rest trial. Thus an EWA vector magnitude of 100 means that the EWA vector was 100 times as large as an EWA vector constructed from noisy EMG data. Thus the EWA vector magnitude is a signal-to-noise ratio.

Representative results show that raw EMG signals can be used in EWA. The results presented will show how the MAE vectors approximately align with anatomical estimates for the action of these muscles, but show that the MAE vectors shift in direction as the task direction changes. In order to ensure that these shifts were not a trivial consequence of voluntary control or low-frequency correlated oscillations among motor units (Deluca and Erim, 1994), EMG data that had been high-pass filtered above 5 Hz (4th order Butterworth filter with -3 dB at 5 Hz) was used in the EWA analysis. A value of 5 Hz was chosen due to exploratory data analysis that revealed that EMG signal in the 0-5 Hz range generated very large shifts in MAE direction, while results remained qualitatively unchanged over different frequency bands provided that the 0-5 Hz was removed.

Shifts in MAE direction were quantified as follows. Muscle recruitment curves were computed from EMG data and plotted as a function of task direction. Raw EMG traces were first rectified and averaged across the hold period of each trial and the corresponding rest period, with the difference between the two serving as the net EMG. We fitted a cosine tuning curve (Hoffman and Strick, 1999; Todorov, 2002) to net EMG data within each subject and task level (24 values for each task level), minimizing the sum-squared error. The EMG data for each task level and subject were then normalized to the maximum of the fit, thus avoiding normalization to a spurious maximum in the data. Once the EMG data were normalized, comparisons of directional tuning could be made across task levels and subjects. Task direction ranges exhibiting significant EMG for each muscle were determined as follows. Normalized EMG data were grouped by 15° task direction bins. An ANOVA was performed on the normalized EMG data using the task direction bin as the factor. A task direction was defined for each muscle for which the muscle was likely inactive.

A post-hoc multi-comparison test with Bonferroni correction was then performed to identify a range of task directions significantly greater ($p < 0.05$) than the inactive direction.

A linear regression analysis was performed between MAE direction and task direction for each muscle separately over the range of task directions for which the muscle was significantly active. This analysis was performed both across and within subjects.

5.3.4 EWA governing equations and computational model

Simple equations and a computational model were constructed to estimate the probability that the results were generated purely by correlation in the EMGs among multiple muscles without any real changes in muscle action. We assume that the muscle command to muscle i can be measured in the form of an EMG signal $E_i(t)$, where t represents continuous time. We assume that muscle commands are converted into muscle activity by a filter having impulse response $T_i(t)$ for muscle i. Finally, we assume that the net endpoint trajectory can be expressed as a weighted linear sum of the muscle action vectors $a^{()}$, the weighting performed by the activity in each muscle. These assumptions lead to the following equations for the net endpoint trajectory, where $*$ represents the convolution operator:

$$Y(t) = a^{(1)}T_1(t) * E_1(t) + \cdots + a^{(m)}T_m(t) * E_m(t) \tag{5.2}$$

For simplicity of notation, we drop t explicitly so we can illustrate the dependence on *time shift* Δt. The EWA trajectory $z^{(1)}(\Delta t)$ can be computed; for simplicity, we compute $z^{(1)}(\Delta t)$. $\star$ represents the cross-correlation operator

$$z^{(1)}(\Delta t) = [Y \star E_1](\Delta t) = a^{(1)}T_1 * E_1 \star E_1 + \cdots + a^{(m)}T_m * E_m \star E_1 \tag{5.3}$$

If cross-correlation among the EMG signals is modest, Equation 5.3 predicts that $z^{(1)}(\Delta t)$ will have the same direction as $a^{(1)}$. This results from the fact that $[E_i \star E_j](\Delta t)$ is a constant function of Δt while the auto-correlation $[E_i \star E_i](\Delta t)$ is not. Thus, if the cross-correlation is computed over a sufficiently long interval, the EWA trajectory can be expressed as $z^{(1)}(\Delta t) = a^{(1)} q(\Delta t) + c$ for some function $q(\Delta t)$ and constant c.

If $[E_i \star E_j](\Delta t)$ is not constant when $i \neq j$, muscle j will make a contribution to $z^{(i)}(\Delta t)$ in the direction of $a^{(j)}$ depending on how active muscle j is. Thus, it is possible that correlation among EMG signals will cause the EWA trajectory to shift direction as the activity in a group of muscles changes, for instance, as the task direction is changed. To estimate how large the correlation would need to be to produce a certain change in MAE direction, Equation 5.2 was simulated. The muscle action for each muscle came from cadaveric estimates for the 7 muscles that control the human index finger MCP joint (An et al., 1983). Following the modeling work of Haruno and Wolpert (2005), we assume that muscle commands can be represented by a constant function that is corrupted by gaussian noise with standard deviation proportional to the signal mean. We further assume that muscle force is generated by linearly filtering the muscle commands by a second-order filter with time constants of 30 and 40 ms, representing excitation and activation, respectively (Van der Helm and Rozendaal, 2000). The average command to each muscle was calculated by choosing commands to minimize endpoint force variance (Todorov, 2002). Correlation was imposed uniformly between simulated EMG signals to a specified level using standard methods based on the Cholesky decomposition.

In analogy to the experimental data analysis, regions of significant activity were determined for the FDI and EIP, and the slope of the MAE direction versus task

direction was computed. Different amounts of uniform correlation were explored until values were found that matched the observed slopes.

5.4 Results: Muscle action shifts with task direction

These results will demonstrate that MAE direction for both the FDI and EIP muscles changes significantly as task direction changes, and that uniform correlation among all muscles pairs is unlikely to account for these results.

Plots of MAE magnitude versus MAE direction reveal that MAE vectors of large magnitude tend to have their directions clustered near anatomical estimates (Fowler et al., 2001) regardless of task direction (Figure 5.3A). Examining more closely the dependence of MAE direction on of task direction (Figure 5.3B) reveals that MAE direction appears to depend linearly on task direction. This result would not be predicted by Equation 5.3 if EMG signals from pairs of muscles were uncorrelated. In this case, constant MAE direction as a function of task direction would be expected.

Linear regression analysis indicates that MAE direction changes with task direction were highly significant. Linear regression applied to data grouped across subjects (Figure 5.4) revealed that both muscles exhibited regression slopes (FDI slope: 0.13, EIP slope: 0.36) significantly greater than 0 ($p < 0.0001$) and that the EIP slope was significantly greater than the FDI slope ($p < 0.05$). When linear regression analysis was performed on data from each subject individually, similar results were found, except one subject's EIP data did not exhibit a significant slope at the 0.05 level.

The possibility of these MAE direction shifts being obviously related to EMG correlation was examined by looking at the EMG-EMG cross-correlation functions for the FDI and EIP over a region of task directions exhibiting significant coactivation of these muscles. EMG-EMG cross-correlation functions were normalized to auto-

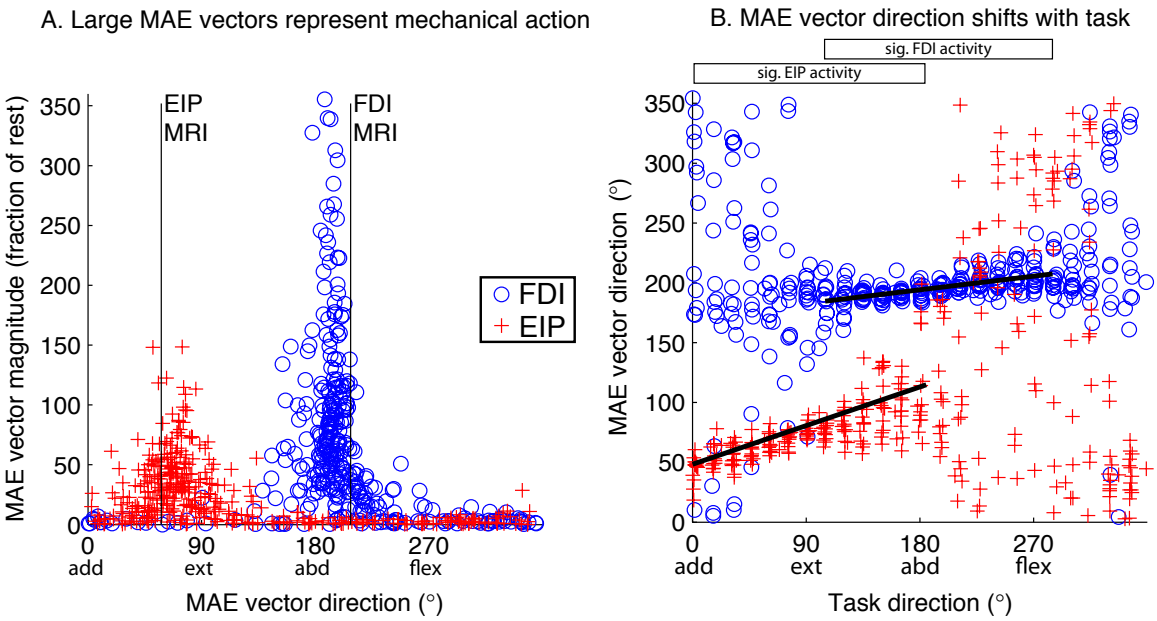

Figure 5.3: Muscle action estimates (MAE) are close to anatomical data, but shift as a function of task. A. The amplitude of the MAE vector for each trial is normalized to the amplitude of the MAE vector during the rest trial. MAE vectors that are relatively large in amplitude cluster near the pulling directions of these muscles as estimated from MRI data (Fowler et al., 2001). B. The direction of the MAE vector shifts gradually toward the task direction as the task direction is changed. Bars indicate task regions of significant EMG activity for the two muscles, and lines show best-fit linear regression lines, computed over the regions of significant EMG activity.

correlation functions, and the results indicate that the cross-correlation functions were small compared to auto-correlation functions (Figure 5.5), indicating that these muscles likely had a limited impact on each other's EWA trajectory. Dividing the peak of the FDI-EIP cross-coorelation function by the peak of the FDI-FDI auto-correlation function gives the FDI-EIP correlation ratio, and provides a measure of the impact the EIP can have on the FDI MAE direction. Dividing the peak of the EIP-FDI cross-correlation function by the peak of the EIP-EIP auto-correlation function gives the EIP-FDI correlation ratio, and provides a measure of the impact the FDI can have on the EIP MAE direction. A model was used to estimate the ratios required among all muscle pairs to obtain the experimentally-observed MAE

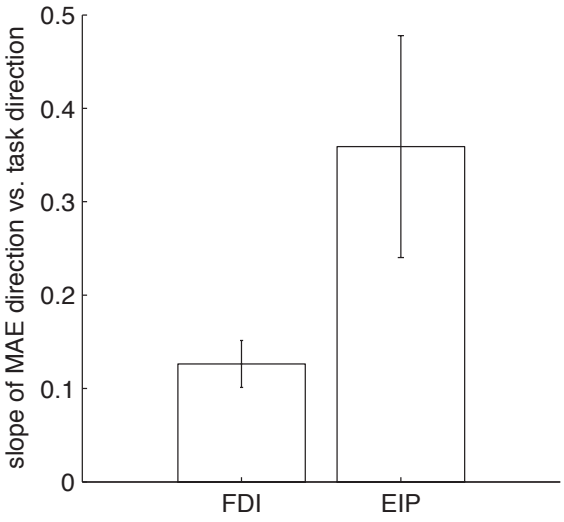

Figure 5.4: Best-fit linear regression slopes for first dorsal interosseous (FDI) and extensor indicis proprius (EIP) across all subjects. The slope describes how quickly the MAE direction changes as task direction changes. Error bars indicate 95% confidence intervals. Both slopes were sigificantly greater than zero ($p < 0.0001$) and the EIP slope was significantly greater than the FDI slope ($p < 0.05$).

direction - task direction slopes. The model predicted that muscle EMG signals would require a uniform correlation ratio of 0.11 to explain the FDI slope, but an FDI-EIP ratio of only 0.0259 was observed. Likewise, the model predicted that muscle EMG signals would require a uniform correlation ratio of 0.19 to explain the EIP slope, but an EIP-FDI ratio of only 0.0375 was observed.

5.5 Discussion: Possibilities and pitfalls

This work has shown that the direction of force associated with electrical activity in two index finger muscles changes as the task direction changes for constant posture tasks. This section explores possible scientific interpretations of this work, along with methodological caveats that need to be considered.

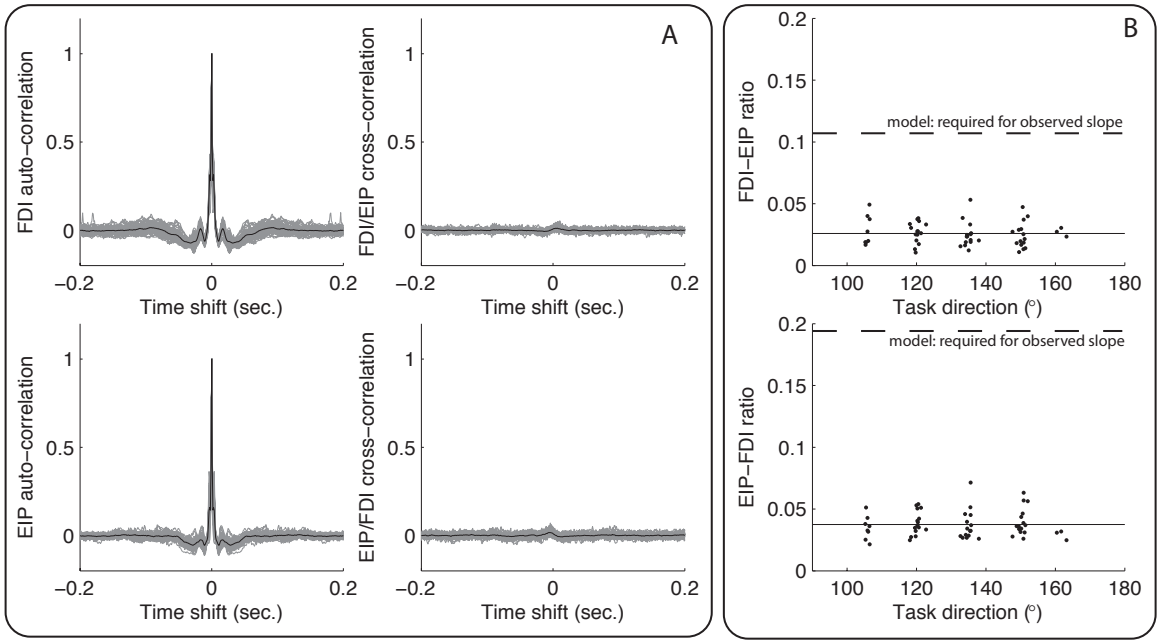

Figure 5.5: Can correlated EMG signals account for the change in muscle action direction? The region of significant EMG activity in both the first dorsal interosseous (FDI) and the extensor indicis proprius (EIP) was determined, indicating the region of likely cooperation between these muscles (105°-165°). A. For every task in this region, the EMG cross-correlation and auto-correlation were calculated as a function of time shift. Within each trial, the FDI/EIP cross-correlation was normalized to the FDI auto-correlation at zero time shift, which was then normalized to have a peak of 1. Within each trial, the EIP/FDI cross-correlation was normalized to the EIP auto-correlation at zero time shift, which was then normalized to have a peak of 1. Dark curves represent averages across all trials while light curves represent the individual trials. B. The likely contribution to the muscle action estimates (MAE) from EMG-EMG correlation was estimated. The FDI-EIP ratio was determined by dividing the peak of the normalized FDI/EIP cross-correlation by the FDI auto-correlation, and represents the potential contribution of the EIP to the FDI MAE. The EIP-FDI ratio was determined analogously. The dots represent the ratios for each trial, while the horizontal lines show the average ratio across all tasks. For this range of task directions, the FDI and EIP are likely two of the dominant muscles, yet the correlation contribution to each others MAE is largely limited. The horizontal dashed lines indicate the model-estimated amount of uniform correlation among all muscle pairs required to explain the observed MAE direction versus task direction slope for each muscle.

5.5.1 Scientific possibilities: variable muscle action

There are two readily apparent mechanisms that could change the action direction for a muscle. First, the muscle could be composed of motor units with different actions, *and* these motor units could be activated differently for different task directions. Second, muscle could transmit their force to compliant structures, such as tendon networks, rather than directly to the skeleton. The precise combination of muscles pulling on the compliant structure could alter the action direction of any muscle connected to the structure.

The FDI is a good candidate for action direction change via the first mechanism. Desmedt and Godaux (1981) observed that 8% of FDI motor unit pairs studied switched their recruitment order when the task direction was switched from MCP abduction to MCP flexion. Thomas et al. (1986), using the spike-triggered averaging technique, found evidence that different FDI motor units had slightly different mechanical action directions in the abduction-flexion task plane. Though no study has provided direct evidence that these two phenomena are coupled to change the FDI action direction, the observed MAE direction shifts for FDI found in this study may reflect these processes.

The EIP is a good candidate for action direction change via the second mechanism - nonlinear force summation due to compliance. The EIP inserts into the compliant extensor mechanism of the finger along with the first palmar interosseous, and first lumbrical muscle, both of which act on the MCP joint in very different directions compared to the EIP (Valero-Cuevas et al., 1998).

This study found that the change in EIP action direction was significantly more substantial compared to the FDI action direction change. Though the FDI tendon may insert into the extensor apparatus (Kamper et al., 2006), its interaction with

the apparatus is likely less than that of the extensors (Long, 1968; Tubiana, 1987). The extensor apparatus may be able to change muscle action quite substantially (Valero-Cuevas et al., 2007). In contrast, the range of mechanical action directions exhibited by FDI motor units may be limited (Thomas et al., 1986), leading to the expectation of smaller muscle action direction changes. Thus, the interaction between the extensor mechanism and the FDI may partially explain the differences in MAE direction shifts observed experimentally for these muscles.

If muscle action does shift by one of these mechanisms, there are consequences for how the CNS coordinates muscles. Are the muscle action shifts reflective of a deliberate motor plan implemented by CNS circuity to optimize movement? Or, are the shifts an inevitable consequence of biomechanical constraints, that must be circumvented or exploited?

5.5.2 Methodological pitfalls: the curse of correlation

There are clear advantages for using EWA to estimate muscle action. For superficial muscles, such as those investigated in this study, changes in EMG can be readily detected by surface electrodes and cross-correlated with changes in force. Of course, the same process can be applied to deeper muscles using a fine-wire electrode, without the need for electrical simulation which may lead to faster fatigue of the muscle (Kamper et al., 2006), and will not reveal the complexities of muscle action that may arise from natural excitation by the CNS.

The main pitfall of EWA is the potential effect of significant EMG-EMG cross-correlation. This affect is analogous to the effects of weak synchronization on STA based on motor unit discharges, and has been well-described in the literature (Taylor et al., 2002; Keen and Fuglevand, 2004b; Kutch et al., 2007). The main difference is that EWA only relies on the condition that EMG signals between *muscles* don't

have significant cross-correlation. This requirement is likely to be less stringent than requiring that there is no significant weak synchronization between spike trains in motor unit pairs within a muscle, needed for STA to be accurate.

We have suggested that the amount of cross-correlation between the FDI and EIP may be insufficient to explain the observed MAE direction changes, if that amount of cross-correlation were found uniform across all muscle pairs. This analysis does not rule out the possibility that cross-correlation is non-uniform among muscle pairs. Further study, involving EMG recordings from all index finger muscles that could contribute to the tasks, is required to make certain that the results are not generated by EMG-EMG cross-correlation.

EWA relies on the condition that relatively high EMG in a particular muscle consistently signals an imminent force contribution from that muscle, while not signaling force contributions from other muscles. To a degree, this condition can be checked by calculating EMG-EMG cross-correlation between muscle pairs, as was done in this study. However, such cross-correlation functions being flat simply implies that increases in EMG in one muscle do not signal imminent events in the EMG of another muscle. There is the possibility, however, that increases in EMG in one muscle could consistently signal imminent muscle force contributions from multiple muscles without signaling increases in EMG in the other muscles. Such a situation could potentially impact the MAE estimates based on EWA without EMG-EMG cross-correlation being detectable. This situation is discussed in (Keenan et al., 2007), and requires further consideration.

EWA uses the size of the EMG signal at any given instant to weight the subsequent net endpoint trajectory. Thus, this process will naturally weight the EWA trajectory toward the mechanical action of motor units that generate larger potentials, either by

being larger motor units or being closer to the recording electrode. However, using intraneural microstimulation, Westling et al. (1990) showed that human thenar motor unit strength was not correlated with action direction, so larger motor units should not skew the EWA trajectory direction. Therefore, if cross-talk from other muscles to the recording electrode is minimized, and thus motor units from other muscles are not close enough to the electrode to generate large potentials, EWA trajectories likely reflect changes in the net endpoint trajectory correlated with the muscle of interest.

5.6 Conclusion

A new method for estimating muscle action *in vivo* was described. This method reveals that muscle action estimates change direction as the task direction changes for constant posture tasks. If such shifts were not observed, it would be difficult to conclude that muscle action could change. Therefore, this study supports the hypothesis that various mechanisms could change muscle action, but does not disprove the hypothesis that muscle action is constant. The question remains: Does muscle mechanical action change depending on the task direction?

5.7 Acknowledgments

The authors would like to thank C. Chikando for help developing the experimental protocol and B. Sinder for writing the computer simulation. This work was supported by NIH NRSA training grant 1F31NS057855-01 to JJK and WZR.

CHAPTER VI

Summary and future work

6.1 Summary

Prior to this work, the role of motor unsteadiness in exploring central nervous system function appeared in three main contexts: 1) examining trial-to-trial variability as subjects repeated ill-posed tasks (uncontrolled manifold analysis), 2) coupling unsteadiness with motor unit discharges (spike-triggered averaging), and 3) examining scaling properties of force variability (signal-dependent noise). This work has significantly broadened the spectrum of approaches to motor unsteadiness by demonstrating additional sources of signal in what otherwise would have been considered motor noise, and increasing the specificity with which this unsteadiness can be processed to make inferences about physiological function.

The first approach, force covariance mapping (FCM), took a multidirectional geometrical approach to motor unsteadiness. FCM simply generates a map of the second-order statistics of endpoint forces exerted across a range of tasks in fixed postures. As was demonstrated experimentally, this deceptively simple approach reveals differences in net endpoint vector fluctuations that are consistent with the CNS using different muscle control strategies for different tasks. For some tasks, the CNS may use a set of motor units having mechanical action highly tuned to the task direction.

For other tasks, the CNS may use a less specific set of motor units with very different mechanical actions. The key insights of this work were that the phenomena of signal-dependent noise in muscle force generation would allow inferences about average muscle activity from measurements of force fluctuations, and that measurements of multidirectional net endpoint vector fluctuations would allow the visualization of CNS control strategies beyond the traditional variability measurements in a single degree of freedom.

The rigorous mathematical analysis of spike-triggered averaging presented in Chapter IV showed that STA was a potential method for estimating motor unit action direction, and made the relation between STA estimates for action direction and weak synchronization precise. In addition, the equations of Chapter IV implied that STA can estimate the direction of muscle action if applied to a merged spike train formed from all active motor units. Though this merged spike train is not typically available experimentally, the surface EMG signal from a muscle of interest contains relatively brief electrical signals occurring when any motor unit in the recording volume discharges. This realization lead to the development of EMG-weighted averaging (EWA) described in Chapter V.

EWA was the second approach to motor unsteadiness presented in this work. Traditionally, net endpoint trajectories have been cross-correlated with a single motor unit spike train to understand motor unit mechanical properties. This work demonstrated that net endpoint trajectories can also be cross-correlated with the surface EMG signal from a muscle of interest to estimate muscle mechanical properties. EWA applied to experimental data from the human index finger support the hypothesis that muscle mechanical action can change for tasks in different directions even when the limb is held in a fixed posture. Future work will be necessary to uncover the

exact mechanism that is producing changes in muscle action.

Descriptions of potential future experimental work are provided here, along with proposals for further new approaches to human motor unsteadiness that are suggested by the current work but not implemented. The first suggests using net endpoint vector statistics to estimate the activity in *each* active muscle for a given task. This contrasts with the less specific conclusions derived from FCM. The second suggests that muscle action estimates could potentially be made directly from the detailed temporal structure of the net endpoint trajectory, thus enabling the determination of the entire set of active muscles, and their action directions, without electrical recordings from any muscle.

6.2 Future experiments

For scientific work testing the predictions of quantitative models, there are usually a set of "unchecked scenarios." In drawing appropriate conclusions from experimental results in this dissertation, these potential scenarios were carefully considered and it was argued that they were unlikely to produce the results. However, experimental checks of these scenarios would likely further the impact of this work, so they are described here.

What these future experiments require most are electrical recordings from a complete set of muscles contributing to tasks in the task space. For these experiments to be as effective as possible, a new experimental system would be invaluable. The index finger was convenient for the experiments described in this work because the net endpoint vector fluctuations were previously known to be large enough to extract useful information (i.e. spike-triggered averages). This disadvantage of this system is that it is controlled by 7 muscles, requiring difficult placements of intramuscular

electrodes. The wrist may be a suitable alternative, as it is acceptable to perform surface EMG recordings from most of the 5 muscles controlling the wrist (Hoffman and Strick, 1999). The disadvantage of the switching to the wrist system is that it is presently unknown whether a load cell apparatus can be engineered that is sensitive enough to detect variability in a muscle's endpoint vectors.

The following sections describe how scenarios could be checked with electrical recordings from a full muscle set.

6.2.1 FCM: EMG evidence of the prime mover strategy

Using force covariance mapping (FCM) results, non-task-directed covariance ellipses were shown to be associated with the cooperation of multiple muscles with different mechanical actions. In order to show definitively that task-directed covariance ellipses are associated with the prime mover strategy, EMG recordings from a complete muscle set would be required.

To illustrate the desired dataset, computer simulated data was generated. A fictive set of 5 muscle action vectors was generated. The standard deviation of activity in each muscle was assumed to be $\sigma_i = 0.05\bar{u}_i$, and muscle activity between muscle pairs was assumed to be uncorrelated. The ellipse field for one task level was simulated (Figure 6.1): muscle activity was chosen to minimize net endpoint vector variance. By comparing the muscle activity tuning curves and the covariance ellipse field, it is possible to see that task-directed covariance ellipses are associated with "activity holes": task directions for which one muscle dominates. Looking for activity holes is only rigorously possible if all activity tuning curves are recorded. Applied experimentally, this analysis would support the contention that task-directed ellipses result directly from the use of a prime mover strategy, and are not an epiphenomenon of muscle activity correlation.

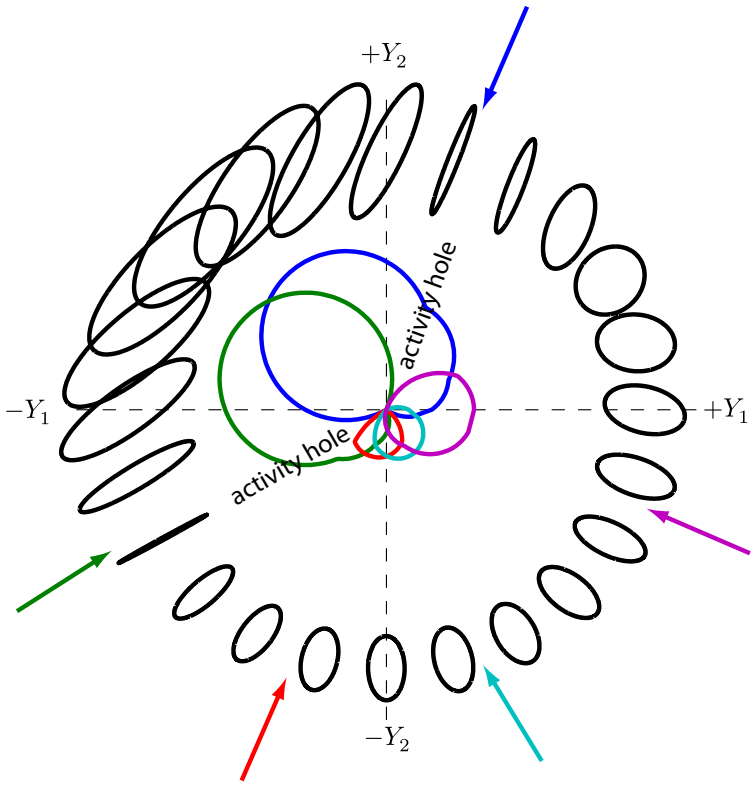

Figure 6.1: Simulated ellipse field compared to muscle activity tuning curves. A fictive system with 5 muscles was generated. Outer arrows indicate muscle action directions. The standard deviation of muscle activity was assumed to be 5% of average muscle activity for all muscles, correlation between muscle pairs was assumed to be 0, and activity tuning curves and ellipse field were simulated by minimizing total net endpoint vector variance. Notice that task-directed (skinny) ellipses correspond to "activity holes"–task directions in which one muscle is the prime mover.

6.2.2 EWA: checking correlation

Following the previous section, if electrical signals from a complete set of muscles were recorded, it would be possible to check if EMG-EMG correlation between muscle pairs was responsible for the shifts in EWA direction observed as task direction changed.

An interesting possibility that arises from having a full set of muscle electrical signals is that correlation can be "inverted out" of MAE estimates based on EWA, in much the same way that weak synchronization could be removed from MUAE

estimates based on STA (Chapter IV). The STA equations presented in Chapter IV are special cases of the more general EWA governing equations presented in Chapter V. Therefore, there will be a matrix of "contribution functions" mapping muscle action vectors to EWA trajectories, and if the correlation between all muscle pairs is known, the contribution function matrix can be estimated and inverted. Muscle action vectors determined in this way could be compared with those estimated from electrical stimulation, so both a direct estimate and an estimate under conditions of physiological excitation could be computed.

6.3 Proposals

A main advantage of using motor unsteadiness as opposed to EMG to study movement is that there is a natural information transmission pathway between the force generated in every motor unit and the endpoint vector; the primary purpose of motor units is to move the endpoint, not to emit electrical signals. The next two sections describe proposals for extending the ideas FCM and EWA to generate a complete picture of muscle action and activity from net endpoint vector measurements alone.

6.3.1 Determining muscle activity from endpoint measurements

The experiments presented in Chapter IV were largely focused on determining if, for a particular task, there is significant activity in muscles with different mechanical actions. We can immediately ask a more general question: can the net endpoint covariance ellipse exactly determine the activity in each muscle with known action directions?

Consider again the simulated ellipse field of Figure 6.1. Task-directed and non-task directed ellipses arise, but there is more information to a covariance ellipse than whether or not it is task-directed. The covariance ellipses in the second quadrant

between $+Y_2$ and $-Y_1$ are "leaning back", and immediately give the qualitative impression that these variability patterns were generated by muscles acting $> 90°$ apart. A covariance ellipse actually holds 5 pieces of information. The 5 muscle action vectors in Figure 6.1 are anatomical estimates for muscles acting in the abduction-adduction/flexion-extension task space of the human index finger task space, with the two flexors and two extensors each represented by a single average vector. So it is possible to have roughly 5 muscles acting in a 2 dimensional task space, and each ellipse can provide 5 equations to try and solve for the unknown muscle activities without measuring any electrical activity in any muscle.

Consider the case of 5 muscles acting in a two-dimensional task space. Assume that the mechanical action vector $a^{(i)}$ is known for every muscle i. These mechanical actions are placed as columns of a matrix A. Assume also that the force variance in every muscle scales linearly with average force, so ${\sigma_i}^2 = k_i \bar{u_i}$ with known k_i for every muscle. The net endpoint vector is Y. Both its mean vector $\bar{Y}$ and its covariance matrix $\mathrm{cov}[Y]$ are measured. Since this matrix is 2×2 and symmetric, it can have at most 3 elements that are distinct.

Under these conditions, the following matrix equation for the vector of average force in each muscle can potentially be solved:

(6.1)

$$\begin{bmatrix} \bar{Y_1} \\ \bar{Y_2} \\ \mathrm{cov}[Y]_{11} \\ \mathrm{cov}[Y]_{12} \\ \mathrm{cov}[Y]_{22} \end{bmatrix} = \begin{bmatrix} a_1^{(1)} & a_1^{(2)} & a_1^{(3)} & a_1^{(4)} & a_1^{(5)} \\ a_2^{(1)} & a_2^{(2)} & a_2^{(3)} & a_2^{(4)} & a_2^{(5)} \\ {a_1^{(1)}}^2 k_1 & {a_1^{(2)}}^2 k_2 & {a_1^{(3)}}^2 k_3 & {a_1^{(4)}}^2 k_4 & {a_1^{(5)}}^2 k_5 \\ a_1^{(1)} a_2^{(1)} k_1 & a_1^{(2)} a_2^{(2)} k_2 & a_1^{(3)} a_2^{(3)} k_3 & a_1^{(4)} a_2^{(4)} k_4 & a_1^{(5)} a_2^{(5)} k_5 \\ {a_2^{(1)}}^2 k_1 & {a_2^{(2)}}^2 k_2 & {a_2^{(3)}}^2 k_3 & {a_2^{(4)}}^2 k_4 & {a_2^{(5)}}^2 k_5 \end{bmatrix} \begin{bmatrix} \bar{u_1} \\ \bar{u_2} \\ \bar{u_3} \\ \bar{u_4} \\ \bar{u_5} \end{bmatrix}$$

We can write this equation more succinctly as $S_Y = M\bar{f}$, where S_Y represents

statistics about the endpoint force vector Y, and M represents the map that converts average muscle forces into task vector statistics. We can recover the mean forces given the covariance ellipse and its center using $\bar{u} = M^{-1}S_Y$ provided that M^{-1} exists. M^{-1} will not exist if any of the mechanical actions are the same or linearly dependent, otherwise, it will exist.

This process can be further explored on a more complex model using computer simulations. For this analysis, assume that muscle activity standard deviation is proportional to average muscle activity. This assumption rules out the simple linear system of equations described above, replacing them with a nonlinear set of equations that convert action and activity into quantities defining the covariance ellipse:

$$\bar{Y} = A\bar{u} \tag{6.2}$$

$$\mathrm{cov}[Y] = A(kk^T \overset{*}{\cdot} \rho \overset{*}{\cdot} \bar{u}\bar{u}^T)A^T \tag{6.3}$$

Equations 6.2-6.3 are the forward equations mapping muscle activity and action to the covariance ellipse center $\bar{Y}$ and the covariance matrix $\mathrm{cov}[Y]$. Important parameters are the standard deviation scaling factors k and the muscle activity correlation matrix ρ. The idea is to solve these equations in the "inverse direction": knowing the average net endpoint vector and its covariance matrix, find the average muscle activity for each muscle and each task. Assume that the muscle action vectors have been estimated by some other means, such as EWA. There are four basic cases to consider for these nonlinear equations: 1) all parameters are known (Figure 6.2B), 2) k is known but ρ is unknown so it is assumed that there is no correlation (Figure 6.2C), 3) ρ is known but only the average k across all muscles is known (Figure 6.2D) (Appendix of Chapter III shows how the average k can be estimated experimentally), and 4) only the average k is known and it is assumed that there is no correlation

(Figure 6.2E). When simulating Equations 6.2-6.3 in the forward direction, we assume that elements of the scaling vector k are uniformly distributed between 0.05 and 0.15, and that the muscle activity correlations are uniformly distributed between 0 and 0.2. Preliminary computer simulations indicate that using the net endpoint vector statistics to solve for the average muscle activity is reasonable in all cases, but it is more important to know the standard deviation scaling factor k_i as precisely as possible for all muscles i and relatively unimportant to know the muscle activity correlation matrix ρ.

Implementing this process on experimental data will require significant future work. First, knowledge of the mechanical action vectors for each potentially active muscle must be known *a priori* or else there will be too many parameters. Finally, if there are more than 5 active muscles, this process will require the use of higher order statistics. However, if the task space dimension is expanded, the average tension in more muscles can be determined by second order statistics. For instance, if the task space dimension is 3, then a matrix equation similar to Equation 6.1 will be generated with 9 equations, thus potentially accommodating 9 muscles. The number of muscles for which second order statistics in a task space of dimension d could determine the activity in every muscle exactly is given by

$$\#\text{ of muscles} = \frac{d^2 + 3d}{2} \tag{6.4}$$

Computing muscle activity from net endpoint vector variance is exciting because a complete ensemble of muscles could potentially be studied with reduced need for the placement of fine wire electrodes in deep or sensitive muscles. A muscle is deep and hard to access only because of its position relative to the skin surface. Preliminarily, there appears to be less of a concept of a deep muscle with regard to the force fluctuations it generates at the endpoint. It may be discovered in subsequent study

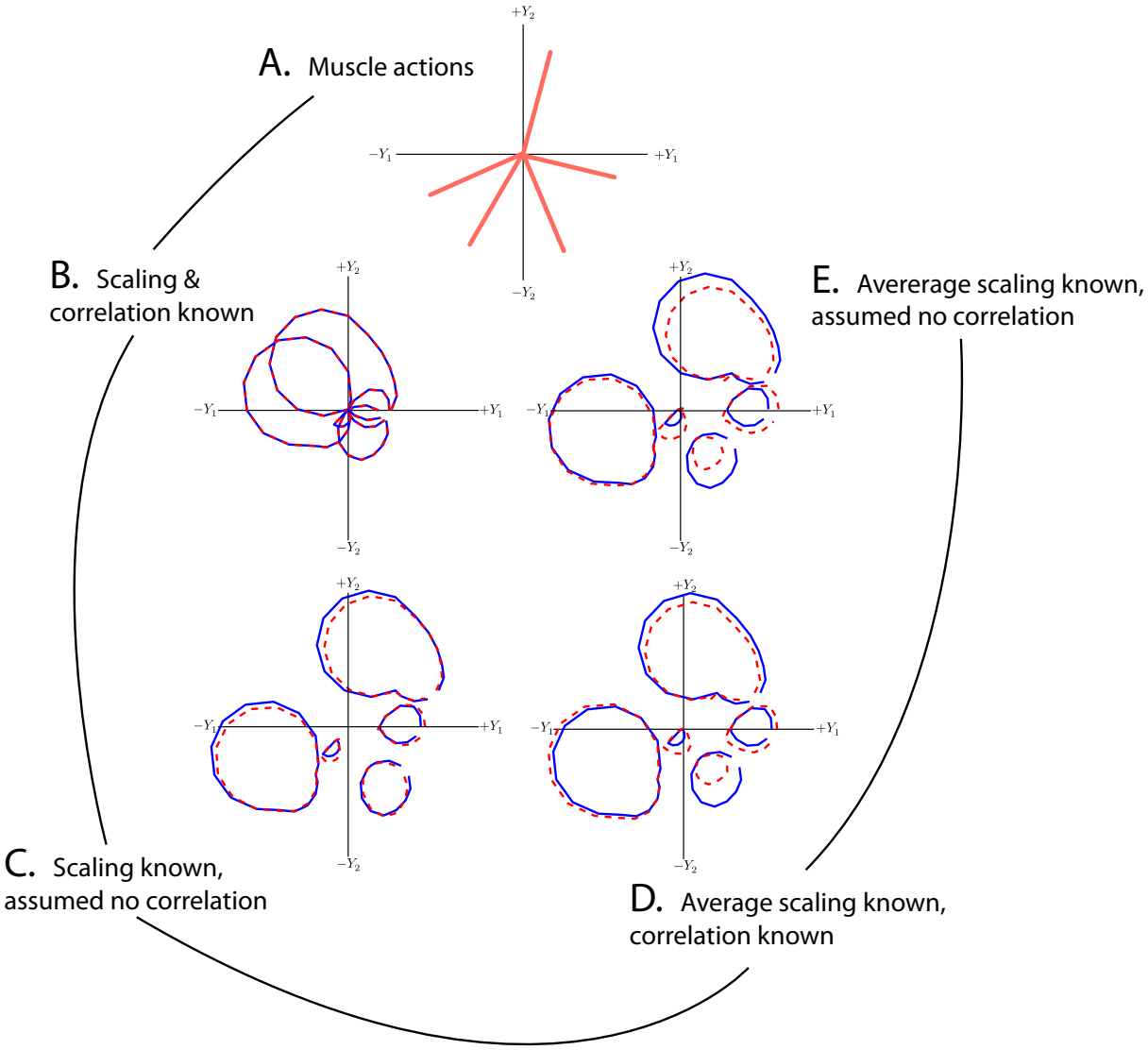

Figure 6.2: Nonlinear force covariance mapping equations can be solved for average muscle activity in a set of 5 muscles. A. Muscle actions are shown for a fictive system of 5 muscles operating in a 2-dimensional task space. Muscle activity is calculated by minimizing net endpoint vector variance, and Equations 6.2-6.3 are used to calculate the covariance ellipse for each task. Since the covariance ellipse and its center are measurable, Equations 6.2-6.3 are then used in reverse to estimate the average muscle activity for each task under various assumptions about what parameters are known. B. If relevant parameters are known, the muscle activity tuning curve can be estimated exactly for each muscle. C. If scaling factor relating activity standard deviation to average activity is known for each muscle, but correlation is assumed to be absent, reasonable estimates of muscle activity curves can be made for each muscle. Tuning curves are shifted away from the origin to facilitate viewing. D. If the correlation between the activity in all muscle pairs is known, but only the average standard deviation scaling factor is known, greater errors are made estimating the tuning curves from the endpoint vector covariance, but estimates are still reasonable. E. If neither the exact standard deviation scaling nor the correlation is known, estimate errors are similar to D, indicating that knowing exactly how activity standard deviation scales with average activity is more important than knowing the exact activity correlation matrix.

that examining muscles through motor unsteadiness is just as problematic because some muscles may have mechanisms of transmitting force but not force variability to the endpoint. Nonetheless, potentially inferring muscle activity from endpoint measurements seems to be a fruitful area for further research.

6.3.2 Determining muscle action from endpoint force accelerations

The computations of section 6.3.1 really require that some *a priori* information is available about the mechanical actions of the active muscles. While these may be estimated by electrical stimulation or EMG-weighted averaging, this would make for complicated and difficult experiments. Thus, it is reasonable to ask if there are ways of estimating the mechanical actions of the active muscles for a given task directly from fluctuations in endpoint force.

Motor unit action potentials generate force twitches. Thus, for a brief time after a motor unit action potential, the endpoint force should be rapidly accelerating along the mechanical action direction of the motor unit that most recently discharged. It is possible that, by looking at directions in which the endpoint force trajectory is accelerating, we may infer directions of likely muscle mechanical action.

Consider a typical waveform of a human motor twitch (Figure 6.3). The general structure of the twitch waveform can be represented by 3 parabolas: there is an initial period of relatively large positive force acceleration, followed by a period of lower negative acceleration, ended with a period of relatively low positive acceleration.

Assuming that the twitches from all motor units in all active muscles sum together to generate the net endpoint force, it is likely that the endpoint force trajectory will have some interesting temporal derivatives based on the twitch structure. We performed a simulation of the Fuglevand model in which we activated the EDC, FDI, and FDS equally. We chose a minimal level of excitation so that each muscle had

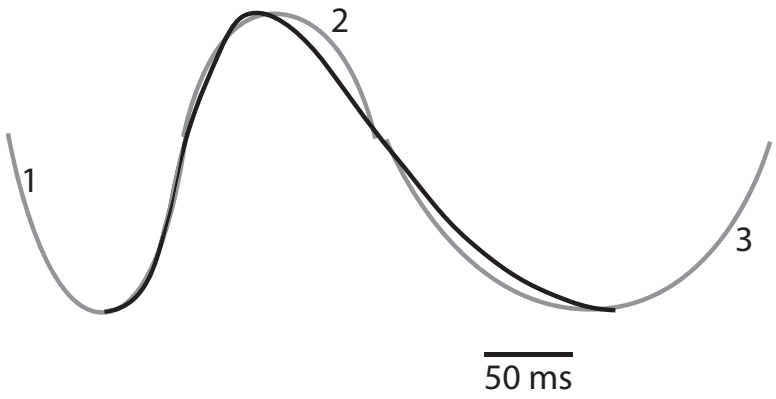

Figure 6.3: A measured human motor unit twitch (Thomas et al., 1990b) shown in dark, can be approximately broken up into three parabolic phases, highlighting the regions of positive and negative acceleration.

18 active motor units. The mechanical action of these three muscles generated a force trajectory (Figure 6.4A). The second derivative of the force trajectory reveals directions along which the force trajectory accelerates, which correspond closely to the mechanical action directions of the active muscles (Figure 6.4B).

There are many obstacles to overcome if endpoint force acceleration can be used experimentally to identify muscle mechanical action directions. First, computing the acceleration will involve differentiation of a potentially noisy signal. Specialized filters, such as Savitzky-Golay differentiators, will need to be designed to smooth out non-differentiable noise while preserving fast changes in force necessary for this analysis. Second, even in simulation, this process becomes less feasible as the number of active motor units is increased, because the time region over which one muscle dominates the force acceleration shrinks to zero. Nonetheless, examining the endpoint force trajectory time course in more detail will likely provide further clues about muscle mechanical action.

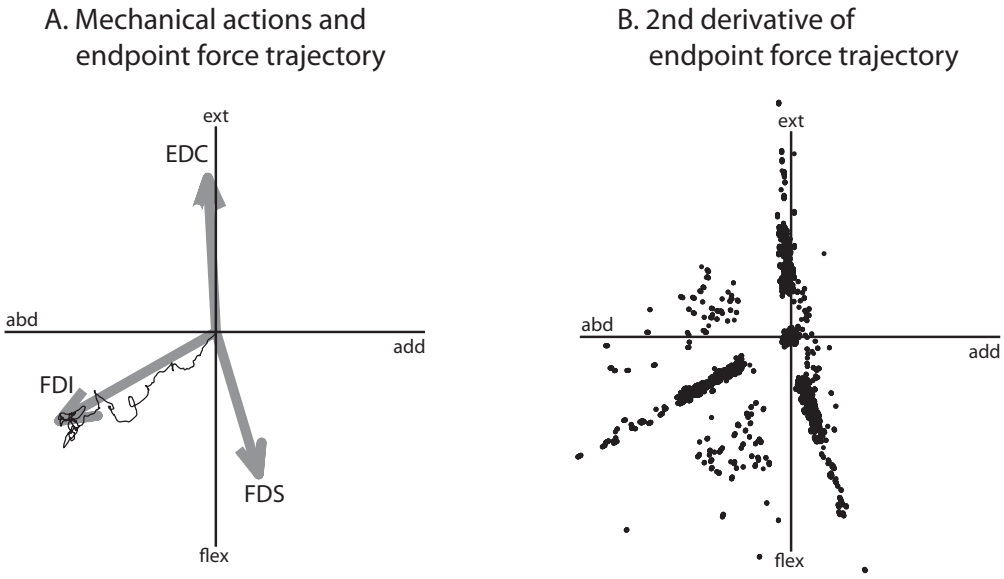

Figure 6.4: Endpoint force trajectory accelerations reveal muscle mechanical action directions in a simulated contraction. A. Three muscles (FDI, EDC, and FDS) with mechanical actions shown were equally activated to produce an endpoint force trajectory (shown). B. If the second derivative of the endpoint force trajectory is taken, and plotted as equally spaced points in time, the muscle mechanical actions appear as directions of relatively large acceleration magnitude.

6.4 Final thoughts: the past and future of motor unsteadiness in movement neuroscience

Figure 6.5 presents one possible diagram that gives some chronology and attempts to link some concepts of motor variability, showing specifically how force covariance mapping and EMG-weighted averaging came from other approaches.

Previous sections of this chapter have described possible research directions in the immediate future. What are the longer term prospects for using motor unsteadiness to study physiology and pathology? The first question is, can movement unsteadiness generated by muscle contraction always be measured, or was the choice of model system used in this work just extremely fortunate? In Chapter II, motor unsteadiness due to muscle contraction was built up from first principles as an intrinsic process; anytime motor neurons discharged to excite muscle, some oscillation in the tension

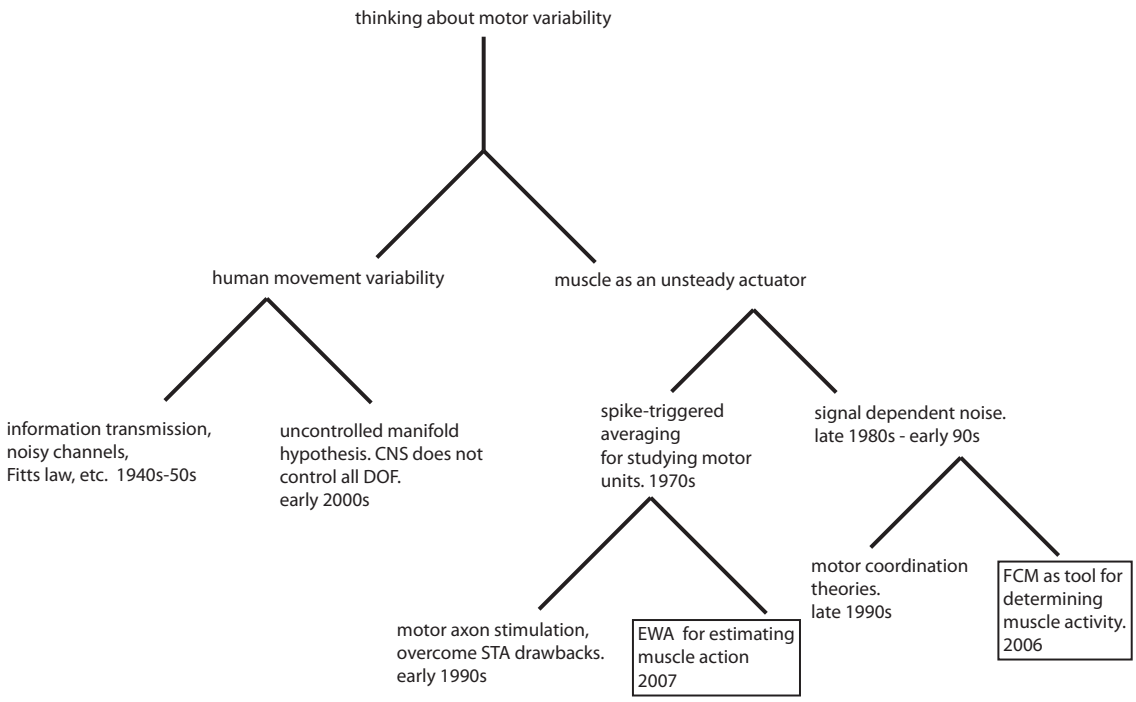

Figure 6.5: Tree view of thinking about motor variability.

generated by the excited muscle is inevitable. These oscillations were experimentally measurable for the human index finger, but it is quite possible that they may be dissipated in the surrounding tissues for other joints and limbs. Performing the techniques described in this work on other parts of the musculoskeletal system may require a large number of technical "tricks." It is intuitive that unsteadiness increases when handling large loads, and for a given movement of the hands, the head of a golf club moves more. Unsteadiness may be amplified using the choice of task magnitude and construction of experimental setup, but other problems may follow, such as finding a load transducer that is both exquisitely sensitive and operates over a large range of loads. It may be necessary to explore unsteadiness using non-mechanical means such as high-speed video or medical imaging. Many technical hurdles exist, but do not seem insurmountable.

The scientific questions this work chose to address with motor unsteadiness were the muscle redundancy problem and the problem of flexible muscle action direction. After the technical hurdles of measuring unsteadiness, it is important to consider broadening the scientific reach of unsteadiness. Philosophically, it seems that movement unsteadiness is a secret whispered by the body: what other information might it contain? One possibility is that unsteadiness holds information about the recruitment of motor units within a muscle. When the force demand of a task is increased, more motor units are recruited. After a motor unit is recruited, it begins to discharge more rapidly. The fluctuation in endpoint force due to a single motor unit would be expected to decrease as the discharge rate increases. Thus, net endpoint vector variability might contain information about the relative rate at which new motor units are recruited compared to the rate at which previously recruited motor units are increasing their discharge frequency. A map of all the scientific questions motor unsteadiness can address is needed to determine which problems are most tractable and should be tackled first.

Some neuro-motor pathologies may give rise to observable phenomena in the pattern of motor unsteadiness that could be exploited to design better treatments. Before treatments options are explored, the existence of embedded information must be established. Does the multidimensional structure of movement fluctuation in patients with tremor hold any clues about the underlying cause? Can force covariance mapping detect and study abnormal muscle coordination following CNS lesion? Can EMG-weighted averaging be used to assess the mechanical contribution of particular muscles after surgery or injury? These and related questions will require extensive future work, but it is hoped that the approaches described in this dissertation will play some role in answering these questions.

BIBLIOGRAPHY

An KN, Ueba Y, Chao EY, Cooney WP, Linscheid RL (1983) Tendon excursion and moment arm of index finger muscles. Journal of Biomechanics 16:419–425.

Andreassen S, Baron E (1983) Estimation of motor unit twitches. IEEE Transactions on Biomedical Engineering 30:742–748.

Bernstein N (1967) The co-ordination and regulation of movements Pergamon Press, Oxford.

Binder MD, Powers RK (2001) Relationship between simulated common synaptic input and discharge synchrony in cat spinal motoneurons. J Neurophysiol 86:2266–75.

Bremner FD, Baker JR, Stephens JA (1991a) Correlation between the discharges of motor units recorded from the same and from different finger muscles in man. J Physiol 432:355–80.

Bremner FD, Baker JR, Stephens JA (1991b) Effect of task on the degree of synchronization of intrinsic hand muscle motor units in man. J Neurophysiol 66:2072–83.

Bremner FD, Baker JR, Stephens JA (1991c) Variation in the degree of synchronization exhibited by motor units lying in different finger muscles in man. J Physiol 432:381–99.

Buchanan TS, Almdale DPJ, Lewis JL, Rymer WZ (1986) Characteristics of synergic relations during isometric contractions of human elbow muscles. Journal of Neurophysiology 56:1225–1241.

Buchanan TS, Rovai GP, Rymer WZ (1989) Strategies for muscle activation during isometric torque generation at the human elbow. Journal of Neurophysiology 62:1201–1212.

Buchanan TS, Shreeve DA (1996) An evaluation of optimization techniques for the prediction of muscle activation patterns during isometric tasks. Journal of Biomechanical Engineering-Transactions of the Asme 118:565–574.

Buchthal F, Schmalbruch H (1970) Contraction times and fibre types in intact human muscle. Acta Physiol Scand 79:435–52.

Calancie B, Bawa P (1986) Limitations of the spike-triggered averaging technique. Muscle Nerve 9:78–83.

Chanaud CM, Macpherson JM (1991) Functionally complex muscles of the cat hindlimb .3. differential activation within biceps-femoris during postural perturbations. Experimental Brain Research 85:271–280.

Chanaud CM, Pratt CA, Loeb GE (1991) Functionally complex muscles of the cat hindlimb .2. mechanical and architectural heterogenity within the biceps-femoris. Experimental Brain Research 85:257–270.

Datta AK, Stephens JA (1990) Synchronization of motor unit activity during voluntary contraction in man. J Physiol 422:397–419.

d'Avella A, Portone A, Fernandez L, Lacquaniti F (2006) Control of fast-reaching movements by muscle synergy combinations. Journal of Neuroscience 26:7791–7810.

d'Avella A, Saltiel P, Bizzi E (2003) Combinations of muscle synergies in the construction of a natural motor behavior. Nature Neuroscience 6:300–308.

Deluca CJ, Erim Z (1994) Common drive of motor units in regulation of muscle force. Trends in Neurosciences 17:299–305.

Deluca CJ, Roy AM, Erim Z (1993) Synchronization of motor-unit firings in several human muscles. J Neurophysiol 70:2010–2023.

Desmedt JE, Godaux E (1981) Spinal moto-neuron recruitment in man - rank deordering with direction but not with speed of voluntary movement. Science 214:933–936.

Dewald JP, Pope PS, Given JD, Buchanan TS, Rymer WZ (1995) Abnormal muscle coactivation patterns during isometric torque generation at the elbow and shoulder in hemiparetic subjects. Brain 118 (Pt 2):495–510.

Fagg AH, Shah A, Barto AG (2002) A computational model of muscle recruitment for wrist movements. Journal of Neurophysiology 88:3348–3358.

Farmer SF, Gibbs J, Halliday DM, Harrison LM, James LM, Mayston MJ, Stephens JA (2007) Changes in emg coherence between long and short thumb abductor muscles during human development. Journal of Physiology-London 579:389–402.

Farmer SF, Halliday DM, Conway BA, Stephens JA, Rosenberg JR (1997) A review of recent applications of cross-correlation methodologies to human motor unit recording. J Neurosci Methods 74:175–187.

Fetz EE (2007) Volitional control of neural activity: Implications for brain-computer interfaces. Journal of Physiology-London 579:571–579.

Fetz EE, Cheney PD (1980) Postspike facilitation of forelimb muscle-activity by primate corticomotoneuronal cells. J Neurophysiol 44:751–772.

Fisher RJ, Galea MP, Brown P, Lemon RN (2002) Digital nerve anaesthesia decreases emg-emg coherence in a human precision grip task. Experimental Brain Research 145:207–214.

Flament D, Goldsmith P, Buckley CJ, Lemon RN (1993) Task dependence of responses in 1st dorsal interosseous muscle to magnetic brain-stimulation in man. Journal of Physiology-London 464:361–378.

Fowler NK, Nicol AC, Condon B, Hadley D (2001) Method of determination of three dimensional index finger moment arms and tendon lines of action using high resolution mri scans. Journal of Biomechanics 34:791–797.

Fuglevand AJ, Winter DA, Patla AE (1993) Models of recruitment and rate coding organization in motor-unit pools. J Neurophysiol 70:2470–88.

Galganski ME, Fuglevand AJ, Enoka RM (1993) Reduced control of motor output in a human hand muscle of ederly subjects during submaximal contractions. Journal of Neurophysiology 69:2108–2115.

Harris CM, Wolpert DM (1998) Signal-dependent noise determines motor planning. Nature 394:780–784.

Haruno M, Wolpert DM (2005) Optimal control of redundant muscles in step-tracking wrist movements. Journal of Neurophysiology 94:4244–4255.

Henneman E, Somjen G, Carpenter DO (1965a) Excitability and inhibitibility of motoneurons of different sizes. Journal of Neurophysiology 28:599–&.

Henneman E, Somjen G, Carpenter DO (1965b) Functional significance of cell size in spinal motoneurons. J Neurophysiol 28:560–80.

Herrmann U, Flanders M (1998) Directional tuning of single motor units. J. Neurosci. 18:8402–8416.

Hoffman DS, Strick PL (1995) Effects of a primary motor cortex lesion on step-tracking movements of the wrist. Journal of Neurophysiology 73:891–895.

Hoffman DS, Strick PL (1999) Step-tracking movements of the wrist. iv. muscle activity associated with movements in different directions. Journal of Neurophysiology 81:319–333.

Jones KE, Hamilton AF, Wolpert DM (2002) Sources of signal-dependent noise during isometric force production. J Neurophysiol 88:1533–44.

Kamper DG, Fischer HC, Cruz EG (2006) Impact of finger posture on mapping from muscle activation to joint torque. Clinical Biomechanics 21:361–369.

Keen DA, Fuglevand AJ (2004a) Common input to motor neurons innervating the same and different compartments of the human extensor digitorum muscle. J Neurophysiol 91:57–62.

Keen DA, Fuglevand AJ (2004b) Distribution of motor unit force in human extensor digitorum assessed by spike-triggered averaging and intraneural microstimulation. J Neurophysiol 91:2515–23.

Keenan KG, Farina D, Meyer FG, Merletti R, Enoka RM (2007) Sensitivity of the cross-correlation between simulated surface emgs for two muscles to detect motor unit synchronization. J Appl Physiol 102:1193–201.

Keenan KG, McNamara RVI, Backus S, Schieber MH, Valero-Cuevas FJ (2006) Index finger abduction is a complex motor task 655.18 In Society for Neuroscience, Atlanta, GA. Neuroscience Meeting Planner.

Kernell D, Eerbeek O, Verhey BA (1983) Relation between isometric force and stimulus rate in cat's hindlimb motor units of different twitch contraction time. Exp Brain Res 50:220–7.

Kilner JM, Baker SN, Salenius S, Jousmaki V, Hari R, Lemon RN (1999) Task-dependent modulation of 15-30 hz coherence between rectified emgs from human hand and forearm muscles. Journal of Physiology-London 516:559–570.

Komatsu Y, Nakajima S, Toyama K, Fetz EE (1988) Intracortical connectivity revealed by spike-triggered averaging in slice preparations of cat visual-cortex. Brain Res 442:359–362.

Krishnamoorthy V, Scholz JP, Latash ML (2007) The use of flexible arm muscle synergies to perform an isometric stabilization task. Clinical Neurophysiology 118:525–537.

Kuo AD (1994) A mechanical analysis of force distribution between redundant, multiple degree-of-freedom actuators in the human - implications for the central-nervous-system. Human Movement Science 13:635–663.

Kuo A (2000) The action of two-joint muscles: The legacy of w.p. lombard In Zatsiorsky VM, Latash ML, editors, Classics in movement science, pp. 289–316. Human Kinetics, Champaign, IL 540.

Kutch JJ, Buchanan TS (2001) Human elbow joint torque is linearly encoded in electromyographic signals from multiple muscles. Neurosci Lett 311:97–100.

Kutch J, Suresh N, Bloch A, Rymer W (2007) Analysis of the effects of firing rate and synchronization on spike-triggered averaging of multidirectional motor unit torque. Journal of Computational Neuroscience 22:347–361.

Latash ML, Scholz JF, Danion F, Schoner G (2001) Structure of motor variability in marginally redundant multifinger force production tasks. Experimental Brain Research 141:153–165.

Latash ML, Scholz JP, Schoner G (2002) Motor control strategies revealed in the structure of motor variability. Exercise and Sport Sciences Reviews 30:26–31.

Lawrence JH, Nichols TR, English AW (1993) Cat hindlimb muscles exert substantial torques outside the sagittal plane. Journal of Neurophysiology 69:282–285.

Lee WA (1984) Neuromotor synergies as a basis for coordinated intentional action. Journal of Motor Behavior 16:135–170.

Lim KY, Thomas CK, Rymer WZ (1995) Computational methods for improving estimates of motor unit twitch contraction properties. Muscle Nerve 18:165–74.

Loeb E, Ghez C (2000) The motor unit and muscle action In Kandel ER, Schwartz JH, Jessell TM, editors, Principles of neural science, pp. 674–694. McGraw-Hill, New York, 4th edition.

Long C (1968) Intrinsic-extrinsic muscle control of fingers. Journal of Bone and Joint Surgery-American Volume A 50:973–&.

Lowery MM, Erim Z (2005) A simulation study to examine the effect of common motoneuron inputs on correlated patterns of motor unit discharge. Journal of Computational Neuroscience 19:107–124.

Macpherson JM (1991) How flexible are muscle synergies? In Humphrey D, Freund HJ, editors, Motor control: Concepts and issues, pp. 33–47. Wiley Press, New York.

Mannard A, Stein RB (1973) Determination of frequency-response of isometric soleus muscle in cat using random nerve-stimulation. J Physiol (Lond.) 229:275–296.

Marsaglia G, Olkin I (1984) Generating correlation-matrices. Siam Journal on Scientific and Statistical Computing 5:470–475.

Matsumura M, Chen DF, Sawaguchi T, Kubota K, Fetz EE (1996) Synaptic interactions between primate precentral cortex neurons revealed by spike-triggered averaging of intracellular membrane potentials in vivo. J Neurosci 16:7757–7767.

Moritz CT, Barry BK, Pascoe MA, Enoka RM (2005) Discharge rate variability influences the variation in force fluctuations across the working range of a hand muscle. J Neurophysiol 93:2449–59.

Murray WM, Delp SL, Buchanan TS (1995) Variation of muscle moment arms with elbow and forearm position. Journal of Biomechanics 28:513–525.

Nordstrom MA, Miles TS, Veale JL (1989) Effect of motor unit firing pattern on twitches obtained by spike-triggered averaging. Muscle Nerve 12:556–567.

Perotto A (2005) Anatomical guide for the electromyographer Charles C. Thomas, Springfield, IL, 4th edition.

Rieke F, Warland D, Ruyter van Steveninck R, Bialek W (1997) Spikes: Exploring the neural code MIT PressIM - Image, Cambridge.

Saltiel P, Wyler-Duda K, D'Avella A, Tresch MC, Bizzi E (2001) Muscle synergies encoded within the spinal cord: Evidence from focal intraspinal nmda iontophoresis in the frog. Journal of Neurophysiology 85:605–619.

Sandercock TG (2005) Summation of motor unit force in passive and active muscle. Exerc Sport Sci Rev 33:76–83.

Schmied A, Vedel JP, Pagni S (1994) Human spinal lateralization aassessed from motoneuron synchronization - dependence on handedness and meter unit type. J Physiol (Lond.) 480:369–387.

Sears TA, Stagg D (1976) Short-term synchronization of intercostal motoneuron activity. Journal of Physiology-London 263:357–381.

Semmler JG (2002) Motor unit synchronization and neuromuscular performance. Exerc Sport Sci Rev 30:8–14.

Semmler JG, Nordstrom MA (1998) Hemispheric differences in motor cortex excitability during a simple index finger abduction task in humans. Journal of Neurophysiology 79:1246–1254.

Stein RB, Yemm R, French AS, Mannard A (1972) New methods for analyzing motor function in man and animals. Brain Res 40:187–192.

Taylor AM, Steege JW, Enoka RM (2002) Motor-unit synchronization alters spike-triggered average force in simulated contractions. J Neurophysiol 88:265–76.

ter Haar Romeny BM, Denier van der Gon JJ, Gielen CCAM (1982) Changes in recruitment order of motor units in the human biceps muscle. Experimental Neurology 78:360–368.

ter Haar Romeny BM, Denier van der Gon JJ, Gielen CCAM (1984) Relation between location of a motor unit in the human biceps brachii and its critical firing levels for different tasks. Experimental Neurology 85:631–650.

Thomas CK, Bigland-Richie B, Johansson RS (1991) Force-frequency relationships of human thenar motor units. J Neurophysiol 65:1509–16.

Thomas CK, Bigland-Ritchie B, Westling G, Johansson RS (1990a) A comparison of human thenar motor-unit properties studied by intraneural motor-axon stimulation and spike-triggered averaging. J Neurophysiol 64:1347–51.

Thomas CK, Johansson RS, Westling G, Bigland-Ritchie B (1990b) Twitch properties of human thenar motor units measured in response to intraneural motor-axon stimulation. J Neurophysiol 64:1339–46.

Thomas CK, Ross BH, Stein RB (1986) Motor-unit recruitment in human first dorsal interosseous muscle for static contractions in three different directions. J Neurophysiol 55:1017–29.

Ting LH, Macpherson JM (2005) A limited set of muscle synergies for force control during a postural task. Journal of Neurophysiology 93:609–613.

Todorov E (2002) Cosine tuning minimizes motor errors. Neural Comput 14:1233–60.

Todorov E, Jordan MI (2002) Optimal feedback control as a theory of motor coordination. Nat Neurosci 5:1226–35.

Towles JD, Murray WM, Hentz VR (2004) The effect of percutaneous pin fixation of the interphalangeal joint on the thumb-tip force produced by the flexor pollicis longus: A cadaver study. J Hand Surg [Am] 29:1056–62.

Tresch MC, Cheung VCK, d'Avella A (2006) Matrix factorization algorithms for the identification of muscle synergies: Evaluation on simulated and experimental data sets. Journal of Neurophysiology 95:2199–2212.

Tubiana R (1987) Extensor apparatus of the fingers In Schneider L, Macklin E, editors, Tendon surgery in the hand, pp. 319–324. C.V. Mosby Company, St. Louis.

Valero-Cuevas FJ, Yi JW, Brown D, McNamara RV, Paul C, Lipson H (2007) The tendon network of the fingers performs anatomical computation at a macroscopic scale. Ieee Transactions on Biomedical Engineering 54:1161–1166.

Valero-Cuevas FJ, Zajac FE, Burgar CG (1998) Large index-fingertip forces are produced by subject-independent patterns of muscle excitation. Journal of Biomechanics 31:693–703.

van Bolhuis BM, Gielen C (1999) A comparison of models explaining muscle activation patterns for isometric contractions. Biological Cybernetics 81:249–261.

Van der Helm F, Rozendaal L (2000) Musculoskeletal system with intrinsic and proprioceptive feedback In Winters J, Crago P, editors, Biomechanics and neural control of posture and movement, pp. 164–174. Springer-Verlag, New York.

Westling G, Johansson RS, Thomas CK, Bigland-Ritchie B (1990) Measurement of contractile and electrical properties of single human thenar motor units in response to intraneural motor-axon stimulation. J Neurophysiol 64:1331–8.

Winslow J (1732) Exposition anatomique de la structure du corps humain Chez Guillaume Desprez et Jen Desesszrtz, Paris, France.

Yao W, Fuglevand RJ, Enoka RM (2000) Motor-unit synchronization increases emg amplitude and decreases force steadiness of simulated contractions. J Neurophysiol 83:441–52.

Zhou P, Rymer WZ (2004) Factors governing the form of the relation between muscle force and the emg: A simulation study. Journal of Neurophysiology 92:2878–2886.

Zhou P, Suresh NL, Rymer WZ (2007) Model based sensitivity analysis of emg-force relation with respect to motor unit properties: Applications to muscle paresis in stroke. Annals of Biomedical Engineering 35:1521–1531.